ALMA MATER STUDIORUM
UNIVERSITÀ DI BOLOGNA

DOTTORATO DI RICERCA IN

Scienze e Tecnologie della Salute

Ciclo XXXVI

Settore Concorsuale: 09/G2

Settore Scientifico Disciplinare: ING-IND/34

DEVELOPMENT AND PRE-CLINICAL VALIDATION OF A COMPUTER-ASSISTED PREDICTOR OF THE RISK OF VERTEBRAL FRACTURE

Presentata da: Chiara Garavelli

Coordinatore Dottorato

Prof. Igor Diemberger

Supervisore

Prof. Marco Viceconti

Co-supervisori

Prof. Uberto Pagotto

Dott. Alessandra Aldieri

Esame finale anno 2024

A Michele.

You were my sunshine,
My only sunshine,
You made me happy,
When skies were grey.

Summary

Vertebral fragility fractures are difficult to predict since, by definition, they do not occur due to accidents. In fact, these fractures typically arise during daily activities, following conditions like osteoporosis or cancer metastasis that increase the vulnerability of the vertebrae. Assessing the residual bone competence in these pathological patients remains a complex task. Although the Vertebral Fracture Assessment (VFA) tool is currently used, it primarily evaluates the severity of fractures once they have already occurred rather than estimating the risk of occurrence. Areal bone mineral density (aBMD), a reliable predictor for proximal femur fractures, does not yield a similar accuracy for the spine. Additionally, Spinal Instability in Neoplastic Disease (SINS) is clinically used for metastatic patients, but it presents some difficulties in discriminating between the central levels of classification.

Patient-specific computational tools based on clinical images may address this challenge and provide valuable support for clinical decision-making. However, before these methodologies can be used in clinical practice, it is necessary to demonstrate that they provide reliable and accurate predictions. To achieve this, the model's predictions require to be validated against the results of controlled experiments. Vertebral fracture experiments can be conducted on cadaver bones. Still, their use for models' validation is challenging: a single isolated vertebral body is not sufficiently slender to assume valid Saint-Venant's principle, while on the other hand experimental tests on a spine segment raise issues with the interaction between bones and intervertebral discs.

This PhD thesis aims to define the accuracy of subject-specific finite element models of multi-vertebrae segments. Homogenised finite element (hFE) models of the spine were generated from clinical computed tomography (CT) or micro-computed tomography (µCT) data; *in vitro* full-field measurements were used in the validation experiments to compare numerical outcomes with the corresponding experimental ones.

The first part of the work focused on assessing whether the construction of multi-vertebrae FE models uniquely based on CT was feasible. To achieve this aim, cadaveric spinal segments were tested experimentally, and Digital Image Correlation (DIC), an optical full-field technique, was used to track the displacements and strains on the vertebrae surface. The spinal segments were also CT-scanned, and FE models were built and subjected to boundary conditions replicating the experimental tests. Numerical outcomes on the vertebrae surface were then compared to the available experimental ones. Because CT does not provide any information about the intervertebral disc material properties, the hypothesis of a linear elastic and isotropic material was done.

More in detail, the analysis was divided into two distinct parts. Firstly, experimental and numerical displacements were compared in the case the intervertebral disc Young's modulus was identified by

fitting the numerical force-displacement curve to the experimental one. Secondly, superficial principal strains on the vertebrae were compared exploring the full range of Young's modulus values assigned to the intervertebral discs in the literature.

Although the kinematics could be correctly reproduced for any of the Young's modulus tested, numerical and experimental strains showed considerable differences. Only 25-30 MPa Young's modulus values yielded comparable order of magnitudes between FE- and DIC-derived strains.

Hence, in the second part of this thesis the focus was shifted to assessing whether, when working on individual vertebrae, the three-dimensional displacements and strains obtained from FE models matched the experimental ones. If this hypothesis were confirmed, then the analysis of a multi-vertebrae FE models would require more accurate modelling of the discs. Specifically, µCT scans of multi-vertebral segments were acquired before and after pure compressive tests. These images were used as input to a Digital Volume Correlation (DVC) algorithm that allowed the extraction of the full 3D deformation field within the bone structure. Then, both micro-FE (µFE) and hFE models were generated from the unloaded µCT scans and were subjected to experimentally matched boundary conditions. hFE models results in terms of displacements were compared pointwise against DVC data and µFE results. Using the same µCT scans as input for both *in silico* model and *in vitro* measurement allows to avoid registration errors. However, considering that µCT scans cannot be acquired *in vivo*, the outcomes of the µCT-based hFE model were compared to the ones of a clinical CT-based hFE model (using the CT scans acquired during the first part of the work). Additionally, a qualitative comparison between the hFE model and DVC strains was performed, to assess the models' ability to highlight the regions showing higher deformations. DVC and hFE displacement fields showed good agreement, both for healthy (R^2 = 0.69÷0.83, RMSE% = 3÷22% and max errors < 45 µm) and metastatic (R^2 = 0.64÷0.93, RMSE% = 5÷18% and max errors < 55 µm) vertebrae. µCT based and clinical-CT based outcomes presented strong correlations (R^2 = 0.99, RMSE% < 1.3% and max error = 6 µm) as well as hFE and µFE models (R^2 = 0.95÷0.97, RMSE% = 3÷29% and 95th percentile = 2÷61 µm). Also, hFE models were able to qualitatively identify the regions which experimentally showed the highest strain concentration.

The main conclusion of this work is that when the boundary conditions are accurately modelled, subject-specific hFE vertebral models built from clinical CT data can predict displacements and strains with accuracies comparable to that of the experimental method (DVC) used for the validation; µFE models show accuracies comparable to hFE models. But in multi-segment models, the model's predictions are highly sensitive to the biomechanical properties of intervertebral discs; thus, we believe accurate models can be built only if the disc's properties are personalised.

Contents

Chapter 1

Introduction

The first chapter aims to provide a priori knowledge relevant to understand the decisions taken for the workflow implementation in the following chapters. Firstly, a brief description of the vertebral bone anatomy and physiology is reported. This is followed by the description of the clinical problem which motivates this thesis, namely the vertebral fragility fracture, analysing the more frequent pathologies that increase its occurrence. The methods currently used to identify patients with high vertebral fracture risk and their limitations are also reported. Then, the state of the art for the generation and the validation of vertebral subject-specific finite element models is presented, with a focus on the models of the pathological vertebra. Subsequently, the experimental methodologies which allow to obtain full-field information on displacements and deformations useful for models validation are briefly described. The first chapter will conclude reporting the motivation behind this thesis and its specific objectives.
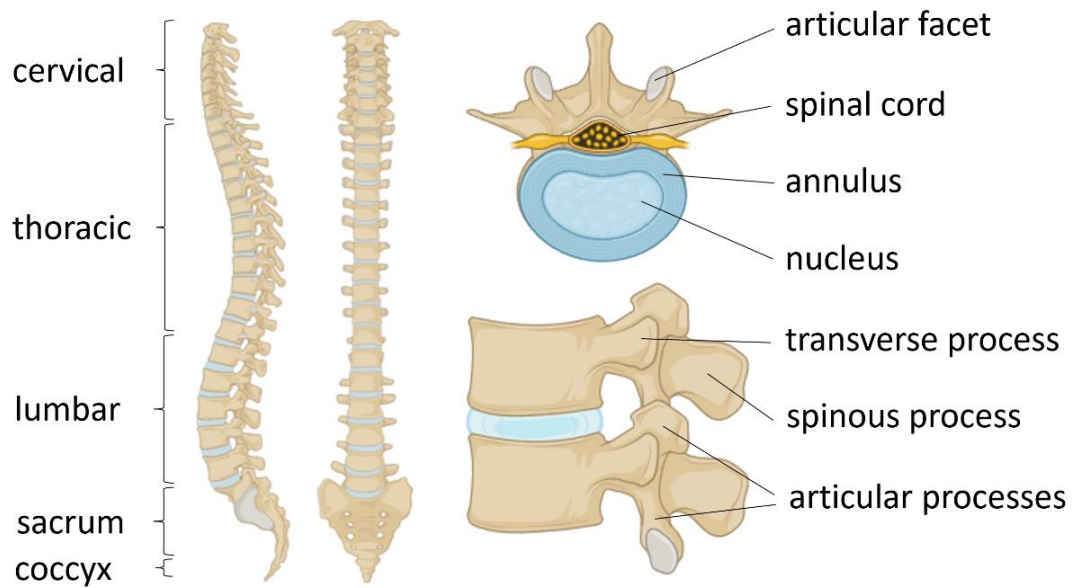
1.1.   Anatomy

The spinal column is a complex anatomical structure that provides fundamental support to the human body, imparting both stability and flexibility, allowing human movement and, at the same time, protecting the spinal cord (Gray, 1858).

Vertebrae are primarily composed of cancellous bone, a network of trabeculae, which are bundles of lamellae in which the collagen fibrils are oriented with strong parallelism (Reznikov et al., 2015). The interstitial space between the trabeculae is filled with the medulla, contributing to the bone's stiffness. The cancellous bone can absorb shocks and is light and inexpensive in metabolic terms; however, it does not guarantee sufficient mechanical strength. Consequently, the structural optimisation is manifested in the vertebrae with a thin layer of superficial cortical bone, mechanically resistant but also heavy and expensive in metabolic terms, inside which is the cancellous bone. In this way, vertebrae provide maximum resistance at minimum cost, avoiding waste of material. The trabeculae in the cancellous bone are oriented mainly in a vertical direction, this being the main direction of load acting on them (Cristofolini, 2015).

The functional unit of the spine is composed of two adjacent vertebrae, the interposed disc, and the capsule-ligamentous structures (Fig. 1.1). In this perspective, the vertebra is classified as a type I lever or "interlocking", in which the inter-apophyseal joints are the point of support, the disc makes a direct and passive cushioning, and the muscles an indirect and active cushioning. The front pillar has a support function, while the rear has a dynamic one. The inter-apophyseal joints have little resistance to compressive or tensile forces while responding with good resistance to torsional stress and slippage. In the healthy spine the vertebral body withstand about 80% of the compressive loads while the posterior column about the 20% of the loads (Mobbs et al., 2013). Most of the stresses are then transmitted from one vertebra to the adjacent one through the interposed disc.

The intervertebral disc has three main functions, namely, to withstand the loads, to dampen and reduce stress transmission, and to allow relative movements between consecutive vertebrae. From a structural point of view, it is composed of two different elements (Cassidy et al., 1989). In the centre there is the nucleus pulposus, a gel rich in proteoglycans that loses part of its water content under pressure. It is surrounded by the annulus fibrosus, a structure of fibrotic tissue with high content of collagen (Disney et al., 2018).

Fig. 1.1: Anatomy of the spine. On the left, lateral and anterior views of the spine with the different portions highlighted. On the right, the functional spine unit, composed by two vertebrae and the interposed discs (bottom), and its section in correspondence to the intervertebral disc. It is possible to distinguish the annulus and the nucleus (top). Imaged created with BioRender.com.

1.2. Vertebral fragility fracture

A vertebral fracture is the disruption in the structural integrity of the vertebral body. It results from excessive mechanical forces, often related to trauma such as accidents or falls. Still, when considering fragility vertebral fractures, the emphasis lies on fractures occurring with minimal or low-energy trauma in individuals with compromised bone quality and reduced bone mineral density. These fractures predominantly affect the thoracic and lumbar regions of the spine, especially at the thoracolumbar junction.

The failure mechanism of the vertebra has been studied, both for healthy and pathological vertebrae, using the application of quasi-static load on multi-vertebral specimens in order to account for the action of the intervertebral discs (Palanca et al., 2023). For both groups it has been shown that the failure frequently originates at the endplate level. In case of metastatic specimens (composed by metastatic vertebra and adjacent radiologically healthy one used as control), typically fractures occurred in the lytic or mixed metastatic vertebra, whit the exception of the specimens presenting blastic metastases where the failure is mainly reported in the control vertebrae.

The most used classification of vertebral fractures is the one presented by Genant et al., 1993, which considers the decrease in the height of the vertebral body (mild 20-25%, moderate 26-40% or severe >40%) and the location of collapse (wedge anterior, biconcave central or crush posterior).

The mechanism of failure seems to be strongly influenced by the way in which the load is applied. Jackman et al., (2016) analysed initiation and progression of the fracture when the spinal segment is subjected to axial compression versus presso-flexion (performed using a combined loading). During the former tests the failure seems to start in the central part of the endplates, generating a biconcave fracture. Vice versa, in the latter test the deflection of the endplate was concentrated in its anterior part, i.e., shifted in the direction of the flexion, producing an external bulge in the anterior cortex. This typically results into wedge-shaped deformity on clinical imaging, with a reduction of the vertebral height and the forward curvature of the spine (kyphosis), affecting the overall spinal alignment and biomechanics. Another crucial aspect emerging from the study was that not only the type but the risk itself of the fracture is dependent to the type of loading. In fact, they showed that vertebrae, even after their ability to support anterior flexion is already compromised, can support significant compressive force. Aware of this and considering that fragility fractures derivate from daily activities, it is interesting to report that many studies have tried to assess the range of loads acting in the vertebra during the most frequent tasks of the daily routine (Rohlmann et al., 2014). The activities that transmit higher loads among a thousand analysed exercises are the flexion of the upper body, the staircase walking and the lifting of a weight from the ground.

More than half of the vertebral fractures are asymptomatic and often they are never diagnosed (Kado et al., 1999). Nevertheless, they can have strong implications on the patients' quality of life, causing spinal compression and consequently pain (Dionyssiotis, 2010) as well as increasing the risk of new fractures (Klotzbuecher et al., 2000).

1.2.1. Pathologies

In the following paragraphs, the main pathologies which affect the vertebral bone mechanical competence increasing the risk of fracture will be presented.

1.2.1.1.   Osteoporotic Disease

Osteoporosis is a skeletal disorder characterised by reduced bone density and progressive deterioration of bone microarchitecture (Morita et al., 1994). Reduced bone density predisposes to bone fractures due to low energy trauma, which would not lead to fracture in physiological bone density conditions (Johnell & Kanis, 2006). The cause of this pathology is the loss of balance in the action of osteoblasts and osteoclasts within the bone remodelling process (Fig. 1.2 A). The first category of cells contributes to bone formation, while the second manages bone resorption; consequently, if the action of osteoclasts is considerably greater than that of osteoblasts, the bone starts to deteriorate. During the menopause period, osteoclasts' increased production is caused by the loss of oestrogen, which leads to a possible increase in cytokines related to the production of osteoclasts. In addition, advancing age decreases the activity of osteoblasts. These facts explain the spread of this pathology in women over 50 (Melton, 1997; Old & Calvert, 2004). However, it can afflict individuals of any age and gender, making it a significant public health concern (Johnell, 1997). When the pathology is achieved by related conditions, like hyperparathyroidism or assumption of osteotoxic drugs, the osteoporosis is defined secondary. The phenomenon is typically asymptomatic and manifested by decreased calcium tone in bone mass (osteopenia). The skeletal districts most easily affected by the decrease in calcic tone are the thoracolumbar vertebrae, the femur, and the wrist (Cooper & Melton, 1992).

Diagnosis and risk assessment are paramount to managing osteoporosis effectively. Traditionally, areal bone mineral density (aBMD) measured using Dual-energy X-ray Absorptiometry (DXA) has been the gold standard for diagnosing the condition. Nowadays, the following thresholds are used to evince the gravity of the disease (WHO, 1994) (Fig. 1.2 B):

- **Normal**: BMD within 1 standard deviations below the young adult average
- **Osteopenia**: BMD between 1 and 2.5 standard deviations below the young adult average
- **Osteoporosis**: BMD higher than 2.5 standard deviations below the young adult average

- **Severe osteoporosis**: BMD higher than 2.5 standard deviations below the young adult average and presence of at least one fragility fracture

However, experts acknowledge that relying solely on aBMD may not capture the complete picture, as it fails to account for bone quality and microstructural changes (Fonseca et al., 2014). Consequently, clinicians now emphasise the integration of clinical risk factors alongside DXA measurements to refine fracture risk assessment (Kanis et al., 2017).

Treatment of osteoporosis primarily revolves around two major goals: reducing fracture risk and preserving bone mass. Lifestyle modifications, such as regular weight-bearing exercises and ensuring adequate calcium and vitamin D intake, are pivotal in maintaining bone health (Albrecht et al., 2022). Various pharmacological interventions have also been instrumental in managing the disease and preventing fractures, including bisphosphonates, selective oestrogen receptor modulators, and monoclonal antibodies targeting specific bone-regulating pathways (Tu et al., 2018).

Despite these advances, challenges remain in optimising osteoporosis management. Some patients may experience side effects from medication, while others may struggle with treatment adherence. Moreover, identifying individuals at high risk for osteoporotic fractures remains a complex task, demanding a comprehensive approach encompassing clinical assessment, advanced imaging techniques, and emerging biomarkers.
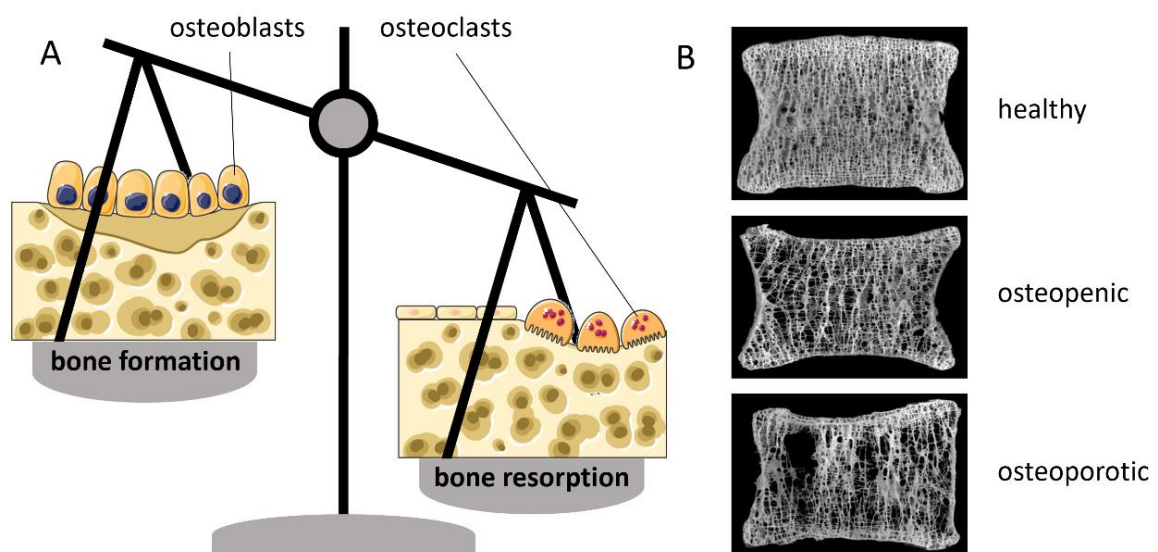
Fig. 1.2: Osteoporosis is caused by a lack of balance in the bone remodelling cycle (A). The original elements used in the figure are from Servier Medical Art (http://smart.servier.com/); Image created with BioRender.com. This imbalance leads to a progressive degradation of the trabecular tissue (B). Image adapted from https://www.medimapsgroup.com/.

1.2.1.2. Bone Metastatic Disease

Bone metastatic disease, a consequence of advanced cancer, inflicts devastating effects on patients' quality of life. This occurs when malignant cells from primary tumours invade blood capillaries, move to a different region elsewhere in the body, create adhesion to the vessels' walls, infiltrate and colonise the bone tissue (Coleman et al., 2019) (Fig. 1.3A). Among patients with metastatic cancer, approximately 70% will experience bone metastases, with common primary sites being breast and prostate cancers (Huang et al., 2020). In Italy, for example, the Italian Association of medical oncology (AIOM) reports 35.000 new cases of bone metastases every year.

Vertebral metastases bring forth many complications, ranging from debilitating pain and fractures to hypercalcemia, spinal cord compression, and impaired mobility. The interplay between cancer cells and the bone microenvironment is complex, leading to bone destruction and tumour growth. Tumour cells are attracted to the bone's rich blood supply and to the release of bone-derived growth factors. Vertebral bones are consequently one of the most common locations of metastasis in light of their high vascularization.

It is possible to highlight three different types of metastases (Guise et al., 2006) (Fig. 1.3B):

- **Lytic**: a disintegration of the trabecular lattice due to an imbalance of regulatory factors (as a result of the presence of primary cancer) that translates into an increase in the resorption of old bone tissue by osteoclasts and a reduction in the deposition of new material by osteoblasts. It's the most common damage in cancers that have spread from the lung, thyroid, kidney, or colon.
- **Blastic**: an anomalous densification of the bone structure. The interstitial space is reduced and sometimes disappears. The deformed bone is weaker since the normal architectural arrangement of the lamellae is no longer present. Furthermore, the morphological alteration of the vertebral body can lead to the compression of the nerve roots and spinal cord, resulting in neurological complications. This type of metastasis is most often diagnosed following prostate, bladder, or stomach tumours.
- **Mixed**: the simultaneous presence of both lytic and blastic metastases inside the same bone.

The diagnosis of bone metastatic disease requires the integration of various imaging modalities, including computed tomography (CT) scans, positron emission tomography (PET), and magnetic resonance imaging (MRI). Early detection is crucial, as timely intervention can alleviate suffering and improve outcomes. Corticosteroids, which are commonly used in therapies to treat tumours, have been shown to cause bone tissue degradation, degenerating into secondary osteoporosis (Adachi et al., 2000). Bisphosphonates and denosumab are frequently prescribed to inhibit bone resorption, mitigate skeletal complications, and improve bone strength.
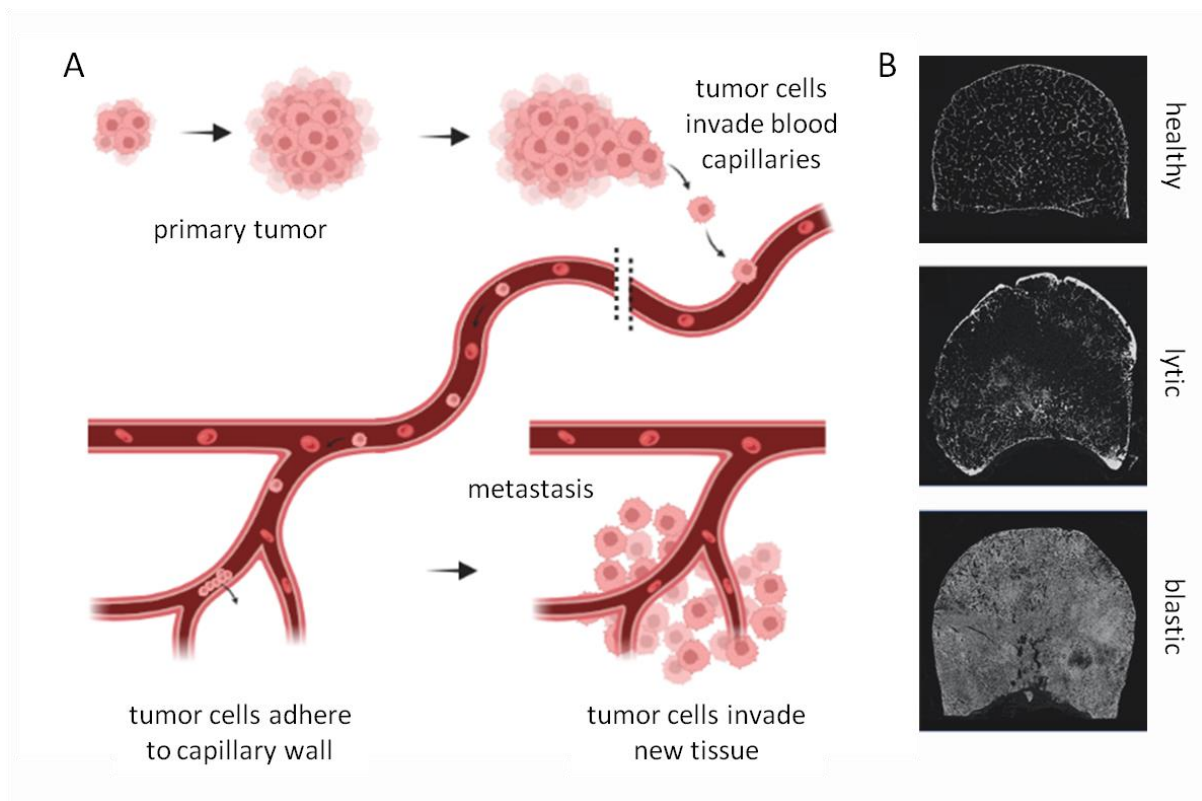
Fig. 1.3: On the left (A), a schematic representation of the metastatic diffusion. Image created with BioRender.com. On the right (B), section of a healthy vertebral scanned inside a µCT machine, followed by sections of vertebrae presenting the signs of bone metastasis, specifically lytic (middle) and blastic (bottom). Image adapted from Cavazzoni et al., 2023 (Reproduced under the terms of the CC BY 4.0 license. © 2023 Cavazzoni, Cristofolini, Dall'Ara and Palanca).

1.2.2. Limitations in the current fracture risk predictors

Nowadays, different indexes are clinically used to assess bone fracture risk in subjects potentially at risk because of their clinical conditions. Still, their ability to discriminate between subjects at risk of fracture and those who have a deteriorated but non-critical condition is limited. T-score derived from a DXA exam is commonly used (Choplin et al., 2014). Still, its lack of specificity and sensitivity in predicting hip and vertebral fractures connected to osteoporosis has been reported (Crandall et al., 2014). T-score measures how much the BMD value of the examined subject deviates from the reference bone mineral density value, which is the healthy population of 25-30 years and the same sex. Moreover, more than 50% of the fractures do not occur in subjects classified as osteoporotic (Cranney et al., 2007; Pasco et al., 2006), pointing out that T-score alone is not sufficient in providing a complete fracture risk assessment (Fonseca et al., 2014).

In addition to this, the Fracture Risk Assessment Tool (FRAX) has been developed by the University of Sheffield to assess the 10-year probability of a major osteoporotic fracture (hip, clinical spine,

humerus, or wrist fracture) and the 10-year probability of a hip fracture specifically in individuals (McCloskey et al., 2012). The FRAX index takes into account various clinical risk factors, including age, sex, body mass index, history of previous fractures, parental history of hip fractures, smoking status, glucocorticoid use, alcohol consumption, and the presence of certain medical conditions such as rheumatoid arthritis. FRAX may only be used in untreated patients (FRAX Implementation Guide, NOF, 2009); in fact, tested on different cohorts of cancer patients treated with androgen deprivation therapy has shown a limited fracture prediction ability. Moreover, the BMD input is limited to the femoral neck based on available population data (LeBoff et al., 2022).

The Vertebral Fracture Assessment (VFA) is also used (McCloskey et al., 2008). It considers a vertebra fractured if its original height is reduced for more than the 20%. Still, its focus is more on detecting an occurred fracture or at least estimating the risk of a secondary fracture after the occurrence of the first one.

Lastly, the clinical index specifically developed for patients presenting metastatic disease is the Spinal Instability in Neoplastic Disease (SINS), which is widely used to predict the degree of spinal instability. It aims at predicting the possible occurrence of a vertebral fracture based on pathological vertebra level, extension of the lesion, pain perceived by the patient, the quality of the bone, the radiographic alignment, the vertebral body collapse, and the involvement of posterior process (Fourney et al., 2011). However, it fails in discriminating between levels 7 to 12 for whom it would be more interesting to have quantitative support in the clinical decision, leaving the decision very dependent on the doctor's experience. Furthermore, it has some difficulties identifying false negatives (specificity equal to 79.5%) (Fisher et al., 2014), leading to the overtreatment of patients already weakened due to chemotherapies they must face because of the primary cancer.

Considering the limitation of the aforementioned indexes, an accurate prediction of the risk of vertebral fracture would be crucial, especially for pathological subjects. Patient-specific models developed from clinical images could might improve the current vertebral fracture risk assessment, as they already demonstrated to be successful in providing accurate estimates of bone strength at the hip (Aldieri, Bhattacharya, et al., 2022; Johannesdottir et al., 2018).

1.3. Homogenized finite element modelling of the spine

During the last years, interest in in-silico strategies applied to medial field increased exponentially (Combes & Shah, 2016; Gaweda et al., 2022; Qasim et al., 2016; Viceconti et al., 2018). Focusing on the bone fracture risk assessment, the most used computational strategy is the finite element (FE) method, which can be applied to subject-specific virtual reconstructions of the patient's bone generated from clinical CT data (Basu et al., 1985). Since its first appearance in the literature, several studies have integrated and improved CT-to-FE methodology (Fleps & Morgan, 2022; Molinari & Falcinelli, 2022; Schileo & Taddei, 2021).

FE analysis technique involves subdividing an object into subdomains, each of which can be represented through a finite number of interconnected elements through a grid of shared nodes (this structure is called mesh) (Zienkiewicz, 1971). The innovation of this method is the possibility of managing complex structures through the discretization of their domains. It is therefore ideal for the biomechanical field, where each structure has very specific geometry, at the same time different from one individual to another.

The procedure for the generation of subject-specific model of the bone require to follow specific steps, that will be briefly reported below, with particular attention to what is required for vertebra models.

1.3.1.   Imaging

The study of bone geometry, structure, and density at different spatial resolutions has been widely done using imaging techniques. *In vivo*, techniques such as DXA and Quantitative Computed Tomography (QCT) are the primary methods used at the macroscopic level to provide apparent measurements of bone mineral density. In fact, intensity values can be converted into a hydroxyapatite-equivalent density using calibration phantoms during image acquisition (Griffith & Genant, 2008), providing volumetric measurements of BMD. Otherwise, *ex vivo*, the 3D microstructure of vertebrae can be resolved and studied using higher resolution imaging techniques like micro–CT (μCT) (Dall'Ara et al., 2012).

Consequently, aiming at generating subject-specific FE models to evaluate bone strength in a patient, the most used source is certainly the QCT. However, it is important to consider that this imaging limited resolution lacks in describing the trabecular bone microstructure and the thin cortical shell present in certain skeletal sites, such as the vertebrae. The low resolution can also lead to partial

volume effects, which may result in an underestimation of the BMD of cortical structures (Klintström, 2017). Furthermore, variations in patient size and shape can influence the accuracy of QCT's BMD measurements, as changes in X-ray attenuation levels due to body composition differences may introduce beam hardening artifacts (Goldman, 2007). These artifacts manifest as artificial lower grey level regions in deeper and thicker areas of the acquired object, affecting the overall BMD quantification. Despite these limitations, QCT remains a valuable tool for bone geometry and material properties analysis.

Conversely, when the focus does not involve the clinical practice, µCT images can be used to generate both µFE models as well as FE models at the continuum scale. µFE models allow to study the microstructural behaviour of the vertebral bone (Costa et al., 2017). For the continuum scale model instead, a calibration of the acquisition is required, as already explained for the clinical CT images, and then a coarsening strategy is typical applied (Chevalier et al., 2009; Eswaran et al., 2008).

1.3.2.   Geometry extraction and mesh generation

The extraction of the geometry of interest, the vertebral bone in this case, from the acquired medical images is called segmentation. It defines the boundaries of different anatomical components, providing subject-specific geometrical information necessary to closely replicate them *in silico*.

Segmentation techniques range from manual tracing to automated algorithms, each with its own advantages and challenges. Vertebral bone presents specific features that make it hard to be segmented in a totally automatic way. For example, at a clinical resolution the interapophyseal veneers are not clearly visible and the processes of two subsequent vertebrae seems attached do not allowing the separation of the two bodies.

Mesh generation consists in the spatial discretization of the computational domain. It can be achieved in different ways (Fig. 1.4), the simplest is to directly convert every voxel from the scan to an element. This is the strategy used for the generation of the µFE models (Chen et al., 2017). Anyway, at a continuum level this can lead to an amplification of the partial volume effect and to a decrease in the accuracy of the external surface representation, relatively complex in the case of the vertebral bone (Engelke et al., 2016). Tetrahedral elements mesh instead are smother and can fit well the curvature of the bone (Gustafson et al., 2017). There are different methods to execute the discretization: the most used, thanks to its robustness, is the octree method. It generates an unstructured mesh by recursively subdividing the physical space down to a prescribed resolution, that is spatially varying.
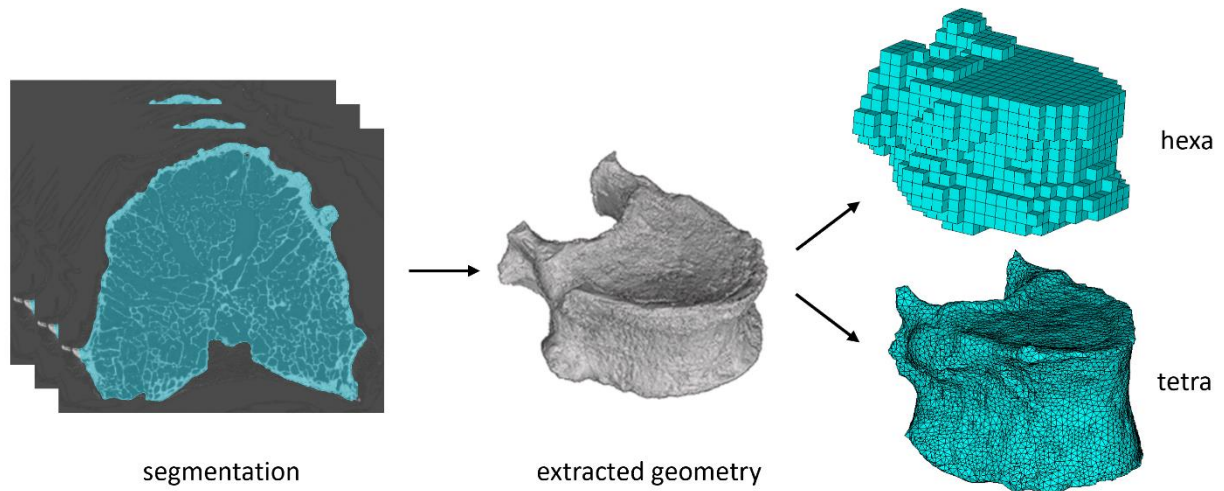
Fig. 1.4: To extract the bone geometry a semiautomatic segmentation is performed on the CT images based on the grey levels. Then, the mesh is generated using a hexaedrical or a tetraedrical elements.

1.3.3.   Material properties assignments

Various relationships between Young's modulus (E) and density (ρ) have been empirically proposed for human bones, following several mechanical tests under different load configurations, using different bone types (cortical or trabecular), and testing different anatomical compartments (Helgason et al., 2008). In subject-specific FE models, the choice of ρ-E relationships is pivotal and should account for the anatomical site (Schileo et al., 2008). ρ-E relationships are reported using both apparent and ash densities. The apparent density pertains to bone sample density under wet conditions, calculated by the ratio of wet weight to bulk volume. Ash density is determined by dividing ash weight by bulk volume, obtained by burning the sample and then measuring the weight after 24 hours. ρ-E relationships have been presented using both linear regression (Keaveny et al., 1997) and power law models (Kopperdahl et al., 2002; Morgan et al., 2003), even if the second ones seem to better fit the data. Moreover, for the vertebra, differently from what happens for other anatomical site, the same equation is used for both cortical and trabecular compartments, because cortical shell can be considered as condensed trabecular bone for this bone type (Jones & Wilcox, 2008). Furthermore, clinical CT images have typically low resolution in order to avoid excessive irradiation on the patient. For this reason, it is not possible to extract information about trabecular orientation, consequently many hFE models of the vertebra apply isotropic material to the bone (Gustafson et al., 2017), or orthotropic (Crawford et al., 2003). Additional and more complex modelling strategies could be found in literature, considering bone anisotropy, through the mean intercept length, but they require high resolution images to be implemented (Harrigan & Mann, 1984).

Moreover, vertebra does not present a fragile behaviour as far as fracture is concerned. For this reason, failure mechanisms involving plasticity and damage accrual have been presented (Dall'Ara et al., 2010, 2012; Imai et al., 2006, 2009). Imai et al., 2006 chose a bilinear elastoplastic model, assuming each element yielded when its Drucker–Prager equivalent stress reached the element yield stress. This allowed to take into account the asymmetry between tensile and compressive behaviour that characterises the bone material. Dall'Ara et al., 2010 implemented an elastic damage constitutive model considering the accumulation of the damage at each element to explain the stiffness reduction. Costa et al., 2019 adopted an isotropic plasticity model based on a Von Mises criteria dependent to the density itself.

1.3.4. Boundary Conditions

Boundary conditions applied to the vertebral models can follow two different strategies. The first, and most common, considers the vertebral bone by its own (Buckley et al., 2007; Dall'Ara et al., 2012; Imai et al., 2006), while the second strategy models all the spine, or a portion of it, as a whole, taking in account also the action of the intervertebral discs (Groenen et al., 2018). They both have some pros and cons that must be taken into account.

Studying the single vertebra by its own allow to have a higher control and the loading pattern applied, both for what concern the experiment as well as for the simulated replication. This is the best way to have a total control on the vertebral bone behaviour, because it is the only tissue examined and simulated. Consequently, when the focus is the vertebral body strength, this is the most common kind of set up. Anyway, taking this choice reduces the ability to study the behaviour of the vertebra under realistic conditions. In most of the cases, a uniform load is applied to the upper vertebral endplates (Chevalier et al., 2009; Crawford et al., 2003). Anyway, some studies have also tried to replicate high-load task like anterior flexion (Dall'Ara et al., 2010).

On the other way, studying multi-vertebrae segments allows to apply more realistic boundary conditions to the specimen (Groenen et al., 2018). Conversely, these long segments force the necessity to model also the intervertebral disc, even if the focus of the study is on the vertebral bone, strongly increasing the complexity of the modelling. Connected to these points, Clouthier et al., 2015, compared experimental measurements with two different models, one in which the vertebra was loaded through the intervertebral discs and the other through a layer of polymethyl methacrylate. The latter kind of boundary conditions resulted unable to reproduce the endplates fracture.

1.3.5.   Validation

Validation allows to assess whether the model can predict accurately the physical phenomena that intend to replicate (Anderson et al., 2007; Viceconti et al., 2005). In the biomechanical field, the phenomena are complex and have a strong subject dependence. For this reason, in many cases at first controlled *in vitro* experiments are performed aiming to replicate what happen *in vivo* and then models predictions under the same experimental boundary conditions are compared to the experimental measurements. This allows to increase step by step the complexity of the modelling, separating the different causes of error. Historically, many different outcomes have been analysed during the validation processes of bone models, but it is possible to group them the following categories:

- Global mechanical properties (e.g., apparent (Buckley et al., 2007; Dall'Ara et al., 2012), yield load (Imai et al., 2006), fracture load (Buckley et al., 2007; Dall'Ara et al., 2012; Imai et al., 2006)).

- Local behaviour of the bone in term of displacements (Gustafson et al., 2017) and strains (Baleani et al., 2023; Schileo et al., 2007), on the bone surface (Grassi et al., 2016) or inside its volume (Palanca et al., 2022). It requires, in addition to the mechanical testing set up, further experimental techniques. Historically, strain gauges attached to the vertebral cortex were the most used tool to assess superficial deformations in the vertebrae (Cristofolini et al., 2013). However, they have two main limits. The first one is that they provide information only at the exact location on which they are attached, and it is impossible to cover all the vertebral surface considering all the instrumentation required. The second one is that they reinforce the cortex, generating a strain underestimation in the range 3÷9% (Cristofolini et al., 2013). An emerging alternative is represented by the optical full-field techniques discussed at paragraph 1.4.

- Damage localization (Imai et al., 2006; Keyak et al., 2001). It requires imaging acquisition both before the test (as the input to generate the model) and after it (to localize the location of the damage).

1.3.6.   Pathological vertebra finite element models

The FE methodologies has already shown several benefits in the study of pathological vertebrae (Naoum et al., 2021). In the following paragraphs the potentiality of the application of FE method to osteoporotic or metastatic spine are highlighted.

1.3.6.1.   Osteoporotic vertebra models

Focusing on osteoporosis, numerous studies have used FE models to assess fracture risk (Rayudu et al., 2022; Zysset et al., 2015) and/or to compare treatments (Viceconti et al., 2016). CT-based FE

models indeed have demonstrated superior discriminative capabilities for vertebral fractures compared to lumbar spine BMD measurements obtained by DXA and quantitative CT (Imai, 2015), suggesting being a viable alternative to the current standards for detecting fractures related to osteoporosis. Some studies proposed to use FE analysis to perform opportunistic examinations on osteoporotic patients whenever a new routinely acquired scan of the subject is available (Rayudu et al., 2022). Response to osteoporotic treatments with teriparatide and alendronate have been analysed with FE models of the lumbar spine (Chevalier et al., 2010; Graeff et al., 2009; Keaveny et al., 2007). Another important application of the FE methodology is the analysis of the stabilization surgeries and their effects both on the instrumented or augmented vertebrae, as well as on the adjacent ones (Wang et al., 2020).

1.3.6.2. Metastatic vertebra models

FE models have shown interesting results also studying of the impact of metastatic lesions on the vertebral bone competence. Subject-specific vertebral models, incorporating either simulated (Galbusera et al., 2018) or actual lytic lesions (Campbell et al., 2017) have been proposed. The effect of parameters such as lesion size and location, vertebral bone quality, and loading rate on the risk of burst fracture (Galbusera et al., 2018). Galbusera et al., 2018 idealized the metastatic lesion as a pseudo-spherical shape randomly centred within the vertebral body and with a random radius in the range 2÷20 mm. The corresponding elements were assigned with an elastic modulus of 1 MPa and a Poisson's ratio of 0.45, representing a highly hydrated material with low compressibility and stiffness. They applied this model to the study of the effect of parameters such as lesion size and location, vertebral bone quality, and loading rate on the risk of burst fracture. Groenen et al., 2018 instead segmented the metastatic lesions form the CT scans and then deactivate the corresponding elements during the simulation. Furthermore, Stadelmann et al., 2018 demonstrated that subject-specific FE models of vertebral bodies predicted ultimate compression force in human vertebral bodies with actual lytic lesions with comparable accuracy to predictions of strength in vertebrae without lesions (R^2=0.73 and R^2=0.77, respectively). These models, generated from resampled μCT images, exhibited similar predictive capability for vertebral mechanical properties compared to μCT-based μFE models generated on the same vertebra. Costa et al., 2019 showed CT-based FE models can improve fracture risk assessment in subjects presenting lytic metastasis, performing better than SINS score. Among the analysed vertebrae, 30% of those classified as prone to fracture were considered mechanically stable by the FE analysis. Recently, the operation of screw fixation in the presence of simulated metastasis has been studied (Bianchi et al., 2022).

Focusing on the material properties assignment, it has been observed that the ρ-E relationship of trabecular bone with metastatic lesions is similar to the one observed for healthy tissues, despite the clear local microstructural changes induced by metastases (Nazarian et al., 2008). Therefore, these

studies suggest that lesioned tissue can be modelled as low-BMD or high-BDM bone with similar constitutive behaviour (Stadelmann et al., 2020) (Fig. 1.5). While the assumption seems reasonable for the osteolytic tissue, for the osteoblastic one instead further experimental studies would be necessary to better inform a subject-specific model.
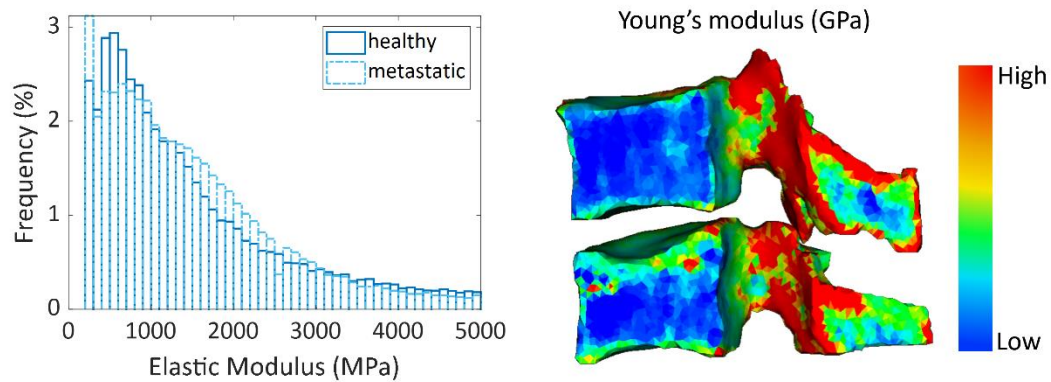

Fig. 1.5: Patient-specific properties are assigned to each element of the vertebral model. In reported example the specimen was composed by a healthy vertebra, the upper one, and a mixed metastatic vertebra, the lower one.

1.4. *In vitro* full-field techniques

The methodologies used to obtain the experimental data for the validation analyses described in this thesis consist in full-field techniques. They are both based on an analogous principle: two images of the same bone in undeformed and deformed configurations are imported and the algorithms compute a field of displacements which minimizes the differences between the deformed images and the registered images (undeformed images after the application of the field of displacement) (Dall'Ara et al., 2017). The field of displacement is then differentiated into a field of strain. The main particularities of each technique are briefly reported hereafter.

1.4.1. Digital Image Correlation

Digital Image Correlation (DIC) is a non-invasive optical technique that involves the acquisition of images of the loaded specimen through a certain number of high-speed cameras (Peters & Ranson, 1982). It can be implemented both in a bidimensional and in a tri-dimensional way, using respectively one single camera or more cameras. The algorithm recognizes and identifies each single point on the surface of the sample, then follows it in the consecutive load steps and, at the end of the experimental test, quantifies the value of the displacement of the individual points for all the duration of the test. To do this, it is necessary that the points in the reference (unloaded) image present a strong correspondence with the points in those acquired in the loaded state. Consequently, the reference image is virtually divided into small rectangular areas (facets), which contain a certain number of pixels and therefore are characterized by a greater amount of information. For each facet, the displacement related to its centroid is calculated once the area matches in the different images (Fig. 1.6).
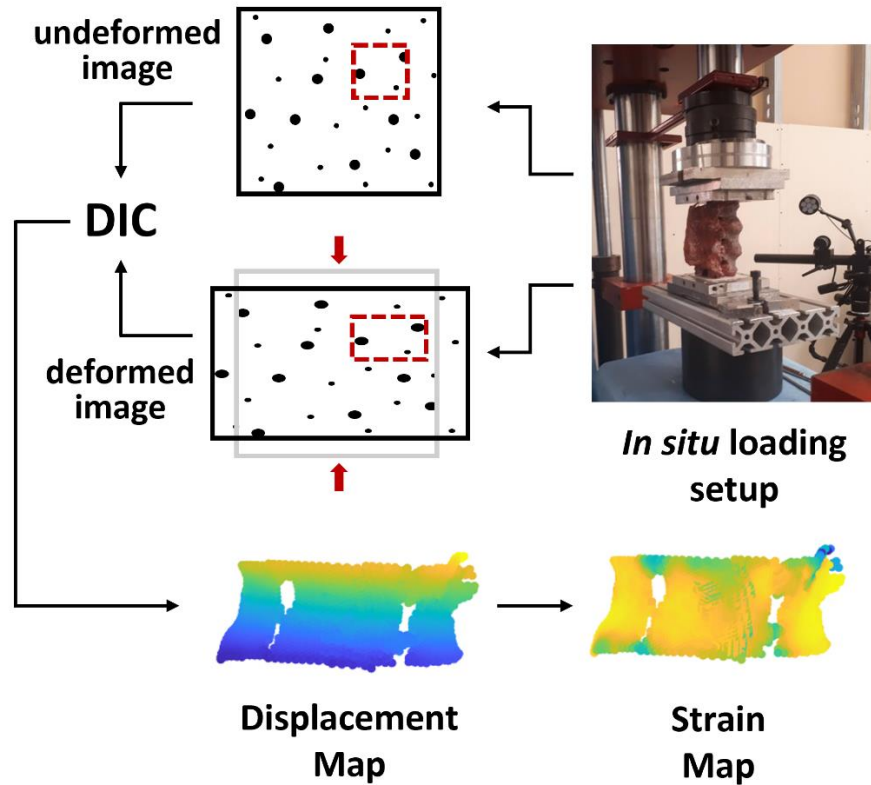
Fig.1.6: Workflow to obtain experimental displacement and strain on the vertebral surface using DIC technique. Images of the specimen in loaded and unloaded conditions are acquired, then a feature recognition algorithm is used to perform the correlation obtaining a displacement field, which is eventually differentiated to obtain the strain field.

1.4.1.1.   Application in experimental biomechanics

DIC showed its benefits in measuring hard tissue deformations compared to previously commonly used strain gauges (Cristofolini & Viceconti, 1997; Yang et al., 2011), since it does not induce any reinforcement on the underlying tissue and does not limit itself to providing a localized measure in a single point but provides data on the entire surface portion of the sample taken by the camera (Schmidt et al., 2003). This is crucial for studying localized peak strains (Sztefek et al., 2010) and for identifying location and modality of fracture in bones (Väänänen et al., 2012, Fig. 1.7B). The technique has been successfully applied to analyse bone tissue at different scales, from tissue level (cortical bone (Hoc et al., 2006); trabecular bone (Acciaioli et al., 2020) and single trabecula (Jungmann et al., 2011)) to organ level (whole bones: Palanca et al., 2018a). Micro-damage and bone remodelling occurrences have been also studied (Hoc et al., 2006; Nicolella et al., 2001). Furthermore, DIC allowed to study the behaviours of vertebrae showing signs of metastatic occurrences, analysing deformations dependence to size, location and type of the lesions (Palanca et al., 2021, Fig. 1.7A).

1.4.1.2.   Application to in-silico models validation

As already mentioned, DIC technique is a powerful tool to validate in-silico models against experimental tests, thanks to its ability to provide full-field data without affect the real conditions of the specimen (Cristofolini et al., 2010). At first, the process has been applied on composite femurs (Dickinson et al., 2011; Grassi et al., 2013, Fig. 1.7C) and then extended to cadaver ones (Op Den Buijs & Dragomir-Daescu, 2011 with 2D-DIC and Helgason et al., 2014; Katz & Yosibash, 2020 with 3D-DIC). First attempts of applying this validation process also on cadaveric vertebral bone have been presented in the literature, both in term of displacements (Gustafson et al., 2017) and strains (Baleani et al., 2023), although these studies performed axial compression on a single vertebra. Moreover, impact loading scenarios have been acquired through DIC and simulated using FE models to investigate cervical spine injuries (Hernandez et al., 2020).
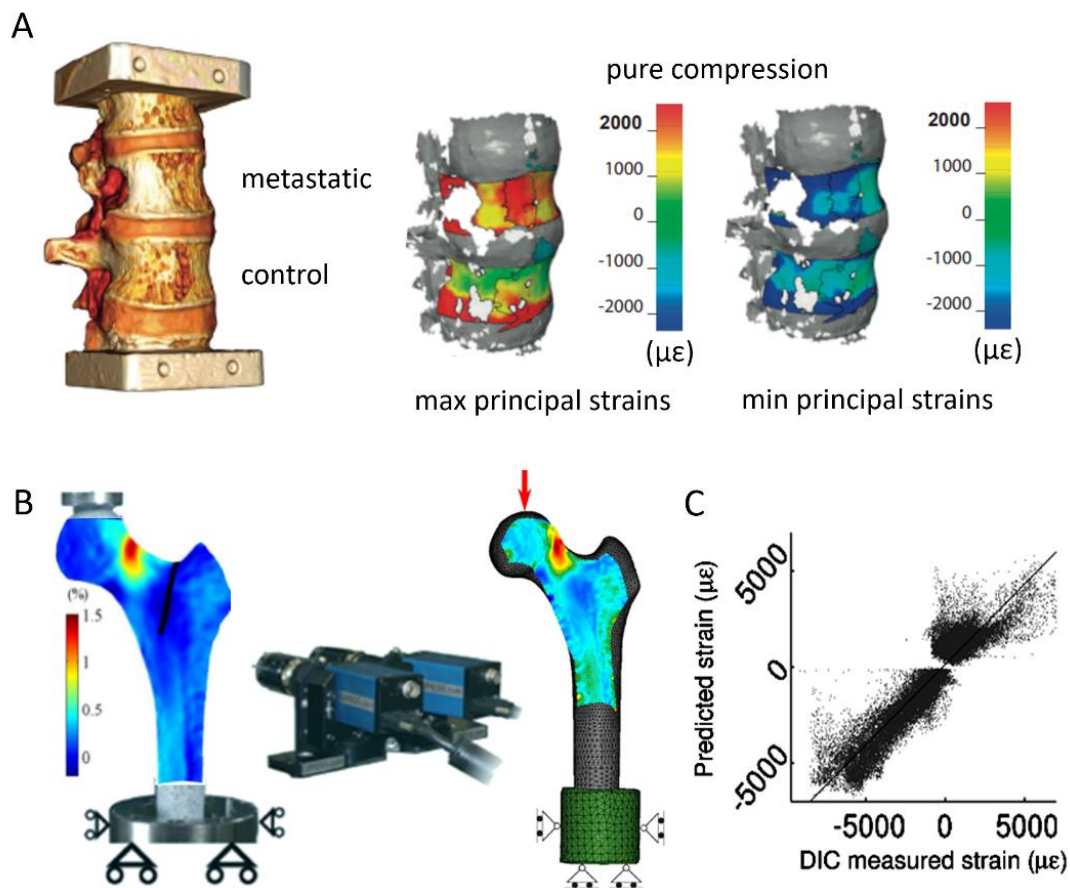
Fig.1.7: Examples of application of DIC technique to study the mechanical behaviour of the vertebral (A. Palanca, 2021, reproduced under the terms of the CC BY 4.0 license. © 2021 The Authors. Published by Elsevier Inc.) and the femoral bone (B. adapted from Väänänen, 2012, reproduced with permission. © 2012 Elsevier Ltd. All rights reserved), and for the validation of FE models (C. adapted from Grassi, 2013, reproduced with permission. © 2013 Elsevier Ltd. All rights reserved).

1.4.2.   Digital Volume Correlation

Digital Volume Correlation (DVC) represents the first experimental technique allowing the analysis of deformation inside the bone (Grassi & Isaksson, 2015) (Fig. 1.8). It requires as input two stacks of computed tomography images, to whom an elastic registration is applied.

There are two main methods for implementing the DVC technique, namely the local and global approaches. The success of both methods depends on the quality of the images used as input and the heterogeneity of the material being studied. Both local and global approaches rely on pattern recognition, hence the more unique and recognizable the tissue is, the more accurate the registration will be.

Local strategies involve dividing the image into sub-regions of interest, and then computing correlation metrics in each sub-region independently. The most widely used correlation metrics are direct correlation (more accurate, Palanca et al., 2016) and fast-Fourier-transform (faster, Palanca et al., 2016). Local methods are generally accurate in predicting local deformations, but if a sub-region lacks well-defined features, it will produce unreliable results because it does not receive information from adjacent sub-regions to correct the computation. For instance, the local approach has been successfully applied to study the propagation of fractures inside a vertebra (Tozzi et al., 2016), using commercial software that implements the direct correlation method.

On the other hand, global approaches minimize the differences between two images by applying a continuous displacement field. To achieve this, the kinematic degrees of freedom are spatially coupled. In the measure of bone strains, global approaches produce lower errors compared to local ones, given a specific spatial resolution (Dall'Ara et al., 2017).

The specific algorithm used to implement this technique on the experiments mentioned in Chapter 4 is called BoneDVC. It has been developed at the University of Sheffield (Dall'Ara et al., 2014) and it is based on a global approach. The procedure computes the displacement map by using the Sheffield Image Registration Toolkit (ShIRT) (Barber & Hose, 2005). A grid with selectable nodal spacing is superimposed to the images to be registered. The deformable registration equations are solved at the nodes of the grid to evaluate the displacement field. The displacement function that transforms the undeformed image into the deformed one are then found. Moreover, using an intensity displacement function, potential changes in the grey levels can be considered. Displacements are interpolated with a tri-linear function between the nodes.
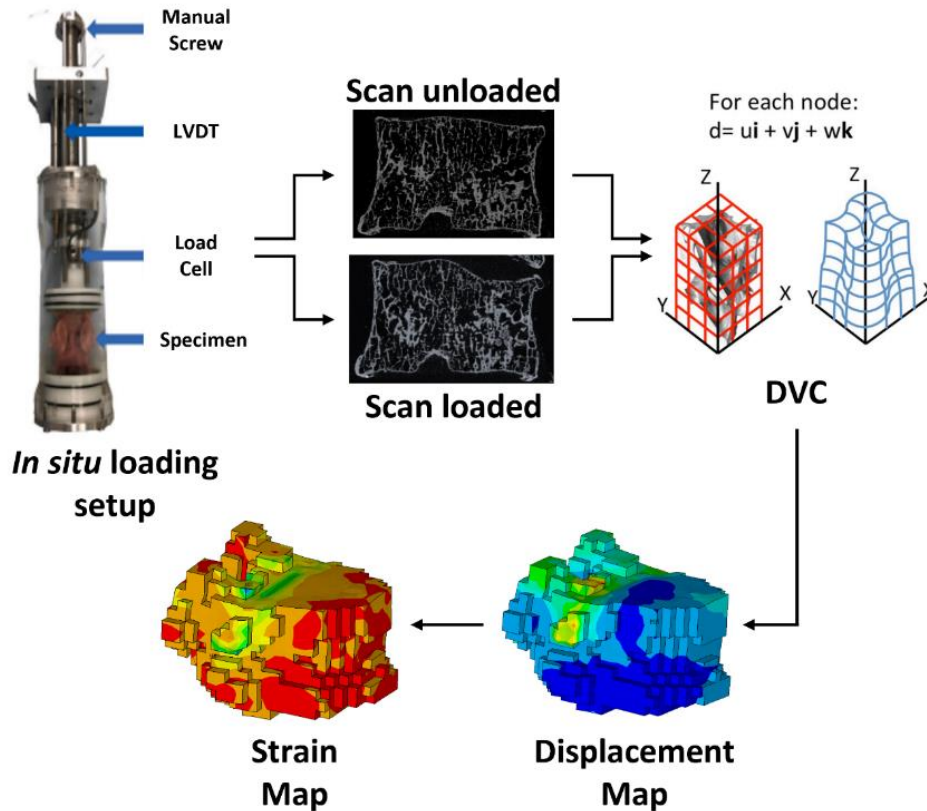
Fig.1.8: Workflow to obtain experimental displacement and strain inside the vertebra using DVC technique. μCT images of the specimen in loaded and unloaded conditions are acquired, then a feature recognition algorithm is used to perform the correlation obtaining a displacement field, which is eventually differentiated to obtain the strain field. Adapted from Palanca et al., 2022 (reproduced under the terms of the CC BY 4.0 license. © 2021 The Authors. Published by Elsevier Ltd) and from Palanca et al., 2017 (reproduced under the terms of the CC BY 4.0 license. © 2017 The Author(s). Published by Elsevier Ltd).

1.4.2.1. Application in experimental biomechanics

DVC technique has been extensively used in the last decade to analyse bone structure and behaviour at different levels (Dall'Ara & Tozzi, 2022), from tissue level using μCT scans (Tozzi et al., 2016, Fig. 1.9A), in order to measure the internal strain from the elastic regime up to failure, to organ level using clinical CT (human subtalar joint, Peña Fernández et al., 2020). First attempts to apply DVC technique on clinical MRI acquisitions to assess internal mechanical behaviour of human bone in vivo have been presented too (Tavana et al., 2020). Different organs and tissues have been studied, including vertebral bodies (Hosseini et al., 2014; Hussein et al., 2018; Palanca et al., 2021), proximal femur (Martelli et al., 2021; Ryan et al., 2020), trabecular bone (Peña Fernández et al., 2021 Fig. 1.9B) and cortical bone (Christen et al., 2012).

1.4.2.2.   Application to in-silico models validation

DVC measurements necessitate complex in situ mechanical testing and often require high-resolution imaging, which may not always be feasible in typical *in vivo* scenarios, on the other hand the experimental evaluation of local displacement and strain patterns can serve as a means to validate computational models constructed from laboratory or clinical images. Indeed, DVC has previously been employed to validate the displacement and strain results of bone FE models created from the images acquired at the undeformed status. This validation was conducted at the microstructural level, encompassing both healthy (Palanca et al., 2022) and metastatic (Costa et al., 2017, as shown in Fig. 1.9C) vertebrae, and also at the continuum level for structures such as osteoarthritic humeral heads (Kusins et al., 2020) and vertebral bodies (Jackman et al., 2016).
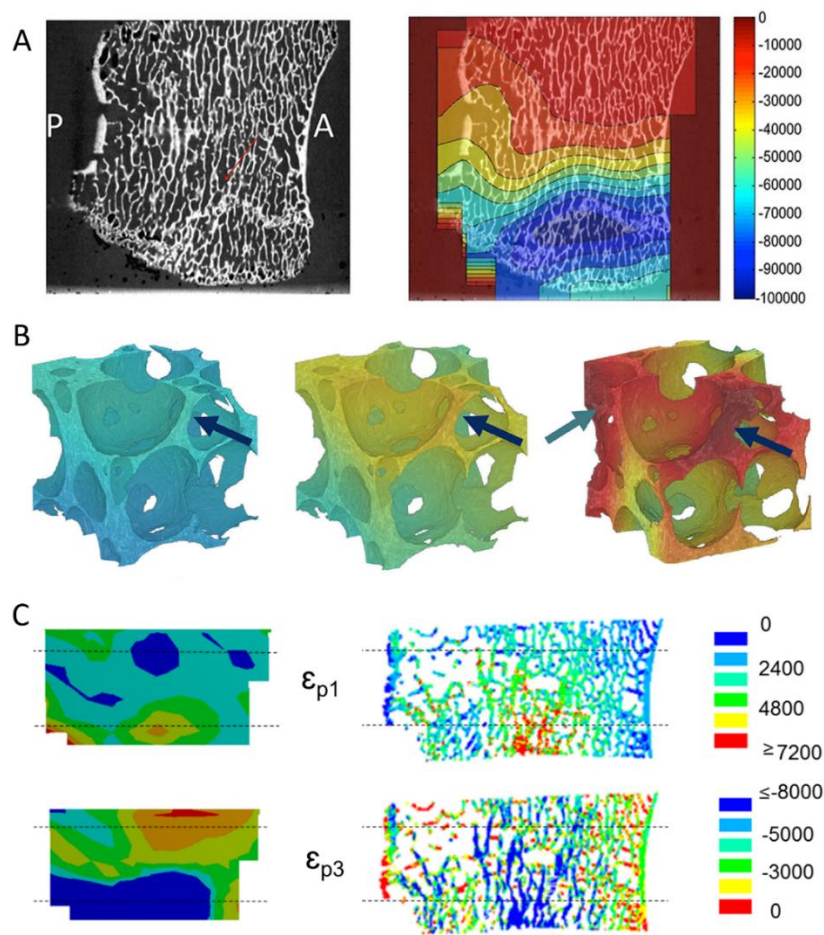
Fig.1.9: Examples of application of DVC technique to study failure in experimental tests on the vertebra (A. Tozzi, 2016, reproduced with permission. © 2016 Wiley Publishing Ltd) and on the trabecular tissue (B. Pena Fernandez, 2021, reproduced with permission. © 2021 Acta Materialia Inc. Published by Elsevier Ltd. All rights reserved.), and for the validation of FE model (C. Costa, 2017, reproduced under the terms of the CC BY 4.0 license. © 2017 Costa et al.).

1.5. Aim and outline of the thesis

The aim of this thesis was the definition of the accuracy of subject-specific continuum finite element models of multi-vertebrae segments. hFE models of the spine were developed from clinical CT and µCT data; in vitro full-field measurements were used to validate the prediction of such models.

The work was divided into two main parts.

In the first one the validation of multi-vertebral model is performed on the surface of the vertebra on displacements and strains using DIC data. The main objectives of that section were:

- To develop a first model validation framework based on the comparison between the vertebral surface displacements predicted by the FE model and the experimentally measured ones using DIC for the same spine segment which included an osteoporotic vertebra and a vertebra with lytic metastatic lesions (Chapter 2).
- To assess the possibility to build a fracture risk predictor of the spine by modelling the intervertebral disc as a linear elastic isotropic material. FE model predictivity accuracy on the strain field was assessed by comparison with experimental DIC data (Chapter 3).

The second part is focused on a single vertebra model validated using DVC data (Chapter 4). The main goals for this part are listed below:

- To validate single vertebra FE models against DVC measurements, in order to assess their ability to predict the local displacements within the bone structure under loading. Using the same µCT scans as input for both *in silico* model and *in vitro* measurement allow to ignore potentially registration errors.
- To compare the predictions of two models (one µCT based hFE and one µFE model) at different scales, generated from the same images and undergone the same loading conditions. This work aimed at understanding deeply whether the mechanical behaviour of the vertebral bone microstructure noticeable at the microscopic level can be reproduced well also at the organ level.
- To locally compare the predictions of two hFE models generated from clinical and µCT, considering that µCT scans cannot be acquired *in vivo*.
- To qualitatively assess the hFE models ability to predict the regions of the vertebral body presenting higher strains concentration in the experiment.

Chapter 2

Experimental validation of a subject-specific finite element model of lumbar spine segment using digital image correlation

Contribution Disclosure

Abstract

Pathologies such as cancer metastasis and osteoporosis strongly affect the mechanical properties of the vertebral bone and increase the risk of fragility fractures. The prediction of the fracture risk with a patient-specific model, directly generated from the diagnostic images of the patient, could help the clinician in the choice of the correct therapy to follow. But before such models can be used to support any clinical decision, their credibility must be demonstrated through verification, validation, and uncertainty quantification. In this study we describe a procedure for the generation of such patient-specific finite element models and present a first validation of the kinematics of the spine segment. Quantitative computed tomography images of a cadaveric lumbar spine segment presenting vertebral metastatic lesions were used to generate the model. The applied boundary conditions replicated a specific experimental test where the spine segment was loaded in compression-flexion. Model predictions in terms of vertebral surface displacements were compared against the full-field experimental displacements measured with Digital Image Correlation. A good agreement was obtained from the local comparison between experimental data and simulation results ($R^2 > 0.9$ and RMSE% $<8\%$). In conclusion, this work demonstrates the possibility to apply the developed modelling pipeline to predict the displacement field of human spine segment under physiological loading conditions, which is a first fundamental step in the credibility assessment of these clinical decision-support technology.

2.1. Introduction

Vertebral fracture is one of the most serious orthopaedic injuries, associated with several adverse consequences including back pain, disability, risk of neurological complications, increased risk of death and a decreased quality of life (Alexandru, 2012; Ensrud & Schousboe, 2011). These fractures are typically traumatic or pathological (the latter being sometime referred in the medical literature with fragility fractures), or more often a combination of both factors. Conditions like osteoporosis, or the presence of metastatic lesions weaken the vertebral body and increase the risk of fragility fractures (Ensrud & Schousboe, 2011; Palanca et al., 2021; Yeung et al., 2021). The incidence of vertebral fragility fractures in women over 50 is around 1%, («Incidence of Vertebral Fracture in Europe», 2002) and it is expected to increase in the next years because of the aging population. Moreover, epidemiology studies show that only about one-third are clinically diagnosed (Schousboe, 2016), (Kim et al., 2018). Physical therapies, pharmacological treatments, and minimally invasive vertebral augmentation techniques such as kyphoplasty and vertebroplasty are usually used to improve the biomechanical strength of the pathological vertebral body. However, because of several possible clinical complications, the choice of treatment is complex and providing a reliable estimate of the risk of fracture is fundamental to support the clinical decision.

Several tools and indexes were proposed in the last decades to predict the risk of vertebral fracture (Ensrud & Schousboe, 2011). The gold standard in the clinical practice, the Vertebral Fracture Assessment (VFA), is a diagnostic method to detect fractures that already occurred and can be used as an indicator for subsequent fractures only. Dual-energy X-ray absorptiometry (DXA) can measure bone mineral density (BMD) that indeed correlates with bone strength (Johannesdottir et al., 2018), even if it does not directly measure it. However, DXA-derived BMD measurement can explain only around the 60% of the variation in vertebral strength (Cheng et al., 1997), because it does not take into account other elements that concur in bone strength assessment, such as inhomogeneity of density distribution and complexity of bone geometry. A promising tool to evaluate vertebral fracture risk is Biomechanical Computed Tomography (BCT) (Keaveny et al., 2020), widely and successfully used to provide a measurement of bone strength at the hip. *Subject-specific* finite element (FE) models are created based on quantitative computed tomography (QCT) images and used to compute the force required to virtually fracture the vertebral body (Buckley et al., 2007; Dall'Ara et al., 2010; Groenen et al., 2018; Gustafson et al., 2017; Imai et al., 2006; Silva et al., 1998). The models demonstrated to be more accurate in predicting vertebral strength and stiffness compared with dual-energy x-ray absorptiometry (Dall'Ara et al., 2012). The BCT works under the assumption that the disease affecting the skeleton modified the quantity of bone tissue, but not its quality. This can be a good enough approximation for diseases like osteoporosis or metastatic disease of lytic type, but could show limitations for other diseases such as osteogenesis imperfecta or blastic metastases. Therefore,

the BCT workflow can also be applied to metastatic bone where the lytic nature of the disease is prevalent.

One of the most crucial aspects that must be properly addressed before applying the BCT technology in the clinical practice is the model validation (Babuska & Oden, 2004). Validation aims at determining the predictive capability of a computational model for its intended use and is usually done by comparing the predicted results against experimental data (ASME, 2018). Several studies focused on this specific problem and different validation metrics were used. Comparisons between computational results and experimental measurements have been performed comparing global mechanical properties (Buckley et al., 2007; Dall'Ara et al., 2010, 2012; Imai et al., 2006). Imai et al., for example, considered four mechanical properties to evaluate the accuracy of the developed FE model: yield load ($r = 0.949$), fracture strength ($r = 0.978$), fracture site and minimum principal strain on the surface of the vertebra ($r = 0.838$) (Imai et al., 2006). In the comparative study presented by Buckley at al. (Buckley et al., 2007), good agreement was found for vertebral strength ($R^2 = 0.80$) while axial stiffness was predicted less well ($R^2 = 0.27$). Also Dall'Ara et al. in their validation study (Dall'Ara et al., 2010), reported stronger correlation for strength ($R^2 = 0.79$) compared to stiffness ($R^2 = 0.49$). Only recently, more detailed and specimen specific validation metrics based on the comparison between predicted and measured displacements extracted on the vertebral bodies with Digital Volume Correlation (DVC) and Digital Image Correlation (DIC) were presented (Gustafson et al., 2017; Jackman et al., 2016). In the study published by Jackman et al., the accuracy of QCT-based FE analyses in predicting vertebral failure patterns was evaluated on three-vertebrae thoracic spine segments comparing the predicted displacements with those measured by DVC. They studied different boundary conditions, loading modes and yield criteria capturing some of the qualitative features of the failure patterns (e.g., vertebral deformation during flexion loading). Gustafson et al. used DIC technique for measuring the displacement fields, and found good FE-experimental agreement ($R^2 = 0.75 - 0.93$ for the surface displacements field and $R^2 = 0.90$ for the specimen stiffness), demonstrating the possibility to use a non-contact optical full-field measurement technique for the validation of vertebral FE models, as also already confirmed for human femur applications (Grassi et al., 2016; Katz & Yosibash, 2020; Palanca, Tozzi, et al., 2016). However, a critically important aspect must be considered: in (Gustafson et al., 2017), compression tests were performed on a single vertebra without intervertebral discs; this choice altered the loading and boundary conditions that may create artifacts (e.g., non-physiological failure mechanics) and neglects what happen *in vivo*. A more clinically relevant validation can be obtained considering at least two spinal units segment so that the load is more physiologically transferred to the vertebral body through the intervertebral discs, as also reported in a recent work (Groenen et al., 2018).

In authors' knowledge, there are no studies in the literature that describe in detail a reliable procedure to validate *subject-specific* FE models of the spine segment using experimental measurements obtained with DIC. Among the possible reasons there is the difficulty in developing complex three-

dimensional FE models of the spine and in accurately reproducing physiological loading conditions defined in the experimental tests. Also, while there is extensive evidence that the attenuation coefficients that a CT provides are correlated to the elastic modulus of the mineralised tissue, there are currently no ways to estimate the biomechanical properties of intervertebral disc from CT images. Thus, an idealised constitutive equation to model the disc should be considered.

The aim of this paper is to present the validation of a multi-vertebrae spine model based on the comparison between the vertebral full-field surface displacements predicted by the FE model against the experimentally measured ones using DIC. In case of multi-vertebrae specimen, it is important to verify that the model reproduces the correct spine kinematics. Considering that the prediction of bone deformation is influenced by the relative movement between two adjacent vertebrae and the overall spine motion, this work is a fundamental preliminary step towards the full validation of spine models.

A cadaveric lumbar spine segment presenting osteoporosis in one vertebral segment, and a metastatic lesion in another was used as case study to demonstrate the possibility to apply the procedure to clinically relevant scenarios.

2.2. Materials and Methods
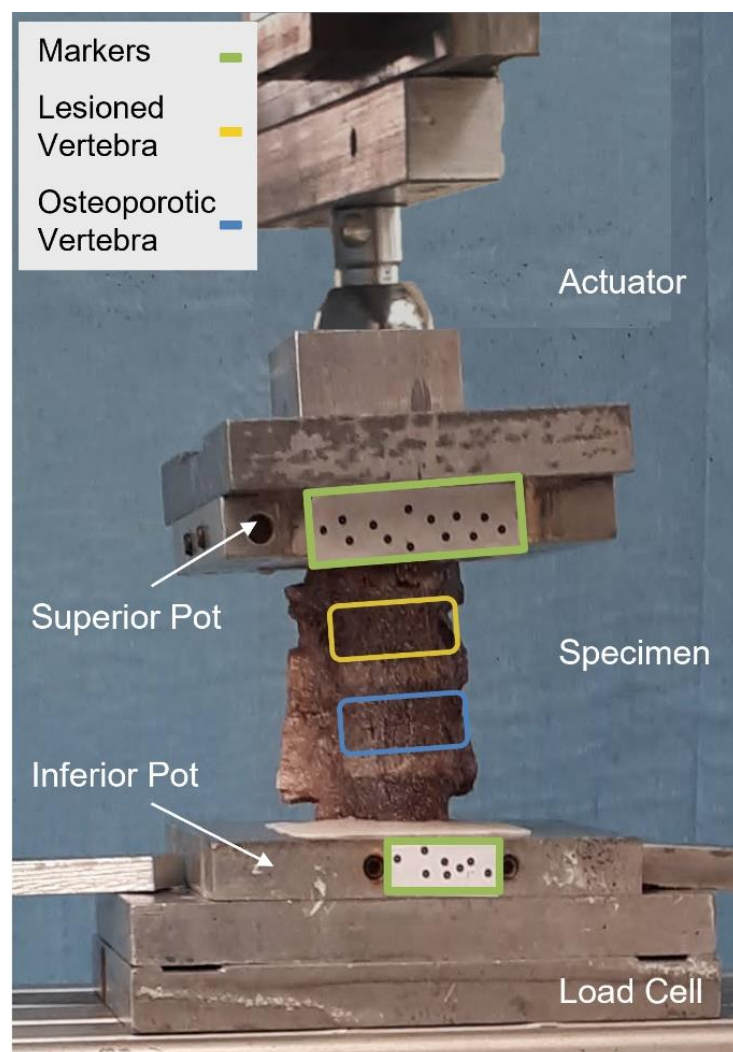
2.2.1. Experimental procedure

The study was conducted on a cadaveric spine obtained from an ethically approved donation program (Anatomic Gift Foundation, Inc.). The subject was a 73-year-old female with a body weight of 72.6 kg, affected by lung cancer with spine metastasis. Lumbar segment from L1 to L4 was extracted from the spine: L2 was evaluated by two expert clinicians as metastatic (Fisher et al., 2010) while L3 did not show any radiographical signs of metastasis. The top half of the most cranial vertebra (L1) and the bottom half of the most caudal vertebra (L4) were embedded in polymethyl-methacrylate (PMMA) (Fig 1) to be mounted on a uniaxial testing machine. The entire segment was aligned following the procedure described by Danesi et al. (Danesi et al., 2014).

Tomograms of a European Spine Phantom (ESP) and of the specimen were acquired with a CT (AquilionOne, Toshiba, Japan) with the following parameters: tube current 200 mA, voltage 120 kVp, without any current compensation. The voxel dimension was 0.24 x 0.24 x 1 mm. The densitometric analysis of the calibrated CT images showed few regions in the L2 segment with mean volumetric Bone Mineral Density (vBMD) of 105 mg/cm^3, about 5 times less than the vBMD measured in the whole vertebral body. On the other hand, the L3 vertebral segment, with its average vBMD of 76 mg/cm^3, would be classified as osteoporotic according to the ACR classification (The American College of Radiology, 2018). The two vertebrae will be referred hereinafter as lesioned (L2) and osteoporotic (L3).

The experimental protocol used to test the specimen was reported in detail by Palanca et al. (Palanca et al., 2021). Briefly, the mechanical test was performed using a uniaxial testing machine (Instron 8500 controller with Instron 25 kN load cell, Instron, UK). A random speckle pattern was prepared on the specimen and an optimized three-dimensional Digital Image Correlation 4-camera system (Aramis Adjustable 12M, GOM, Braunschweig, Germany, with 12MPixels cameras and 75 mm metrology-standard lenses), was used to measure the displacement fields.

In order to load the specimen in compression-flexion, the application point of the force (*F*) was offset toward anterior by 4 mm, i.e., 10% of the antero-posterior dimension (*d*) of the L2-L3 intervertebral disc, similar to (Palanca et al., 2018). To perform the compression-flexion, avoiding any transmission of undesired load components, the superior pot was free to rotate and translate by means of a ball-joint and two low-friction orthogonal linear bearing, while the inferior pot was fixed (Ruspi et al., 2017). The target load to be applied was tuned to reach an average compressive strain of -2500/-3500 microstrain on the anterior surface of L3 vertebral body (monitored in real-time through the DIC system). This is the strain range associated to physiological load (Lanyon, 1987). The specimen was tested applying a monotonic ramp that reached the target load (60 N) in 1.0 second. According to the testing machine report, the uncertainty on the applied load was around 4 N (0.14% at 2500N).

Moreover, the auto-range of the testing machine control allows to reduce it. During the test, images of the spine segment were recorded at 25 Hz to measure the full-field displacement and strain on the external surface of L2 and L3 vertebral bodies, following the procedure described in (Palanca et al., 2015). Processing of the images was performed using a facet size of 30 pixels, a grid spacing of 10 pixels, a median spatial filter on 5 facets, and a median temporal filter on 2 frames. These parameters allowed us to obtain a measurement spatial resolution of about 2 mm, with a strain systematic error of 30 microstrain and a strain random error of 100 microstrain. Systematic and random errors in term of displacements were found around 10 μm and 25 μm, respectively. Flat circular markers were glued on the aluminium pots of the test machine to track the displacement of the superior and inferior pots (Fig 2.1).

Fig 2.1: Experimental set up. Specimen mounted on the testing machine with the set up in the compression-flexion configuration. Reproduced under the terms of the CC BY 4.0 DEED license. © 2022 Garavelli et al.

2.2.2. Computational procedure

Finite element simulations were performed considering subject-specific models of the vertebral bodies and population-averaged models of the intervertebral discs (IVDs).

To create the geometry, all the specimen components (two entire vertebral bodies, two half vertebral bodies and three IVDs) were firstly segmented individually from the CT-images using a threshold-based algorithm with lower and upper Hounsfield Unit (HU) values set to 226 and 3071 respectively, and manual editing (Mimics, Materialise NV, Leuven, Belgium). Solid parts were reconstructed, and body attachments were created through Boolean operations (SpaceClaim V19.3, Ansys Inc., Canonsburg, PA). A mesh of 10-node iso-parametric quadratic tetrahedral elements was generated using an Octree automatic mesh generation algorithm (ICEM CFD V19.3, Ansys Inc.). Octree meshing was selected because it is more robust to topological imprecisions, and thus can be used to mesh directly the polygonal surfaces obtained from the CT-images segmentation. The mesh was generated by imposing a max element edge length equal to 2 mm. The mesh size was selected based on a preliminary convergence test, where the maximum displacement in the two regions of interest change of only 0.01% with a further refinement of the mesh.

Bone tissue was modelled as an heterogenous, locally isotropic, linear elastic brittle material. While more complex formulations have been proposed, this constitutive equation allowed the prediction of bone strains with an accuracy of 93% (Schileo et al., 2008). The heterogenous elastic properties were derived from the CT data, assuming them related to the density of the mineral phase in each point of the bone. The elastic properties of the bone were subsequently mapped on each element (Bonemat® V3.1, Istituto Ortopedico Rizzoli, Bologna, Italy) (Taddei et al., 2007) after converting the HU values of CT images voxel into volumetric bone mineral density equivalent values (ρ_{QCT}) using the following calibration equation, specific for the ESP previously scanned:

$$\rho_{QCT} = -0.016404 + 0.00085164 \cdot HU \tag{1}$$

The density to elasticity relationships (Eq. 2,3) were adopted to convert ρ_{QCT} to ash density (ρ_{ash}) as proposed by Schileo et al. (Schileo et al., 2008) and then to the elastic modulus (E) following the equation provided by Morgan (Morgan et al., 2003), with $\rho_{app} = \rho_{ash}/0.6$ according to (Schileo et al., 2008). Poisson's ratio was set to 0.3. In the Eq. 2,3 E is expressed in MPa and ρ in g/cm^3.

$$\rho_{ash} = 0.079 + 0.877 \cdot \rho_{QCT} \tag{2}$$

$$E = 4730 \cdot \rho_{app}^{1.56} \tag{3}$$

Both osteoporotic and lesioned vertebrae were modeled in the same way, according to (Nazarian et al., 2008; M. Stadelmann et al., 2018). The intervertebral discs were modelled as a single homogeneous isotropic material with a Poisson's ratio equal to 0.1, as proposed in (Argoubi & Shirazi-Adl, 1996). The modulus of elasticity was calibrated for the specified loading condition so

that the global stiffness of the spine segment, as predicted by the finite element model, matched that measured experimentally. A percentage difference less than 0.1 % computed between the predicted axial load and the force measured experimentally was considered acceptable for the study. The resulting modulus of elasticity was 1.92 MPa, which is within the range of values reported in the literature (Argoubi & Shirazi-Adl, 1996).

After the generation of the model, a rigid registration was performed using a feature-based rigid registration algorithm (Mimics, Materialise NV) to align the experimental DIC data of the two free vertebral surfaces at the initial (unloaded) configuration to the segmentation obtained from the CT data (Fig 2.2a). Since the registration tool required a polygonal surface as mover body, a Delaunay triangulation algorithm (Matlab® v2020, MathWorks, Natick, Massachusetts, US) was previously used to transform the DIC point cloud into an open triangulated surface. The rigid transformation matrix (Mt) was then extracted using a single value decomposition algorithm (Matlab® v2020, MathWorks, Natick, Massachusetts, US) that best align the original and the registered DIC point clouds. All the displacement vector components of all the correlated DIC points and the coordinates of the markers placed on the superior and inferior pots were transformed using Mt.

The registration accuracy was assessed computing the Euclidean distance between the points on the DIC-detected surface and the nearest corresponding node on the model surface (Registration Error) and was expressed as the root mean square error (RMSE).
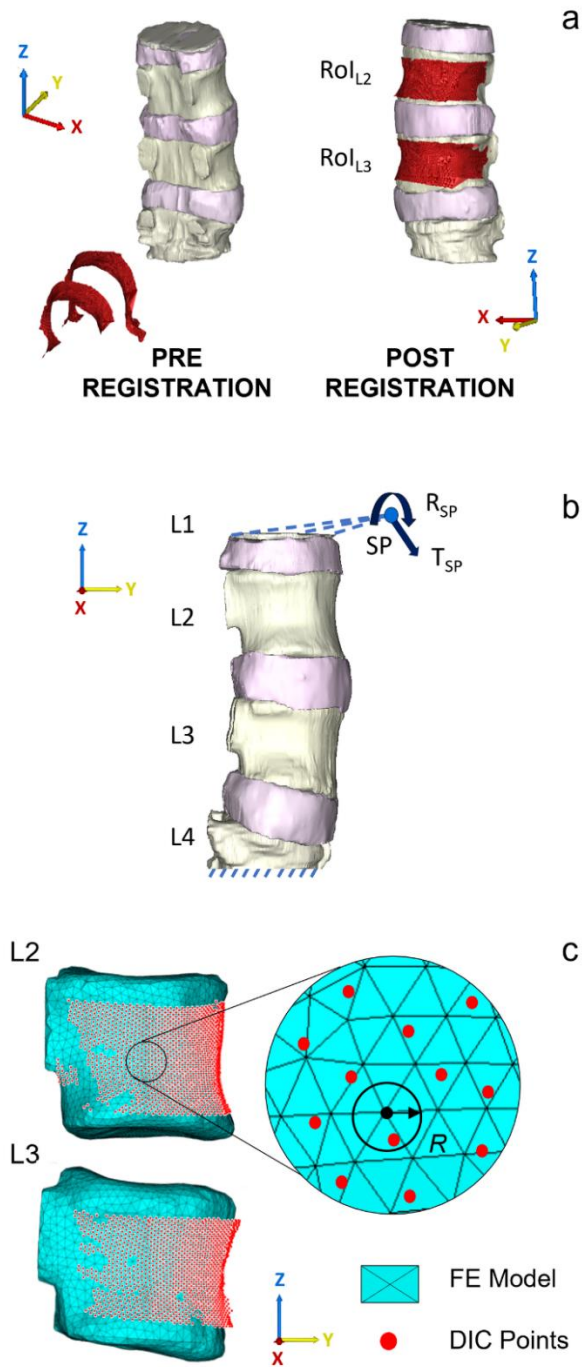
Fig 2.2: Workflow used to compare predicted and experimental local displacements. a) Registration of the DIC points (red surfaces) to the segmentation obtained from the CT data. By aligning the surfaces, it was possible to perform the comparison between the displacements predicted by the FE model and the ones measured using the DIC. b) Boundary conditions applied to the FE model: the inferior surface of the lower vertebral body was fixed while translations (TSP) and rotations (RSP) are applied through a pilot node SP to the superior surface of the upper vertebral body. c) Illustration of the tool used for the local displacement comparison. Reproduced under the terms of the CC BY 4.0 DEED license. © 2022 Garavelli et al.

The boundary conditions (BCs) simulated the experimental test (Fig 2.2b). Particularly, the inferior surface of the lower vertebral body (L4) was fixed while the rigid body motion of the superior aluminium pot, extracted using the single value decomposition algorithm (Sorkine & Rabinovich, 2009), was transferred at the superior surface of the upper vertebral body (L1) using a remote displacement approach (Mechanical APDL V19.3, Ansys Inc.). Both displacements and rotations were prescribed through a pilot node (SP) that corresponds to the centroid of the registration marker cluster placed on the metal pot (Fig. 1). The remote boundary conditions were implemented with the Multipoint Constraint (MPC) technique using the rigid surface-based constraint. The computed translation vector T_{SP} (expressed in mm) and the rotation matrix R_{SP} are reported below:

$$T_{SP} = \begin{bmatrix} 1.321 \\ 5.441 \\ -4.754 \end{bmatrix} \qquad R_{SP} = \begin{bmatrix} 1 & 0.014 & 0.005 \\ -0.014 & 0.996 & 0.088 \\ -0.003 & -0.088 & 0.996 \end{bmatrix} \qquad (4)$$

To investigate the model results and allow the comparison with the experimental data, two regions of interest RoI_{L2} and RoI_{L3} (respectively red and green contours in Fig 2.2b) were defined on the anterior and lateral surface of the two vertebral bodies L2 and L3. These regions correspond to the correlation areas where displacements are captured by the DIC system during loading. In addition to the three displacement components, the axial resultant force was computed as a constraint node reaction solution at bottom surface of the lower vertebra.

The entire FE model had 1,198,125 degrees of freedom and took approximately 2 minutes to solve with Ansys preconditioned conjugate gradient solver, using parallel distributed memory over 6 cores with 64 GB of RAM (Intel(R) Xeon(R) E-2276G CPU 3.80GHz).

2.2.3. Statistics

To compare the simulation results with the experimental data, the DIC displacement measurements were first averaged over a spherical volume with the radius R equal to the registration RMSE (see result and discussion section) and the centre coincident to an FE model node. Then, prediction accuracy was evaluated comparing the displacements predicted by the FE model at each node of the RoI (U_{FEM}) against the measured displacement averaged over the spherical volume of interest centered on that node (U_{DIC}) (Fig 2.2c). The total number of experimental data points used for the validation was 2,452 (1,143 and 1,309 for L2 and L3 vertebral body respectively). Cook's distance method was used to clean data from potential outliers. Specifically, points with a Cook's distance greater than four times the mean Cook's distance value were removed from the comparison (Stevens, 1984). Linear regressions were used to estimate the goodness of the comparisons: determination coefficient (R^2) was used to quantify how well a linear model described the FE to DIC relationship, while RMSE was chosen as a good measure of how accurately the model predicts the response. A normalized RMSE (%RMSE) was calculated using the maximum displacement measured by DIC in

each RoI as normalization factor. The absolute error and the percentage error were computed at each point and for every directional component as follow:

$$Error_{x,y,z} = |U_{DIC_{x,y,z}} - U_{FEM_{x,y,z}}| \qquad (5)$$

$$Error_{x,y,z}\% = \frac{|U_{DIC_{x,y,z}} - U_{FEM_{x,y,z}}|}{|U_{DIC_{x,y,z}}|} \cdot 100 \qquad (6)$$

Maximum values of the absolute error (Max Error) and average values of the percentage error (Average Error %) were then extracted in each RoI. The vector resultant (Diff) was also computed as:

$$Diff = \sqrt{Error_x{}^2 + Error_y{}^2 + Error_z{}^2} \qquad (7)$$

2.3. Results

After registration, DIC surface points and FE external nodes, both extracted in the unloaded condition, had a least square distance of 0.34 mm and a registration RMSE equal to 0.53 mm. A maximum distance of 2.96 mm was found between the DIC points and the corresponding nodes of the model near the upper endplate of the L2 vertebra (Fig 2.3).
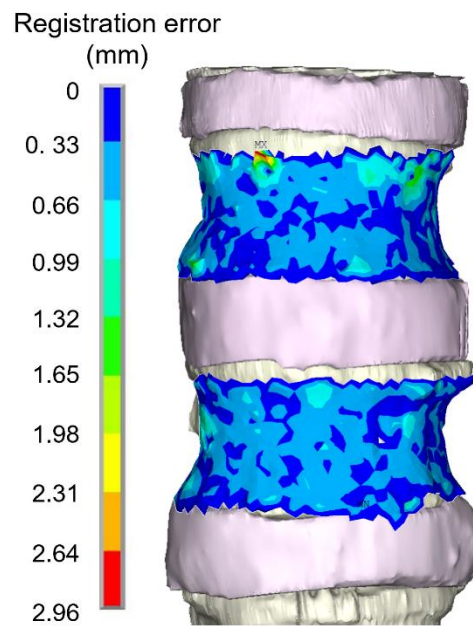
Fig 2.3: Graphical representation of spatial distribution of the registration error. Spatial distribution of the registration error of DIC points on the vertebral surfaces of the FE model. Reproduced under the terms of the CC BY 4.0 DEED license. © 2022 Garavelli et al.

The FE model was able to predict the measured displacements at a load of 60 N with a determination coefficient higher than 0.9 and RMSE less than 0.12 mm (%RMSE less than 7%). A summary of the validation results for the three displacement components are reported in Table 1 while the correlations between the experimentally measured and numerically predicted displacements are shown in Fig 2.4. Highest average percentage errors were found on the right-left and the superior-inferior direction of the displacement components for the lower vertebra (about 8.7 % and 14 % respectively). The %RMSE in all the directions was found to be in the range between 1.8 % and 7.5 %. The magnitude of the error did not seem to depend on the magnitude of the measurements, as can be observed in Fig 2.5 while the plots of the spatial distribution of the vector resultant (Diff) in Fig 2.6 highlighted a trend with higher errors on the left side. Finally, spatial distributions of DIC measured displacement fields and FE predicted ones are reported to show the ability of the model to reproduce the realistic spine kinematics (Fig 2.7).

Table 2.1: Summary of the validation metrics values for local displacement comparisons between DIC and FE results.

	L2			L3		
	RL	AP	SI	RL	AP	SI
R^2	0.98	0.98	0.98	0.97	0.94	0.98
Slope	0.823	0.976	1.073	0.650	0.979	1.071
Intercept	0.054	-0.030	0.054	0.071	-0.023	-0.038
RMSE (mm)	0.055	0.110	0.065	0.028	0.072	0.105
RMSE %	7.5	2.7	3.7	3.8	1.8	6.0
Average Error %	8.7	3.4	3.9	9.4	6.4	14.0
Maximum Error (mm)	0.077	0.225	0.165	0.079	0.181	0.203

Validation metrics for L2 and L3 vertebral surfaces and calculated on the right-left (RL), antero-posterior (AP) and superior- inferior (SI) displacement components.
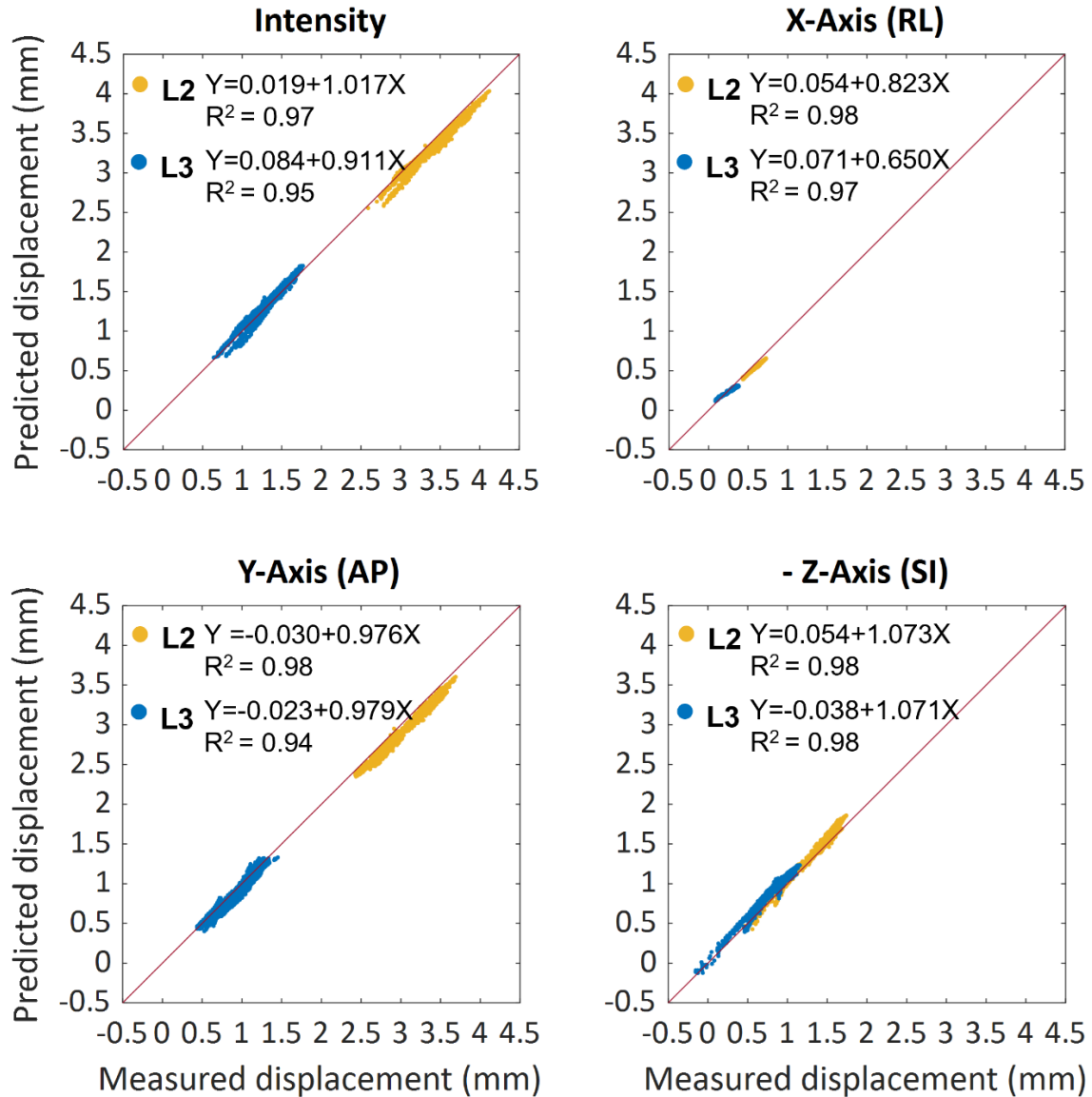
Fig 2.4: Linear regressions plots between predicted and experimental local displacements. Comparison between the displacements measured using DIC and the ones predicted by the FE model for L2 (yellow) and L3 (blue) vertebral surfaces. The Euclidean norms of the displacements, referred as Intensity, and the three displacement components defined in the FE model coordinate reference system are plotted. Linear regression and coefficient of determination are also reported for the correlation plots. It is important to notice that the SI component is plotted with the sign changed to allow comparison with the other subplots. Reproduced under the terms of the CC BY 4.0 DEED license. © 2022 Garavelli et al.
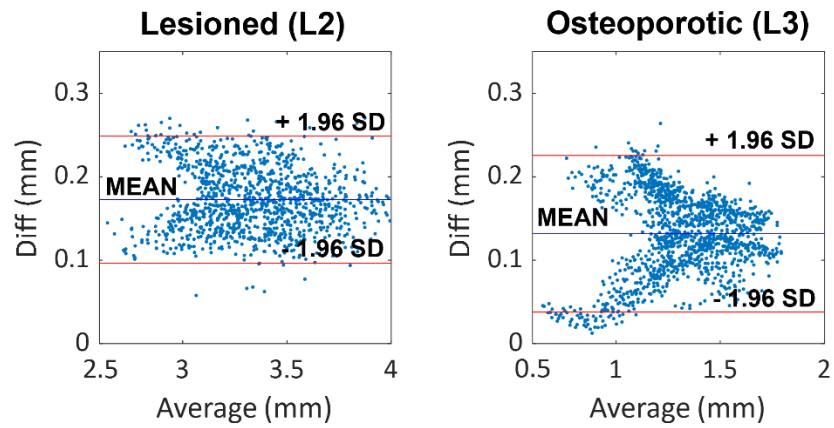
Fig 2.5: Residual analysis estimated between FE and DIC displacements. Bland-Altman plots showing the dependence of the vector sum magnitude (Diff) on the average value between measured and predicted local displacement. Reproduced under the terms of the CC BY 4.0 DEED license. © 2022 Garavelli et al.
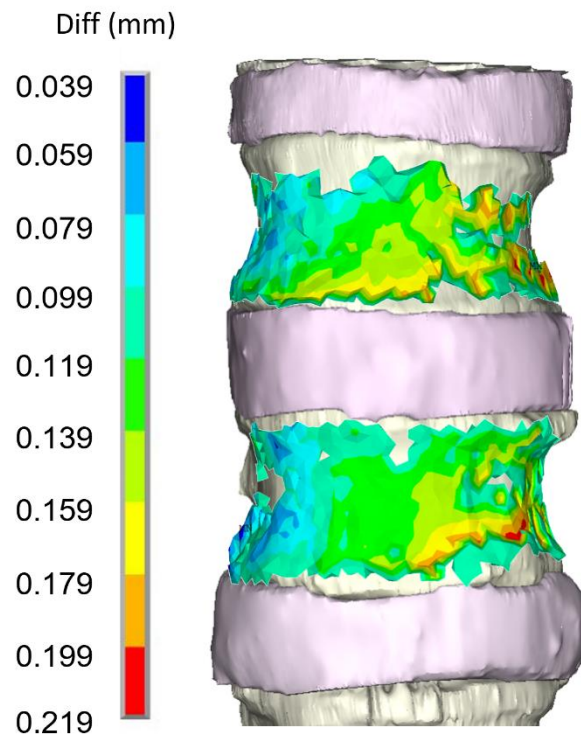
Fig 2.6: Representation of comparison error spatial distribution. Spatial distribution of the vector resultant (Diff) on the vertebral surfaces of the FE model. Reproduced under the terms of the CC BY 4.0 DEED license. © 2022 Garavelli et al.
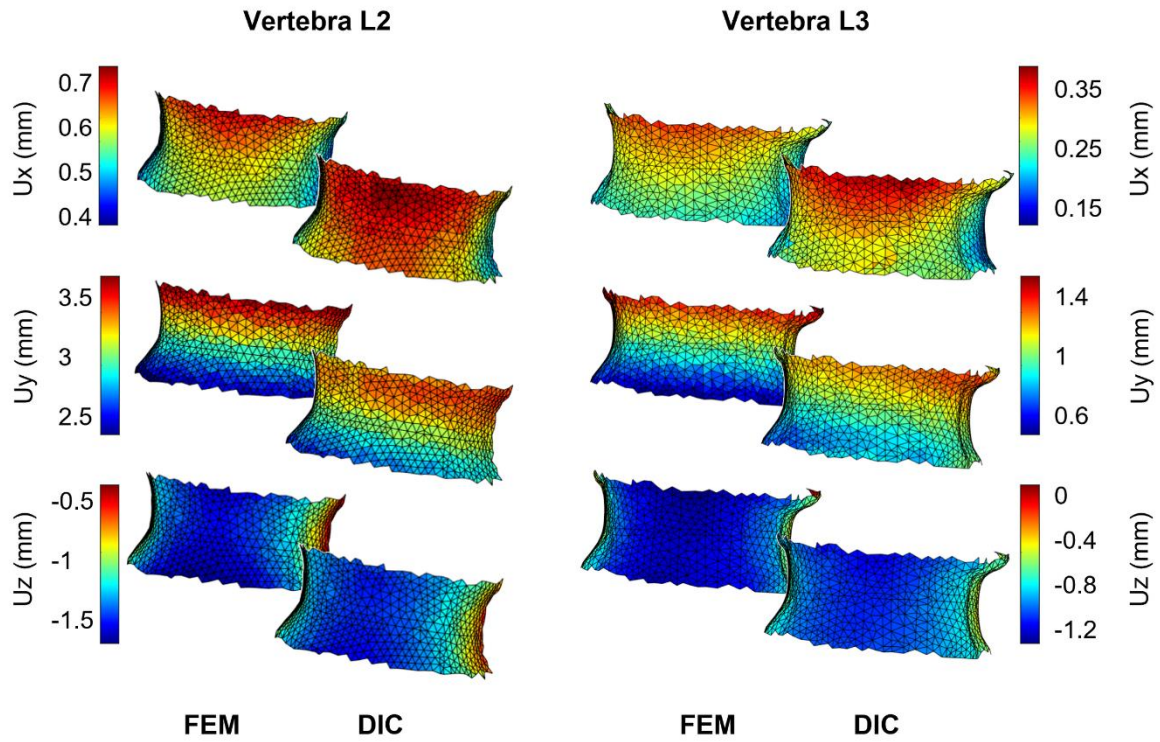
Fig 2.7: Displacement field of the two vertebral surfaces. Comparison between computational and experimental displacement fields in the three directional components X, Y and Z for each vertebra (L2 left, L3 right). To help the reader in appreciating the comparison, both experimental and computational displacements have been interpolated over the same mesh. Reproduced under the terms of the CC BY 4.0 DEED license. © 2022 Garavelli et al.

2.4. Discussion

The aim of this paper was to develop a first model validation framework based on the comparison between the vertebral surface displacements predicted by the FE model and the experimentally measured ones using DIC for the same spine segment which included an osteoporotic vertebra and a vertebra with lytic metastatic lesions.

To achieve this goal, the first challenge was to align the experimental DIC data to the geometry of the FE model. The proposed registration method allowed to obtained good registration results, comparable with those obtained in the state-of-the-art validation studies (Grassi et al., 2013; Gustafson et al., 2017). As already mentioned, the radius R of the spherical volume of interest defined to compute the average of the measured displacements was set equal to the registration RMSE. In a preliminary sensitivity analysis, it has been noticed that this distance ensured that more than 80 % of DIC points had at least a corresponding node of the FE model to be compared with. Also, points whose distance from the closest FE node is more than 0.53 mm were discarded minimizing the influence of the registration errors on the validation results.

The local comparison between the displacements predicted by the developed FE model and the ones measured by the DIC showed robust correlation. The R^2 values along the three directions ranged from 0.94 to 0.98 and RMSE % was found always less than 8%. Highest RMSE % value (7.5%) was observed in the RoI of the lesioned vertebra and related to the right-left displacement direction; nonetheless maximum displacement errors and DIC uncertainty for this displacement component were found of the same magnitude order. The systematic procedure developed to define the boundary conditions proved to be overall efficient to represent the experimental loading conditions and obtain good displacement prediction accuracy.

To the author's best knowledge, no other studies focused on the experimental validation of FE models of human spine segment that include more than two spinal units using DIC. The only study that applied a similar validation approach to FE models of single thoracolumbar vertebral bodies was presented by Gustafson et al. (Gustafson et al., 2017). In their work, a registration method based on the additional acquisition of control points coordinates using a 3D point digitizer was used and the maximum distance between the DIC surface points and FE nodes after the registration was found about 2 mm. The R^2 correlation values between the DIC and FE displacements ranged from 0.75 to 0.93. Nevertheless, it is important to notice that in their study individual vertebrae were tested and the overall spine motion, with the role of the IVD in particular, could not be considered in the displacement comparison. Other studies used DIC data to validate FE models of bones (e.g., cadaveric femora and pelvis) showing good predictive accuracy in term of both displacement and strain measurement comparison (Ghosh et al., 2012; Grassi et al., 2016; Katz & Yosibash, 2020). Commonly used registration methods relied on landmark-based alignment techniques and iterative closest point

algorithm; however, these techniques cannot be easily applied to the antero-lateral surface of the vertebral body as it does not have clearly distinguishing features.

The attempt to replicate *in silico* what happen during experimental tests obviously brings its own set of limitations. A first critical point concerns the mechanical properties assigned to the IVDs. The effect of considering more complex modelling (e.g., nonlinear material properties of the nuclear pulposus and annulus fibrosus) on the simulation outputs is worth studying in future work, that will include a strain-based validation in the workflow. A systematic analysis on the biomechanical response of the discs at different degenerative stages might be required as well as a detailed reconstruction of the IVDs geometry that cannot be easily performed from clinical CT images of the specimen. More complex finite element models will be also needed to investigate the effect of the posterior ligaments and the facet joints that were not included in this work.

Regarding the BCs, one assumption made was that the metal and the PMMA pots were considered as a single rigid body connected to the surface of the vertebral body. This is a realistic assumption because the stiffness of the metal pots is much greater than that of the specimen, and screws ensured a stable connection of the parts. Another important aspect that should be mentioned is that the applied rotations and translations were defined in the coordinate reference system of the FE model considering the transformation matrix extracted after the registration step. This might have introduced some errors due to possible relative motions between adjacent vertebral bodies caused by the insertion of the specimen in the testing machine.

Material properties of the bone were mapped using the same constitutive laws both for osteoporotic and lesioned vertebrae. This choice could have introduced some inaccuracy but was supported by other authors findings (Nazarian et al., 2008; M. Stadelmann et al., 2018), who had shown that the mechanical properties for trabecular bone with and without lesions are similar. However, it should be mentioned that even though not clear blastic formations were identified, the lytic regions were widely spread within the L2 vertebral body and very small and higher density regions were found in other parts of the bone segment that might be also caused by an early onset of fracture. In general, the proposed validation method should be considered valid as long as the hypothesis that the metastatic lesions can be characterized as low-density bone tissue remains true. If evident signs of blastic metastases or primary tumours (e.g., osteosarcoma) are observed, other constitutive models should be included to characterize the mechanical properties of the bone tissue.

Last limitation that is important to underline is that the present work has been developed using one single specimen. Nevertheless, this is a first proof-of-concept validation study that allowed to highlight strengths and weaknesses of the methodology. Despite the limitations, it represents a fundamental step towards the application of the technique to more complex models that can be used to predict bone surface strain and assess fracture risk in pathological vertebrae.

In conclusion, a subject-specific finite element model of a lumbar spine segment with mixed metastasis was developed and validated against experimental displacements measured through digital

image correlation technique. With the proposed methodology good predictivity accuracy (RMSE% < 8% and R^2 > 0.9) was achieved in the simulation of the spine kinematics. The present findings show how the experimental spine displacement field could be adequately reproduced by the developed multi-vertebrae FE model, despite the simplified mechanical modelling of the IVDs.

Chapter 3

Multi-vertebral CT-based FE models implementing linear isotropic population-based material properties for the intervertebral discs cannot accurately predict strains

This chapter is adapted from the manuscript:

C. **Garavelli**, A. Aldieri, M. Palanca, L. Patruno, and M. Viceconti

'Multi-vertebral CT-based FE models implementing linear isotropic population-based material properties for the intervertebral discs cannot accurately predict strains'

Submitted to

Biomechanics and Modeling in Mechanobiology

The preprint version of the manuscript has already been published on ArXiv repository:

arXiv:submit/5404150

Abstract

Vertebral fractures cannot currently be predicted accurately in clinics, where the adopted scores have limitations in identifying subjects at risk. In this context, CT-based finite element (FE) models might improve fracture risk prediction. Many proposed FE models consider single vertebrae only, thereby neglecting the role of the intervertebral discs in load transmission and distribution across vertebrae. Multi-vertebrae models would allow the inclusion of more physiological boundary conditions in the simulation thanks to the discs' inclusion. Nevertheless, while CT allows material properties to be assigned to the vertebrae according to the Hounsfield Units, no information about the discs' mechanical properties is provided. Hence, the aim of this study was to validate a CT-based multi-vertebrae FE model where linear isotropic material properties were assigned to the discs against experimental data. The CT-based FE model of a multi-vertebrae specimen was built, where Young's modulus populations values in the literature range were assigned to the discs. Boundary conditions were assigned coherently with experiments performed on the specimen and the computational strains on the vertebrae surface compared to the experimental strains coming from digital image correlation measurements. The strains on the vertebral surface increased following the increase of the discs' Young's modulus, with no changes in their local distributions. Although Young's modulus values around 25-30 MPa yielded comparable orders of magnitude between numerical and experimental strains, strains local distribution differed substantially. In conclusion, subject-specific discs' material properties should be included in CT-based multi-vertebrae FE models in order to achieve acceptable accuracy in fracture risk assessment.

3.1. Introduction

Vertebral fracture represents a very severe event, which, regardless of the pathology associated with its occurrence, increases morbidity, mortality and decreases the quality of life in already fragile subjects (Hasserius et al., 2005). In addition, it also has economic implications for the healthcare systems (Barlev, 2010). According to the World Health Organization (WHO), by 2030, the number of people older than 60 will increase by 34% compared to 2020 (World Health Organization & United Nations Children's Fund (UNICEF), 2022). Due to risk factors such as increased propensity to fall and deteriorated mechanical properties of the bone tissue, the elderly present a markedly increased bone fracture incidence, mainly at the hip, wrist, and spine. At the same time, the WHO has also reported that almost 20 million new cancer cases are diagnosed every year (Ferlay et al., 2021). In fact, the improved therapeutic protocols for cancer patients have significantly increased their average survival (Miller et al., 2022). In return, an increasing incidence of bone metastases has been observed, primarily located in the spine (Kakhki et al., 2013), which compromises the physiological mechanical competence of the vertebrae (Bishr & Saad, 2012; Laufer et al., 2013). The spine is already per se one of the most fracture-prone anatomical sites (Borgström et al., 2020), and pathological vertebrae are exposed to an even higher risk of fracture (Burke et al., 2017). Therefore, an accurate prediction of the fracture risk turns out to be pivotal so that appropriate preventive interventions are taken.

The available clinical gold standards for bone fracture prediction have shown limited accuracy in stratifying subjects at high risk of experiencing a fracture from subjects who are not. The widely used T-score, for example, was proved to suffer from poor specificity and sensitivity in predicting hip and vertebral fractures connected to osteoporosis (Crandall et al., 2014). Similarly, the Spinal Instability Neoplastic Score (SINS), adopted in clinics for referring patients to surgical/orthopaedic consultation in case of metastatic vertebrae, suffers from a certain degree of subjectivity in the final clinical decision (Fisher et al., 2014) and lacks sufficiently good specificity (Y. R. Kim et al., 2021). Nevertheless, an accurate prediction of the risk of fracture would be crucial, especially in metastatic subjects, as surgeons could decide whether to surgically intervene on subjects already weakened by primary cancer treatment.

In recent years, Computed Tomography (CT)-based digital twins development has highlighted the potentiality of such *in silico* methodologies in this context. Several studies have demonstrated the possibility of adopting *in silico* tools to provide information about bone resistance non-invasively (Dall'Ara et al., 2012; Imai et al., 2006; Viceconti et al., 2018). For some anatomical sites, such as the femur, *in silico* methodologies have successfully outperformed the gold standard for predicting hip fracture (Aldieri, Terzini, et al., 2022; Bhattacharya et al., 2019). On the contrary, due to its complexity, the fracture prediction at the spine *in silico* is not as straightforward.

The spine comprises multiple vertebrae with intervertebral discs (IVDs) interposed, which affect the load transmission and distribution. Consequently, vertebral fracture risk prediction *in silico* based on clinical images (e.g., CT) could be performed by adopting two mutually exclusive strategies. In the first one, the vertebra fracture risk is predicted by only modelling one vertebra and neglecting the IDVs (Allaire et al., 2019; Kopperdahl et al., 2014; X. Wang et al., 2012). This approach intrinsically poses some limitations since it does not allow to impose physiological loading conditions on the vertebral bodies and does not consider to what extent IVD degeneration might impact load transmission to the adjacent vertebrae (Adams et al., 2006; Danesi et al., 2016; Hussein et al., 2013). On the other hand, the second modelling strategy includes the IVDs in the model by modelling at least one entire vertebral unit to account for the real complexity of the spine. In principle, this would require the inclusion of a comprehensive description of the IVD through magnetic resonance imaging (MRI) as an additional input to the model besides CT, as it would allow for the quantification and integration of the patient-specific structure and composition of the IVDs (Antoniou et al., 2013; Rijsbergen et al., 2018), (M. A. Stadelmann et al., 2018). Although this approach would increase the accuracy of the model, allowing to reproduce a more realistic load transmission among vertebrae, it brings its own set of complications (e.g., higher costs and higher clinical workload), preventing its implementation in clinical practice. In fact, the development of a digital twin for vertebral fracture risk prediction based only on the subject's CT would be much more clinically feasible. The CT would allow reconstruction of the geometry and the assignment of patient-specific Hounsfield Units-based material properties to the vertebral bone tissue. However, no information would be provided regarding the disc, forcing to model it with population material properties coming from the literature.

In this light, the aim of this work was to assess the accuracy of a multi-vertebrae FE model uniquely based on CT, where the IVDs were included and modelled in the simplest possible way with homogenous and linear isotropic material properties. A patient-specific FE model of a spine segment with evidence of metastatic disease was developed from CT images of a cadaveric sample. A range of population-based Young's modulus values from the literature (H. Yang et al., 2016) were assigned to the IVDs. The strains obtained from the model were compared to experimental data acquired through Digital Image Correlation (DIC) (Palanca, Tozzi, et al., 2016) on the same sample, and the accuracy of the proposed modelling strategy assessed.

3.2. Materials and methods

3.2.1. Mechanical Testing

The procedures for conducting the mechanical testing have been thoroughly explained in a prior publication (Palanca et al., 2021) and will be briefly summarized here. Experimental tests were performed on a thoracolumbar cadaveric specimen obtained from an ethically approved donation program (Anatomic Gift Foundation, Inc.). The sample included four vertebrae and the interposed three IVDs, from T10 to L1. One of the two central vertebrae showed signs of lytic metastatic lesions (Fig.3.1A). Half of the most cranial and half of the most caudal vertebrae were embedded in polymethyl-methacrylate (PMMA) cement (Fig.3.1B). After the preparation of the specimen, diagnostic images were acquired with a spiral CT (AquilionOne, Toshiba, Japan), to be subsequently used for the FE model development. Scans were performed at 120 kVp with 200 mA tube current, 0.24 mm × 0.24 mm pixel size and 1 mm slice thickness. Afterwards, the specimen was sprayed with white water-based paint to generate a unique speckle pattern recognisable by a three-dimensional DIC 4-camera system (Aramis Adjustable 12M, GOM, Braunschweig, Germany, with 12mPixels cameras and 75 mm metrology-standard lenses). Flat circular markers were glued on the aluminium pots of the test machine to track the displacement of the superior and inferior pots (Fig.3.1C).

The mechanical tests were performed using a uniaxial testing machine (Instron 8500 controller with Instron 25 kN load cell, Instron, UK) in displacement-controlled modality. The load application point was shifted forward by 10% of the anteroposterior dimension of the central IVD to impose an anterior flexion (Palanca et al., 2018). The use of a ball-joint and low friction bearings allowed the top pot to be free to rotate and translate, while bottom one was totally constrained. The load magnitude was identified as the load able to induce minimum principal strains typically associated to physiologic loads (Lanyon, 1987) (i.e. in the order of 2500/ 3000 microstrain) on the anterior surface of the control vertebra. The experimental reaction force was recorded. Further details can be found in (Palanca et al., 2021). During the test, DIC images of the two central vertebrae free from the cement and of the two pots were acquired at 25 Hz (Fig.3.1D). DIC measured the displacements on the visible vertebral surfaces. Systematic and random errors in term of displacements were found around 10 μm and 25 μm, respectively. Maximum and minimum principal strains on the vertebrae surface were then calculated by derivation of the nodal displacements, as described later in the Metrics paragraph. The measurement spatial resolution was about 2 mm.
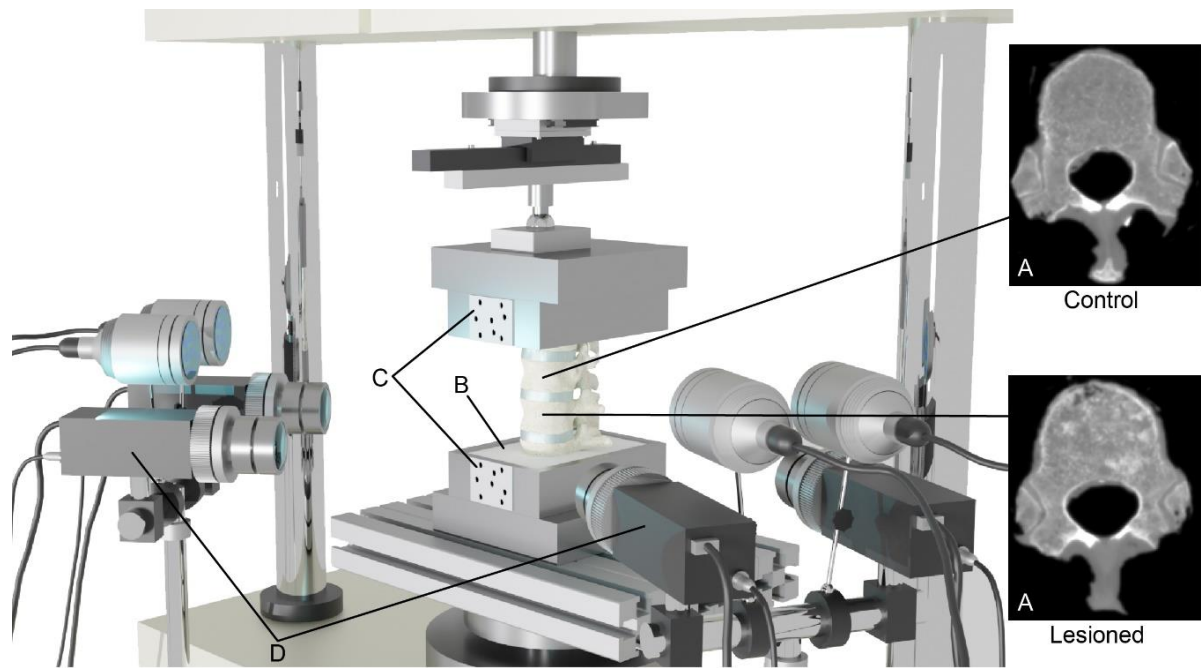
Fig.3.1: Experimental test set-up. The specimen with one control (A, top) and one metastatic (A, bottom) is placed into the testing machine (B). Pots displacements are tracked thanks to glued markers (C). The flexion test is recorded by a three-dimensional DIC system (D).

3.2.2. Finite Element Analysis

The steps required to develop a CT-based homogenised FE model have already been presented in detail in our previous work (Garavelli et al., 2022, reported in Chapter 2) and will be here briefly summarised. Firstly, CT images of the specimen were segmented to extract the geometry of the vertebral bodies, IVDs, and pots separately. A threshold method based on Hounsfield Units (HU) values was used to pick out bone tissue and PMMA cement (200÷3000 HU for bone and 1100÷1800 HU for PMMA), followed by manual editing (Mimics 25.0, Materialise NV, Leuven, Belgium). The IVDs profiles were segmented completely manually: lateral contour was sufficiently well visible from the CT scan, while adjacent vertebrae endplates were used as upper and lower bounds. Secondly, subtraction Boolean operations were performed to glue vertebral bodies with adjacent intervertebral discs to obtain a unique volume object (SpaceClaim V19.3, Ansys Inc., Canonsburg, PA). Eventually, posterior processes were removed, considering that in the flexion test, the posterior ligaments were activated only if the physiological range is exceeded (at this spinal level, the neutral zone and the range of motion for each FSU are around $0.6° \pm 0.1°$ and $3.5° \pm 0.8°$ respectively (Wilke et al., 2017)), which instead was avoided in the presented test-case (total flexion: 2.8°).

A ten-node tetrahedral structural solid mesh was generated following a sensitivity analysis, imposing a maximum edge length equal to 2 mm (ICEM CFD V19.3, Ansys Inc.). Subsequently, material properties were mapped on each element (Bonemat® V3.1, Istituto Ortopedico Rizzoli, Bologna,

Italy) (Taddei et al., 2007). Bone tissue was modelled as a heterogeneous linear elastic isotropic material. Specifically, the voxel HU values were converted to equivalent values of volumetric bone mineral density through a phantom-based calibration and the application of an additional calibration correction (Schileo et al., 2008). A density-elasticity relationship (Morgan et al., 2003) was adopted to assign heterogeneous elastic properties over space to the vertebral elements. A Poisson's coefficient (v) equal to 0.3 was assigned to all bone elements. The IVDs were modelled as isotropic and homogeneous linear elastic materials, all characterised by the same elastic modulus (E_{disc}). Initially, E_{disc} was set to the value that allowed it to fit the experimentally recorded reaction force, as described in (Garavelli et al., 2022). Subsequently, the analysis was extended to the entire range covered by the literature, ranging from 4 MPa to 50 MPa (Keller et al., 1987; O'Connell et al., 2007; Pollintine et al., 2010; H. Yang et al., 2016). A Poisson's coefficient (v) equal to 0.1 was adopted (Argoubi & Shirazi-Adl, 1996). Linear elastic material properties were also assigned to the PMMA pot, with v=0.3 and an elastic modulus (E_{PMMA}) equal to 3 GPa (obtained from in-house experimental tests on cement samples).

Boundary conditions were assigned to the FE model to replicate the experimental test conditions. The metal and PMMA cement pots were assumed to be rigidly connected so that only the second ones were modelled. The positions of the superior metal pot at the initial and final steps of the experimental test acquired through the DIC, were processed using a single value decomposition (SVD) algorithm to extract the rotation components and translation of the rigid pot's motions. The obtained values were imposed on all the external nodes of the FE model superior PMMA pot using a multi-point constraint. The inferior PMMA pot was fixed.

Simulations were solved in the FE software (Mechanical APDL V19.3, Ansys Inc.) with the preconditioned conjugate gradient solver, using parallel distributed memory over 6 cores with 64 GB of RAM (Intel(R) Xeon(R) E-2276G CPU 3.80GHz).

Maximum and minimum principal strains were calculated on the surface of the vertebrae by derivation of the numerical nodal displacements, as described later in the next section.

3.2.3. Metrics

The DIC and FE reference systems had to be aligned prior to the comparison between experimental and numerical outcomes. This was done adopting a procedure based on surface registration (Mimics 25.0) and SVD (Matlab® v2020, MathWorks, Natick, Massachusetts, US), as described in details elsewhere (Garavelli et al., 2022).

Subsequently, DIC vertebral displacements were interpolated onto the locations of the superficial nodes of the FE model. To do this, an inverse distance weighting algorithm based on the Euclidean norm was used, with power equal to 2 and threshold radius set to 1 mm accounting for the surface

registration error. The interpolation allowed to perform pointwise comparison between the experimental and the numerical outcomes (Matlab® v2020), for all the different E_{disc} values applied.

In order to check if the kinematics observed in the experiments was correctly reproduced by the model, DIC and numerical displacements agreement was assessed point wise. To evaluate this, linear regression coefficients, determination coefficient (R^2) and root mean squared error normalized by the maximum measured value (%RMSE) were computed between DIC and FE local displacements.

Experimental and numerical strains on the vertebral surfaces were obtained through derivation of the displacement fields on the superficial nodes of the vertebrae. More in detail, the strains were calculated by defining linear triangular elements as the faces of the mesh tetrahedrons lying on the vertebral surface. Maximum and minimum principal strains were considered. R^2, RMSE, and %RMSE between experimental and FE strain fields were evaluated in order to identify, if possible, the E_{disc} value providing the best match between the two fields. In addition, also percentual differences between FE model and DIC were computed on strains. Kolmogorov-Smirnov test was adopted to compare DIC and FE principal strains distributions.

Each vertebral surface was also divided into three Regions of Interest (RoI), corresponding to the central, the right and the left portion of the external surface, where the experimental and numerical were averaged and compared.

3.3. Results

Numerical and experimental displacements were compared and showed a %RMSE lower than 9% (Fig. 1s in the Appendix A).

A E_{disc} equal to 4.15 MPa allowed fitting of the experimental reaction force. Nevertheless, experimental and numerical principal strains differed of more than one order of magnitude, with the model underestimating the experimental values (RMSE > 85%). As E_{disc} increased from 4.15 to 50 MPa, the numerical strains on the vertebral surfaces increased without changes in the numerical strains local distribution, which resulted in a considerable disagreement (p<0.001) between the numerical and experimental strains distributions (Fig. 2).

The values of R^2, RMSE, and RMSE% between experimental and FE local strain measurements for all the E_{disc} considered are reported in Table 1s in the Appendix A for both the control and the lesioned vertebra. For the E_{disc} assignment (25 MPa) providing the best fitting of the experimental strain field, RMSE% higher than 30% and R^2 lower than 0.55 were found. Average percentual strain differences between FE and DIC settled to 20% and 65% for minimum and maximum principal strains respectively on the control vertebra, and to 35% and 55% respectively on the metastatic vertebra. Errors did not exceed 90% in any case.
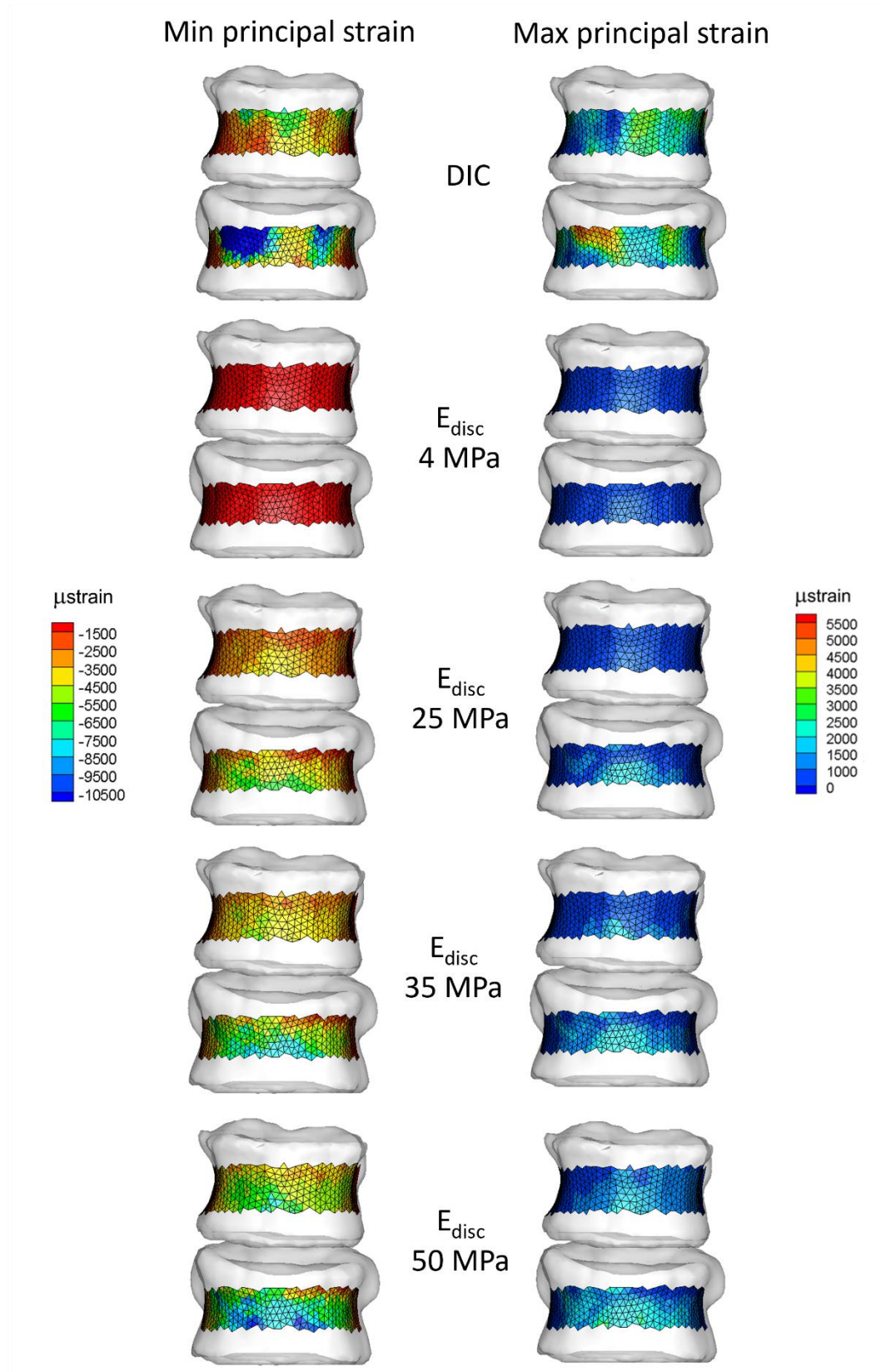
Fig.3.2: Contour plots of the computational principal strains at different E_{disc}. Comparison between experimental (first row) and computational (second to final row) principal strains over the vertebrae surface, for the different E_{disc} implemented.

Fig. 3.3 and Fig. 3.4 present the comparison between the average values of the maximum and minimum principal strains in all the three RoIs. As visible, the twelve times stiffening of the IVDs made the strains intensify about eight times in compression and nine times in traction (Fig.3.3). Moreover, an IVDs E_{disc} equal to 25 MPa was found to minimise the %RMSE computed on the minimum principal strains in particular (Fig.3.4). In fact, it is possible to observe local minima for all the lines in the bottom-left plot. None of the implemented E_{disc} values turned out to be able to minimise the %RMSE computed on the maximum principal strains.
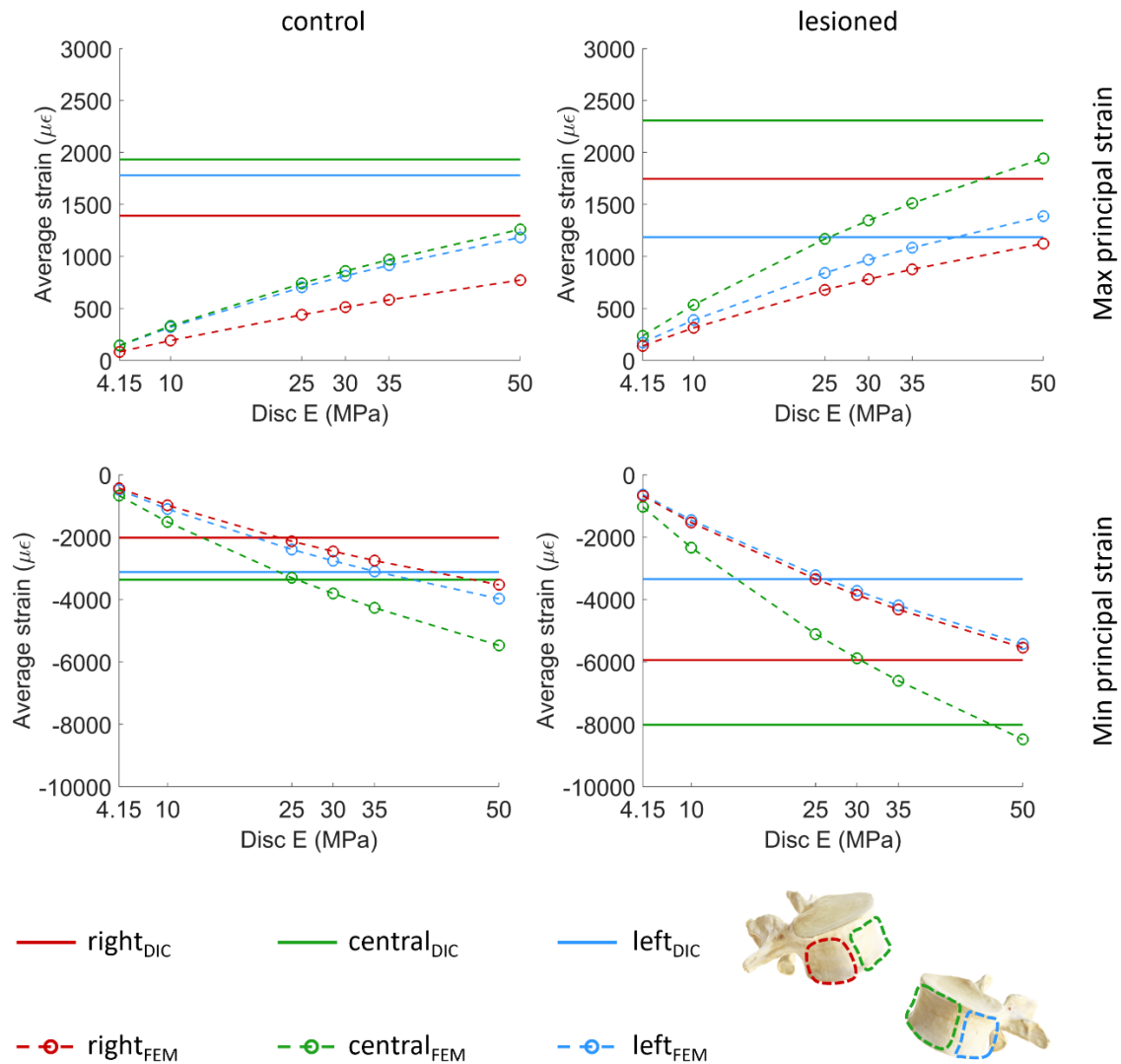
Fig.3.3: Strains dependence to the elastic modulus. Comparison between numerical (dotted lines) and experimental (solid line) averaged on the RoI for the E_{disc} values tested.
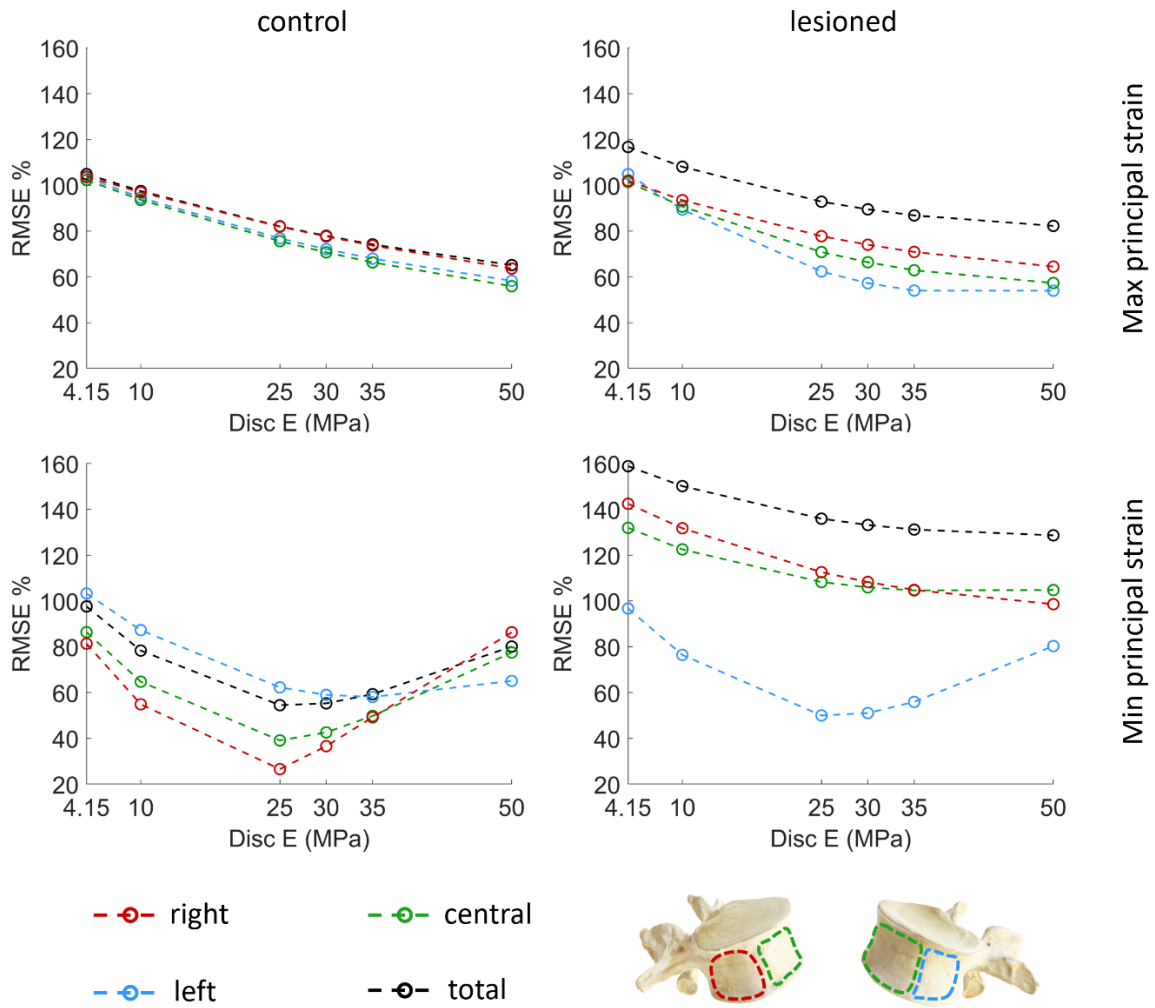
Fig.3.4: Strains error dependence to the elastic modulus. %RMSE computed between numerical and experimental strains for each RoI (red, blue, green dotted lines) and for the whole vertebra (black dotted line) at the E_{disc} values tested.

3.4. Discussion

The purpose of the presented study was to assess whether a CT-based multi-vertebrae FE modelling framework turned out to be accurate and reliable enough to be employed in clinical practice to support and improve the currently adopted tools for vertebral fracture risk prediction. A FE model of the human spine was developed uniquely from CT information and its outcomes compared to corresponding DIC experimental results. The model consisted of four vertebrae, but since two were used for the boundary conditions the comparison was performed on the two central ones.

The accuracy of the developed CT-based FE model was assessed against experimental data coming from compression-flexion tests where a DIC experimental set-up was employed, providing local displacement data on the vertebrae surface (Palanca et al., 2021). A previous study (Garavelli et al., 2022), assessed the capability of the CT-based multi-vertebrae FE model to simulate the experimental kinematics. Herein, the aim was to assess its ability to accurately predict deformations, the biomechanical variable most often employed to assess the onset of a fracture.

In fact, CT-based FE models for assessing the risk of fracture in vertebra are usually developed considering only one vertebra as an isolated body (Crawford et al., 2003) (Matsumoto et al., 2009), but this prevents the application of physiological loading conditions, such as those provided by the IVDs (Anitha et al., 2020), as well as the occurrence of high strain concentration close to the endplates, where fracture often originates (Palanca et al., 2023). The IVDs play a crucial role in load transmission among vertebrae (Hussein et al., 2013). Since IVDs can deeply influence the vertebrae deformation state (Adams et al., 2006), *in silico* vertebral fracture prediction without IVD can be jeopardised. Thus, developing reliable predictive models would require at least one functional spine unit. Having said that, accurate and patient-specific modelling of the IVD mechanical behaviour require information from the MRI imaging technique. This would imply the need for two distinct techniques, MRI and CT, to build a multi-vertebrae FE model for predicting the fracture risk at the spine, making its application in clinical practice more difficult. For this reason, herein, we aimed to assess the accuracy of a multi-vertebrae FE model developed solely from CT, where the simplest possible assumption on the IVDs material properties was made, i.e., that of homogeneous linear isotropic behaviour.

On top of that, the majority of the studies where this approach was adopted have all performed model validation through apparent mechanical properties only (e.g., vertebral strength (Buckley et al., 2007; Dall'Ara et al., 2012; Imai et al., 2006), yield load (Imai et al., 2006), stiffness (Buckley et al., 2007; Dall'Ara et al., 2012)), without considering local biomechanical variables variation within the vertebral body, or by acquiring a μCT scan after the test to visually assess the degree of agreement between the predicted and the experimental site of the fracture onset (Imai et al., 2006).

In light of the considerable underestimation of the deformations by the FE model, where the IVD elastic modulus had been determined to match the experimental load-displacement curve, the elastic modulus was increased to cover the full range available in the literature (Keller et al., 1987; O'Connell et al., 2007; Pollintine et al., 2010; H. Yang et al., 2016). As expected, the magnitude of the strains was highly sensitive to the disc elastic modulus, with typical stiffening of the disc increasing strains throughout the vertebral body. However, the increase in elastic modulus could only shift the numerical deformations' order of magnitude without affecting the distribution of deformations. Hence, although the 30 MPa Young's modulus provided the best agreement between numerical and experimental strains orders of magnitude, a satisfactory agreement between the two could not be achieved.

Considering these findings, more accurate mechanical modelling of the IDV would seem mandatory to achieve sufficient accuracy of the FE models. Further investigation could be carried out to slightly increment the complexity of the adopted constitutive laws and assign different population-based properties to each IVD component (i.e., annulus and nucleus). Still, a CT-based FE model could not include specific information about the IVDs' composition and real mechanical behaviour. Moreover, the IVD elastic modulus was shown to be correlated to their degenerative status in Antoniou et al., 2013, heavily affecting how the load is transferred across the spine and, consequently, the vertebral body deformations. It is then still to be determined whether a multi-vertebrae FE model developed uniquely from CT could provide sufficiently accurate insights into the vertebral fracture risk. In summary, the obtained findings suggest that CT-based multi-vertebrae FE models including subject-specific multiple vertebrae and IVDs modelled with homogenous linear isotropic material properties based on population values cannot accurately predict strain distribution on the vertebral surfaces.

Chapter 4

Validation of homogenized finite element models of human metastatic vertebrae using digital volume correlation

This chapter is based on a manuscript which is currently in preparation:

C. Garavelli, A. Aldieri, M. Palanca, E. Dall'Ara, and M. Viceconti

'Validation of homogenized finite element models of human metastatic vertebrae using digital volume correlation'

The preprint version of the manuscript has already been submitted on ArXiv repository:

arXiv:submit/ 5409326

Abstract

The incidence of vertebral fragility fracture is increased by the presence of preexisting pathologies such as metastatic disease. Computational tools could support the fracture prediction and consequently the decision of the best medical treatment. Anyway, validation is required to use these tools in clinical practice. To address this necessity, in this study subject-specific homogenized finite element models of single vertebrae were generated from μCT images for both healthy and metastatic vertebrae and validated against experimental data. More in detail, spine segments were tested under compression and imaged with μCT. The displacements field could be extracted for each vertebra singularly using the digital volume correlation full-field technique. Homogenised finite element models of each vertebra could hence be built from the μCT images, applying boundary conditions consistent with the experimental displacements at the endplates. Numerical and experimental displacements and strains fields were eventually compared. In addition, because also clinical CT scans were available for the same specimens, the outcomes of a μCT based homogenised model were compared to the ones of a clinical-CT based model. Moreover, μCT based homogenised model were also compared to micro finite element model under the same boundary conditions. Good agreement between experimental and computational displacement fields, both for healthy (R^2 = 0.69÷0.83, RMSE% = 3÷22%, max error < 45 μm) and metastatic (R^2 = 0.64÷0.93, RMSE% = 5÷18%, max error < 54 μm) vertebrae, was found. The comparison between μCT based and clinical-CT based outcomes showed strong correlations (R^2 = 0.99, RMSE% < 1.3%, max error = 6 μm) as did also the comparison between homogenized and micro finite element models (R^2 = 0.95÷0.97, RMSE% = 3÷29%, 95th percentile = 2÷61 μm). Furthermore, the models were able to qualitatively identify the regions which experimentally showed the highest strain concentration. In conclusion, the combination of the experimental full-field technique and the in-silico modelling allowed the development of a promising pipeline for the validation of fracture risk predictors, although further improvements in both fields are needed to better analyse quantitatively the post-yield behaviour of the vertebra.
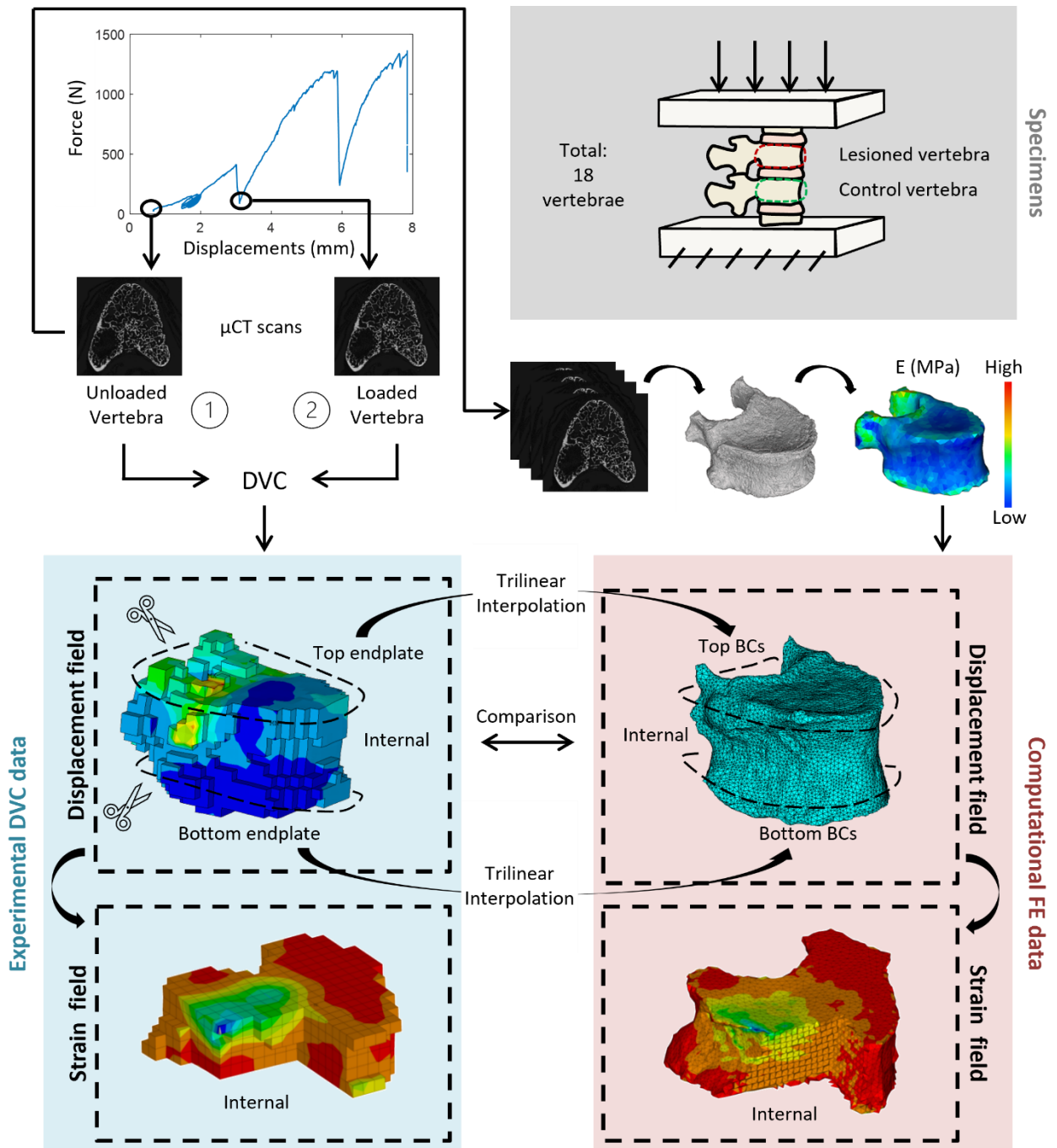
Graphical abstract

4.1. Introduction

In 2020 the World Health Organization (WHO) reported an incidence of more than 18 million cancer occurrences worldwide and presented a prevision of almost 20 million for the year 2040 (World Health Organization, 2020). Among them, one-third of the patients presented signs of spinal metastasis (Van Den Brande et al., 2022). The presence of such metastases, especially lytic, has been demonstrated to increase the vertebral risk of fracture (Kaneko et al., 2004). Although the incidence of this type of metastatic lesions can appear moderate, the comorbidities connected to the fracture events at the vertebrae should be considered (Kado et al., 1999), as well as the associated decrease in the quality of life (Alexandru et al., 2012). In light of this, constant monitoring of vertebral stability in pathological patients is crucial, aiming to prevent the fracture from occurring.

The finite element (FE) methodology has been successfully adopted to evaluate the stability of vertebrae with lytic lesions (Costa et al., 2019) showing the ability to provide information in cases where the Spinal Instability Neoplastic Score lacked in specificity (Fisher et al., 2014). A similar strategy has also been applied to vertebral bone affected by osteolytic lesions, allowing to obtain better assessment of bone fragility compared to volumetric bone mineral density, bone volume fraction and trabecular separation measurements (Campbell et al., 2017). In addition, it has been shown that metastatic vertebrae strengths from experimental tests and from FE models correlated well (R^2 = 0.78) regardless of the lesion phenotype (Stadelmann et al., 2020). However, no direct validation of displacements and strains fields predicted by the models has been presented in these studies. Moreover, they investigated simplified boundary conditions only.

In order to fill this gap, Digital Volume Correlation (DVC) represents a useful tool because it provides full-filed information over the whole bone volume (Grassi & Isaksson, 2015), has been widely used to validate bone models (Dall'Ara & Tozzi, 2022) and can provide experimentally matched boundary conditions (BCs) for the models (Chen et al., 2017; Kusins et al., 2020). Vertebral body FE models have already been validated using DVC both at the tissue level, i.e., µFE models validation (Costa et al., 2017; Palanca et al., 2022) and at the organ one, i.e., hFE models validation (Jackman et al., 2016). Moreover, DVC technique has already been applied to validate vertebral FE models where the load was transmitted through the discs (Hussein et al., 2018). However, in that study the focus was on osteoporotic vertebrae and the validation was carried out by averaging the results within areas of interest where the vertebra had been divided.

The aim of this work was thus to develop µCT-based homogenized finite element (hereinafter referred as hFE) models, for both healthy and metastatic vertebrae, and to validate their prediction in terms of displacements and reaction forces against experimental data. DVC measurements were used to perform the validation. Given that µCT are not performed in clinics, the outcomes of one µCT-based

hFE model were also compared to the ones of clinical-based hFE model of the same vertebra. Additionally, displacements fields of hFE models and micro finite element (µFE) models of the same bones were compared. Eventually, the ability of the hFE models to highlight the regions with higher strain concentrations were assessed.

4.2. Materials and Methods

The following pipeline was applied on 18 vertebrae (Fig. 4.1), divided as follows: 10 healthy and 8 metastatic, specifically 4 lytic and 4 mixed. The comparison between hFE and µFE models based on µCT was performed only on a subsample of 6 vertebrae (Fig. 4.1), composed of 3 healthy and 3 metastatic, specifically 2 lytic and 1 mixed. The comparison between hFE models generated from different resolution scales (clinical CT and µCT) was performed on a single healthy vertebra (Fig. 4.1).
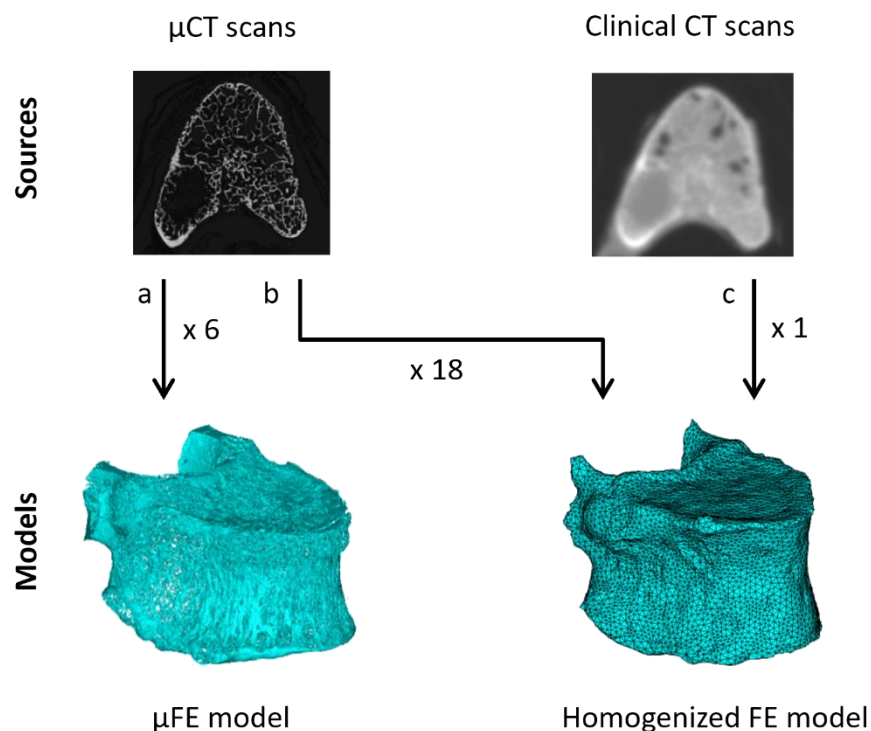
Fig. 4.1: Overview of the developed models. Six µFE models and eighteen homogenized FE models were built from µCT acquisition of the spine specimens, while one homogenized FE was built from clinical CT scans acquired on one among those specimens.

4.2.1. Mechanical Testing

Experimental analyses were conducted on thoracolumbar cadaveric specimens obtained from an ethically approved donation program (Anatomic Gift Foundation, Inc.). Each specimen was composed of four vertebrae: the most cranial and the most caudal ones were embedded in the polymethylmethacrylate and were used to apply the load while the two (one showing signs of lytic or mixed metastatic lesions and one healthy control) in between were free to move through the action of the intervertebral discs. During the preparation of the specimen, posterior elements were removed

(Fig.4.2A). The specimen was mounted on a jig and inserted into a μCT scanner where an unloaded scan (Fig.4.2C) was acquired with 39 μm isotropic voxel size (current: 114mA, voltage: 70kVp, integration time: 300ms, power: 8W). The mechanical test was performed as follows and as described in greater detail in Palanca et al., 2023: 1) a compressive load inducing physiological strains on the surface of the healthy vertebra (Palanca et al., 2021) was applied at the cranial vertebra; 2) the load was increased of three times; 3) the load was increased up to failure (Fig.4.2B). After each load step a μCT scan was acquired following relaxation (Fig.4.2D). DVC, implemented through the BoneDVC algorithm (Dall'Ara et al., 2017), was later performed on each combination of the unloaded scan and one of the loaded scans for the same specimen. Due to the high computational cost required by the BoneDVC algorithm, the original images were cropped, before to start the elastic registration, in order to contain only one vertebra at a time. DVC was carried out based on a 1.95 mm sized grid, where displacements values were thus available (Fig.4.3A). The displacement field was imported into a FE analysis environment (ANSYS Inc., Mechanical APDL), where the strain field was obtained through differentiation. Further technical details about the DVC technique can be found in (Palanca et al., 2023).
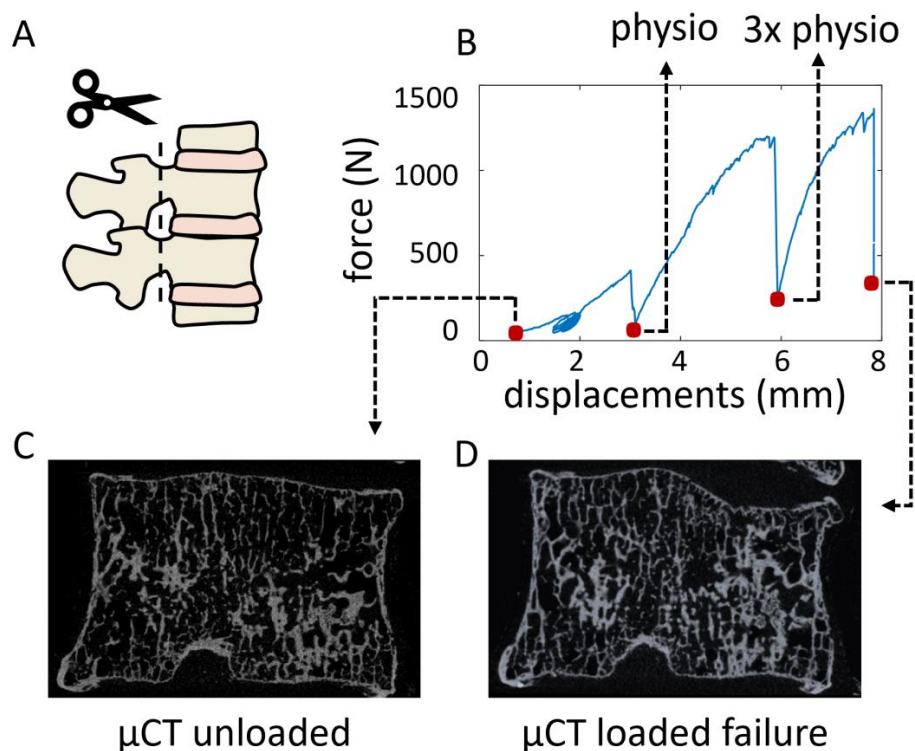
Fig.4.2: Experimental test. The specimens were composed by four vertebrae, but the two extreme ones were used to transmit the load only, and the posterior elements were removed (A). During the compression test (B), μCT scans were acquired at the unloaded condition (C), then after each load step (red dots), until failure (D).

4.2.2. Finite Element Analysis

In analogy with the experimental analysis, where the DVC measurements were carried out on one vertebra at a time, FE models of each vertebra were also created independently. Moreover, both the hFE and the µFE models were generated from the µCT images. In this way, FE models and DVC data shared the same reference system, allowing to reduce errors connected to the registration process. The possibility to generate an hFE model based on a µCT scan has been presented in several works (Kok et al., 2022; Robson Brown et al., 2014; Wijayathunga et al., 2008). Additionally, the outcomes of one µCT-based model were compared to the outcome of the same model mapped on a clinical CT to assess the correctness of the procedure. The steps required for the two kinds of model are reported in the following two paragraphs.

The hFE model was created based on the unloaded µCT scans. First, the µCT images were segmented adopting a semi-automatic segmentation procedure (Materialise Mimics), and a 10-node tetrahedral structural solid mesh was later created (ICEM, ANSYS Inc.), with an edge length equal to 1 mm (Costa et al., 2019). The material properties were assigned analogously for the healthy and pathological vertebrae. µCT grey levels were calibrated to obtain density values, using hydroxyapatite phantoms. Then, Bonemat software developed at Rizzoli Orthopaedic Institute was used to integrate the voxel density over each element of the mesh. Coefficients from the literature were used to define the density-elasticity relationship (Morgan et al., 2003). Subsequently, boundary conditions were assigned to the hFE model in order to reproduce the experiments. For each vertebra, the two DVC grid slices falling inside the bone and closest to the endplates (upperBC and lowerBC) were selected. The displacements of upperBC and lowerBC were interpolated onto the FE nodes at the extremity of the vertebral body through a trilinear interpolation algorithm (Matlab, Mathworks Inc.), such that the FE model could be loaded in displacement using experimental data (Fig.4.3B).

For one specimen, the same hFE tetrahedral mesh already mapped on µCT was roto-translated to a clinical CT acquired on the same specimen for a previous study (Palanca et al., 2021) using a procedure accurately described elsewhere (Garavelli et al., 2022). Then, the hFE was mapped on the clinical CT scans, calibrated using ESP phantom. A correction of the calibration was also applied (Schileo et al., 2008) and eventually a conversion from element density to elasticity (Morgan et al., 2003). After that, the inverse transformation matrix was applied to the hFE nodes to reposition the model back onto the µCT reference system. Eventually, the model was solved by applying the same boundary condition previously described for the µCT-based model.

The hFE simulations were run on a FE analysis environment (ANSYS Inc., Mechanical APDL) and performed on a local computer (parallel distributed memory over 6 cores with 64 GB of RAM (Intel(R) Xeon(R) E-2276G CPU 3.80GHz) and required around 1 hour.

The μFE model was generated following an already published procedure (Chen et al., 2017; Costa et al., 2017; Palanca et al., 2022), which is briefly reported in the following. Firstly, the unloaded μCT scan was filtered with a 3D Gaussian filter (σ = 1.2 and k = 3) and a single-level threshold based on the Max Entropy thresholding algorithm was used to binarize the images (Matlab, Mathworks Inc.). Then, each bone voxel was directly converted into an 8-node linear hexahedral element of the mesh, to which an elastic modulus of 12 GPa and a Poisson's ratio equal to 0.3 were assigned. Boundary conditions were applied consistently to the hFE model of the same vertebra (ANSYS Inc., Mechanical APDL). The μFE simulations were performed on a high-performance computing cluster (ShARC), requesting 10 cores from ShARC's scheduler with 50 GB of memory per CPU core and it takes around 3.5 hours.

Two additional tests were performed on one vertebra only, and are reported in Appendix B. The tests are respectively, the inclusion of an elastoplastic behaviour to the hFE model, and the propagation of the error on displacement to an error on the strains. The addition of plasticity is intended to improve the prediction of deformation in vertebrae that are nearing their elasticity limit. This is particularly useful for predicting fracture risk because once the limit is exceeded, the vertebra is permanently damaged, and we only need to know that it has fractured, not the exact value of the deformation. What's interesting is the moment of damage accumulation in the area just before the fracture. That's why it was important to determine whether adding plasticity would help us better track this phenomenon. The study of error propagation is based on the fact that it isn't possible to use the exact value predicted by the DVC to validate the strain of the models. However, the fracture definition in Chapter 1 is based on the strain. Therefore, we decided to quantitatively validate the displacements and qualitatively validate the strains. Then, we defined a procedure to evaluate the error propagation from displacements to strains.

4.2.3. Validation and Comparison

In order to compare the hFE model against experimental data and μFE model results the hFE nodal displacements were interpolated at the DVC points location using the shape functions of the elements. Specifically, a two-fold validation procedure was followed: at first, all DVC point locations were used, secondly, only a subsample of the aforementioned DVC points, namely the one falling inside a trabecula (Fig.4.3D) or within the cortical shell. The point-to-point validation was always performed on the central 75% of the modelled vertebra, in order to be sufficiently far from the nodes used to apply the boundary conditions (Fig.4.3C).
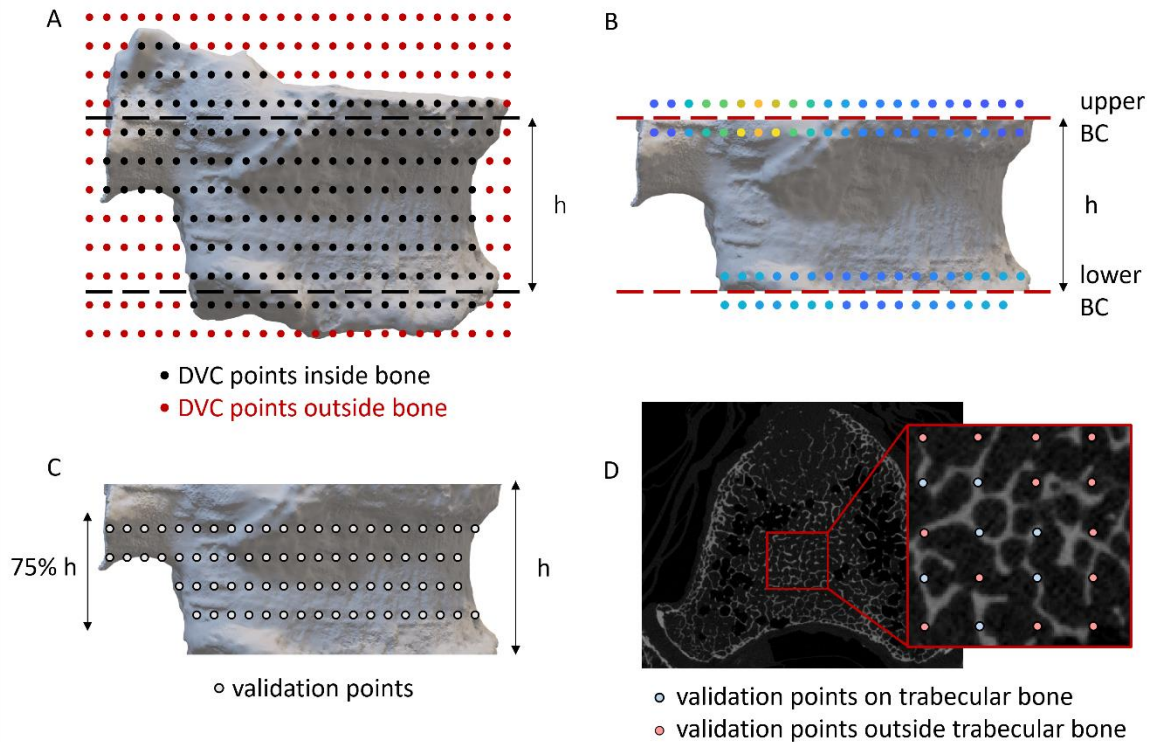
Fig.4.3: Definition of the DVC points (A, only red dots provide usable information) used for BCs assignment (B) and validation of the models (C). Among the latter only the validation points falling inside a trabecular bone were used also in the comparison between hFE and μFE (D).

4.2.4. Metrics

The agreement between hFE and DVC displacements as well as between hFE and μFE displacements was reported by computing the intercept and the slope of the linear regression, the coefficient of determination (R^2), the root mean squared error (RMSE), and the percentage RMSE (RMSE%), obtained normalizing the RMSE by the higher experimental displacement. Maximum and minimum principal strains obtained from the hFE model have been qualitatively compared to the one provided by the experimental test, to compare the location of the regions in which the deformations were concentrated. Conversely, it was not possible to directly compare hFE predictions with the ones from the μFE because the two mesh have different scales.

In addition, the agreement between the axial reaction forces predicted by the FE analysis and the ones measured during the experimental tests was assessed, in term of R^2, RMSE% and maximum error. The numerical reaction forces were computed in the axial direction at the nodes of BClineDOWN.

4.2.5. Exclusion Criteria

Among the tested specimens, some vertebrae needed to be excluded from the validation process. The following exclusion criteria were used: (i) more than 25% of the correlation points present experimental deformations over Bayraktar failure limits (Bayraktar et al., 2004), (ii) the lytic metastatic lesion has destroyed the trabecular lattice of the vertebra, for more than half of its body, and/or (iii) the prediction errors strongly correlate with the DVC uncertainties at the same locations. Each vertebra matching at least one of the criteria was excluded, while the other one from the same specimen was validated as usual.

4.3. Results

The comparison between μCT-based hFE and DVC displacements is shown in Fig.4.4, displayed differently according to the health status of the vertebra (control, lytic metastasis, mixed metastasis) they originated from. It is possible to observe that for all the directions and for all the categories the model slightly underestimated the experimental values. Anyway, no specific dependence of the goodness of fit on the health status of the vertebra was found. In fact, the strongest correlation in the anterior-posterior direction was found for the lytic vertebrae ($R^2 = 0.93$), while in the cranio-caudal direction that was found for the healthy ones ($R^2 = 0.83$). The RMSE% for the control vertebrae were in the range 3-22% and the maximum error was lower than 45 μm, while for lesioned vertebrae RMSE% was in the range 5-18% and the maximum error was lower than 54 μm. For pooled data the RMSE% were 6% for anterior-posterior and 13% for the cranio-caudal. The correlation indexes of each vertebra are also reported in the boxplots in Fig.4.5. The entity of the displacements in the right-left direction resulted to be lower than the voxel size for most of the points. For this reason, these displacements were considered too close to the experimental measurements uncertainties and were therefore excluded from the validation process.
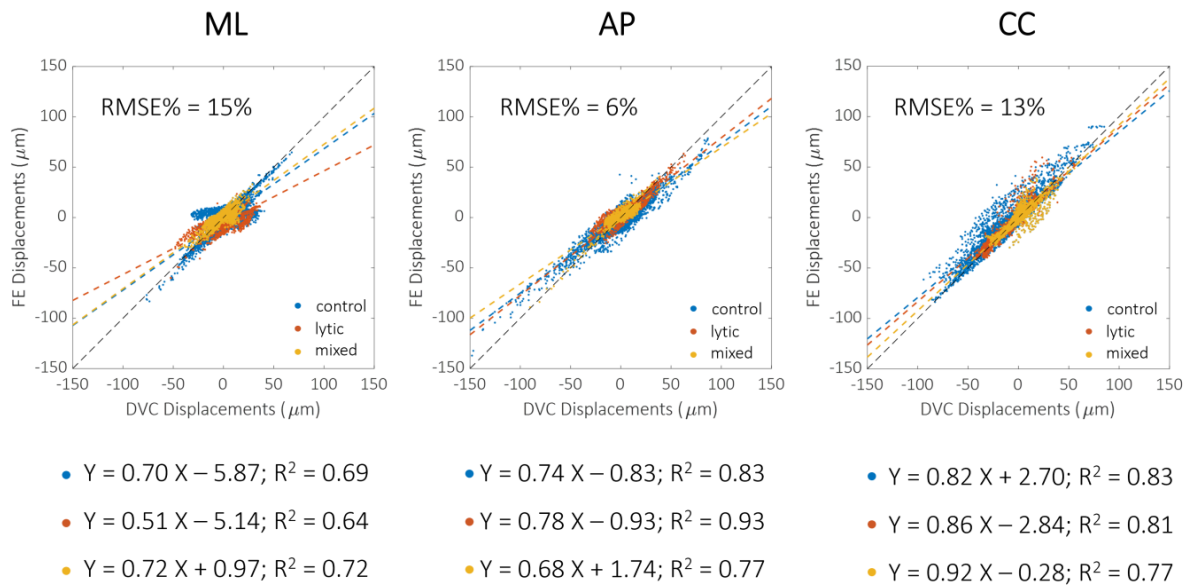
Fig.4.4: Comparison between DVC (horizontal axis) and hFE (vertical axis) displacements, on mediolateral (ML), anteroposterior (AP) and craniocaudal (CC) directions respectively. Control vertebrae are reported in blue, lytic in orange and mixed in yellow. For each type of vertebra regression lines and R^2 are also reported, while RMSE% in reported for the pooled groups.
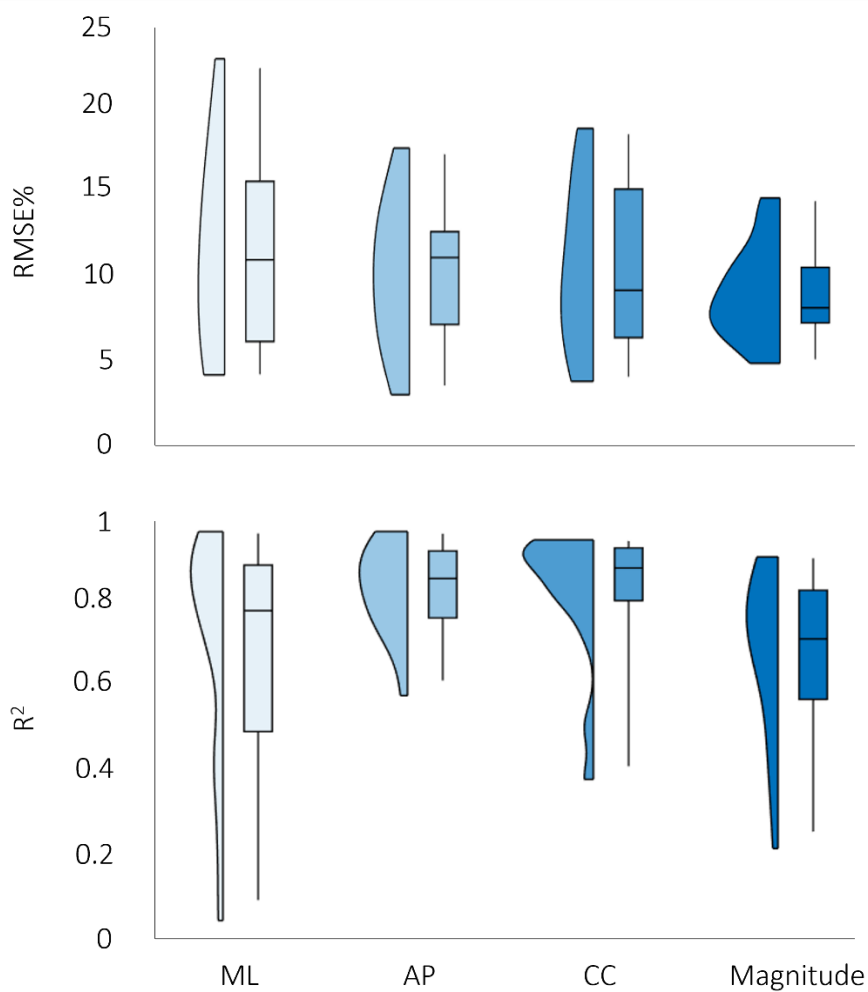
Fig.4.5: Boxplots reporting RMSE% and R^2 for all the vertebrae analysed. Red horizontal lines represent the ideal value for each index. Mediolateral (ML), anteroposterior (AP) and craniocaudal (CC) directions as well as the magnitude are reported.

Narrowing the analysis to those DVC points whose position lies within the trabecular bone, a substantial decrease in RMSE% is observable for the craniocaudal direction, while no strong differences are observed for the anteroposterior direction (Fig.4.6).
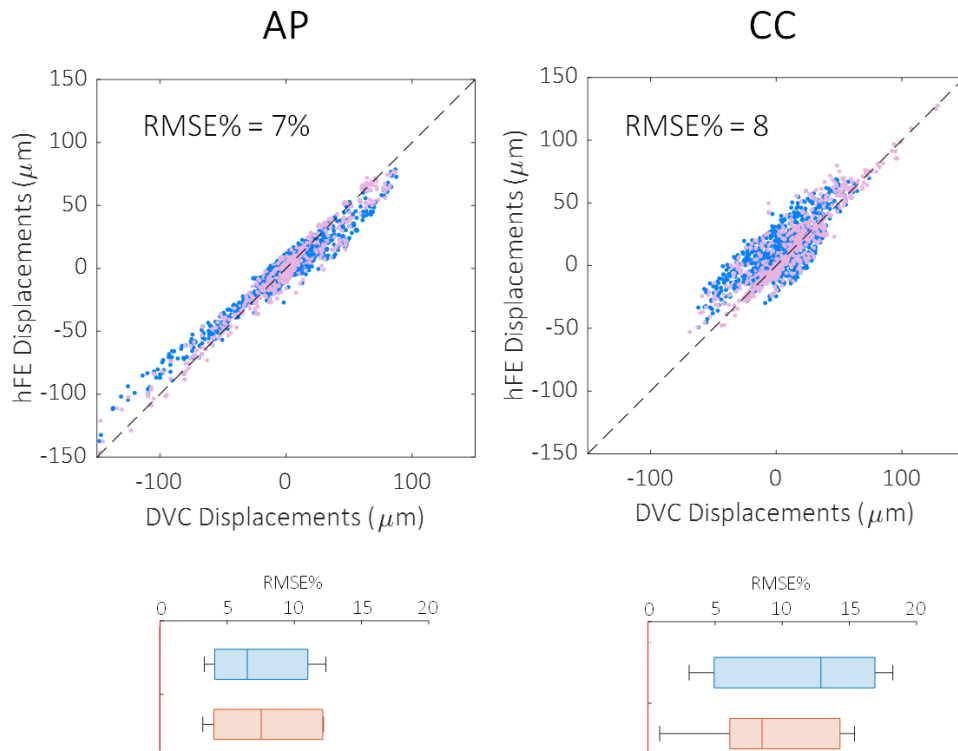
Fig.4.6: Scatter plots between DVC (horizontal axis) and hFE (vertical axis) displacements on trabecular locations only, on anteroposterior (AP) and craniocaudal (CC) directions respectively. Below each direction, the relative changes in RMSE% due to the restriction of the analysed points are reported (light blue before, pink after the restriction).

Furthermore, strong agreement in the displacements field was found between the μCT-based and the clinical-CT-based models, with RMSE lower than 0.75 µm (RMSE% < 1.3%) and R^2 higher than 0.99. The maximum difference among all the nodes and considering the three cartesian directions was 6 µm (Fig.4.7). In terms of predicted reaction forces, the difference between μCT-based and clinical-CT-based models is around 1%, specifically 2088 N in the former case and 2119 N in the latter.
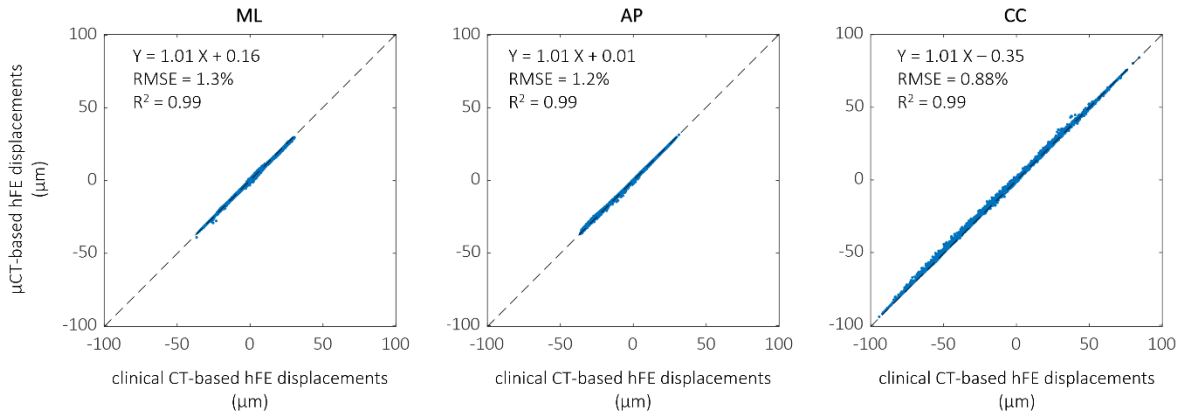
Fig.4.7: Correlations between displacement fields predicted by clinical-CT- (horizontal axis) and µCT-based (vertical axis) models. Regression lines, R^2 and RMSE% are reported.

Looking at the comparison between the hFE and µFE models, the hFE model showed an accuracy in the prediction of the displacements comparable to the µFE model, with determination coefficient higher than 0.95 and root mean squared error equal to a tenth of a voxel (Fig.4.8) for the pooled data. In terms of RMSE% the results were in the range of 3-29%, while the 95-th percentile of the differences between hFE and µFE displacements was in the range 2-61 µm. In Fig.4.8 it is possible to observe that only one model (light blue dots) seems to present a strongly worse behavior than the other, corresponding to a vertebra that has already overcome the elastic regime.

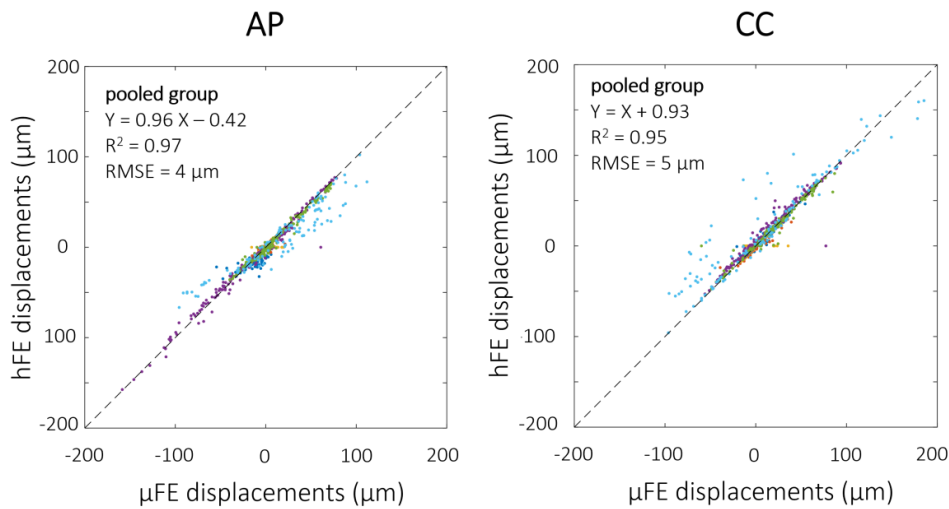**Fig.4.8**: Scatter plots between µFE (horizontal axis) and hFE (vertical axis) displacements, on anteroposterior (AP) and craniocaudal (CC) directions respectively. Regression lines, R^2 and RMSE are reported. Each vertebra is plotted in a different colour to highlight that most scattered points derive from the same vertebra.

A qualitative comparison of experimental and simulated strains is also reported. The distribution of maximum and minimum principal strains highlighted that the hFE models were able to select the regions of the vertebral body providing the highest strain concentration (Fig.4.9).
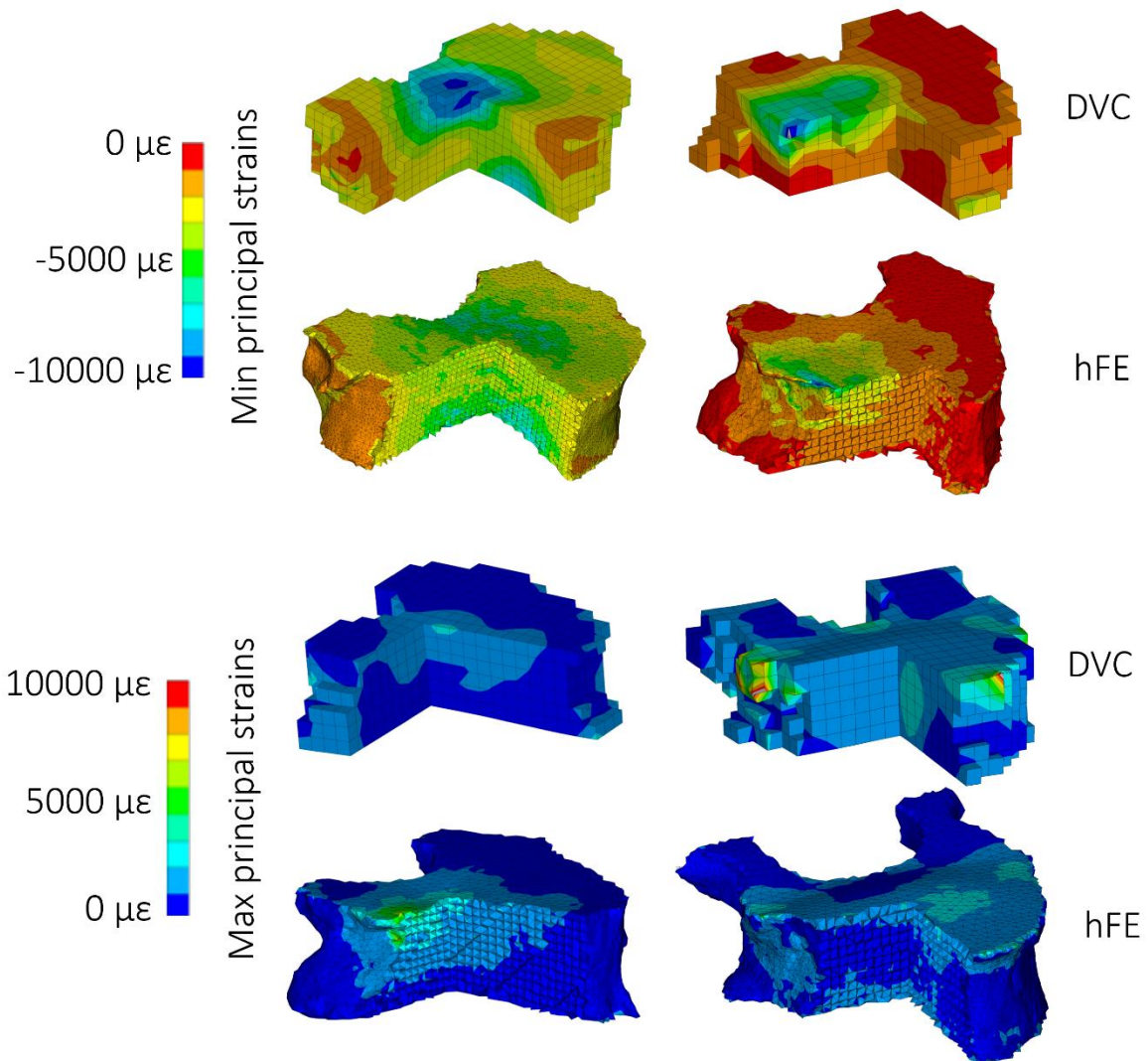
Fig.4.9: Qualitative comparison between DVC and hFE strains. Four different vertebrae are reported as examples; for each one the upper contour plot refers to the DVC hexahedral grid, while the lower refers to the hFE tetrahedral mesh. The figure highlights that for the majority of the specimens the regions presenting higher deformations are correctly predicted (B, C). However, there are still some specimens for whom the FE models fail in founding the highly deformed regions (A, D).

Lastly, quite good correlation was found between the axial reaction forces predicted by the FE analysis and the ones measured during the experimental tests, with $R^2 = 0.65$, RMSE = 19% and maximum error equal to 1368 N (Fig.4.10).
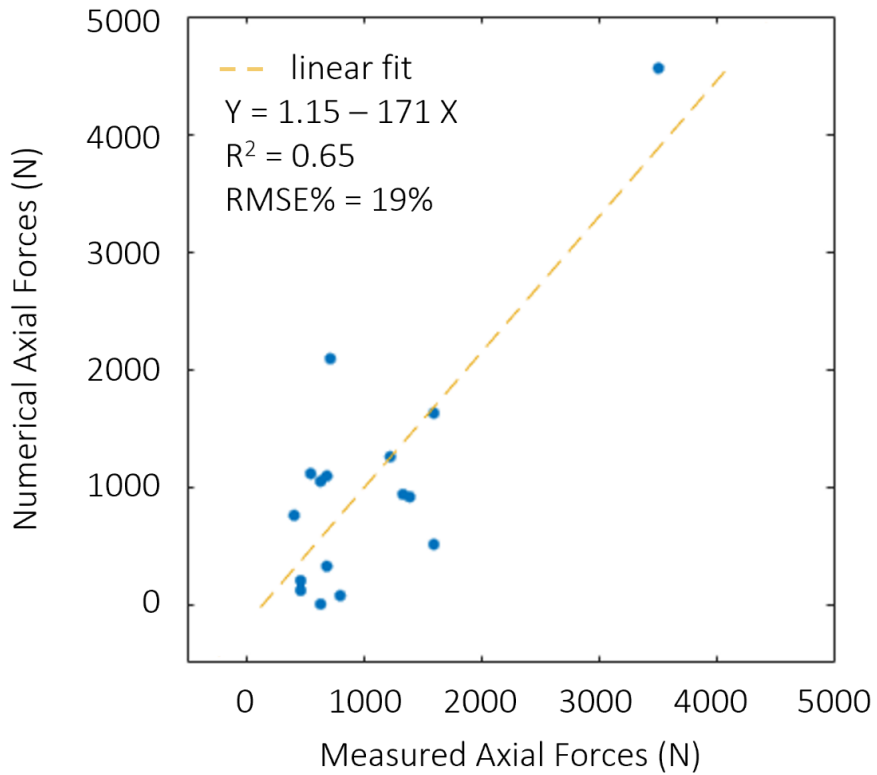
Fig.4.10: Comparison of axial reaction forces predicted by the vertebral hFE models and the experimentally measured ones. Regression line (yellow), R^2 and RMSE% are reported.

Among the analysed vertebrae, three (1 control, 1 lytic and 1 mixed) were excluded from the validation because they fitted one of the Exclusion Criteria (Appendix C).

4.4. Discussion

This study aimed to assess the accuracy of subject-specific hFE models of the vertebra with experimentally matched BCs directly applied in the prediction of displacements and strains compared to a widely used experimental method.

Good agreement between DVC and hFE displacement fields, both for healthy (R^2 = 0.69÷0.83, RMSE% = 3÷22%, max error < 45 μm) and metastatic (R^2 = 0.64÷0.93, RMSE% = 5÷18%, max error < 54 μm) vertebrae, was found. Furthermore, the models were able to qualitatively identify the regions which experimentally showed the highest strain concentration. The derivation of displacements error to strains errors is also reported in Appendix B, with average errors around three thousands of microstrains. However, it is important to highlight that the errors committed by the homogenised FE models were obtained in presence of a DVC uncertainties identified in zero-strain conditions of 6÷9 μm for the displacements field and average errors around two thousands of microstrains for the strains field (Cavazzoni et al., 2023). Consequently, the difference between the prediction errors and the experimental uncertainties were less than two order of magnitude. This does not allow to consider the model validated however the theories embodied by the models have resisted attempts at falsification by the DVC experimental. In addition, quite satisfactory agreement was found in the reaction forces (R^2 = 0.65, RMSE% = 19%) corroborating the density-elasticity law employed.

The presented results in terms of FE displacement prediction of DVC measurements were found to be in agreement with the ones reported by Palanca et al., 2022. There, μFE models of porcine vertebrae were developed and experimental derived displacements were applied as BCs, supporting the implementation performed in this study, to be eventually compared against DVC (RMSE% =1.01-14.51, R^2 = 0.65-1.00, slope = 0.77-1.19). The lower correlation found in this study compared to Palanca et al., 2022 could be explained considering that the work used porcine healthy specimens with induced lesions, while this study tested human vertebrae, some of them with lytic or mixed metastasis, and this aspect increased the difficulty in the material modelling. Jackman et al., 2016 performed human vertebra FE models validation against DVC with an experimental set-up similar to the one in this study. Their findings for the compression tests with experimentally matched boundary conditions showed a median error in displacements in the range of 20-80% (average = 49%). Computing the same value for the presented data the resulting range is 13-109% (average = 39%), highlighting a comparable fitting of the experimental data. DVC techniques have also been applied in the validation of hFE models of the scapular bone, analysing both the displacements (Kusins et al., 2019) and the strains fields (Kusins et al., 2020) respectively with point-to-point and averaged comparisons. This study achieved slightly inferior results in terms of displacement field prediction for the same boundary condition application approach (R^2 =0.40-0.98, slope =0.43-1.32 in this study versus R^2 =

0.79-1.00, slope = 0.87-1.09 in Kusins et al., 2019). Also, the correct identification of the regions which experimentally showed the highest strains concentration by the hFE was confirmed in Kusins et al., 2020. Analysis at different scales for the vertebral mechanics had been already presented by Stadelmann et al., 2020. Even if they did not perform a point-to-point comparison between the two models as well as has been here presented, their conclusions supported our finding that hFE and µFE could provide comparable results inside the physiological range of deformation.

It is necessary to highlight some limitations of this work. Firstly, as explained above, the comparison was made only for vertebrae that did not show visible signs of failure at the time of the loading scan. This is because the developed models were linear elastic and, therefore intrinsically unable to correctly predict deformations beyond the elastic regime. Further improvements in both computational and experimental methods are needed to quantitatively analyse the post-yield behaviour of the vertebra. Secondly, the necessity to sacrifice the endplates regions to inform the models excluded these regions from the validation, although they are known to be of major interest for the failure mechanisms (Palanca et al., 2023). This criticality could be overcome only when it will be possible to obtain accurate DVC measurements for soft tissues (and therefore also of the discs), to be able to move the application area of the boundary conditions externally to the endplates.

In conclusion, the combination of the experimental DVC technique and the FE modelling technique has allowed to develop a promising pipeline for validation of in silico predictors of fracture risk. However, as already mentioned, the models prediction errors identified were not sensitively higher than the experimental data uncertainties, which prevented to consider the model validation successful. Two possible approaches could be followed to overcome this conundrum. On one side, to the use of imaging techniques able to reach a higher resolution, lower than a micrometre. Nevertheless, imaging tools able to achieve this level of resolution cannot currently be applied to a whole vertebra, but only to a portion of it, acquiring only some trabeculae at a time. On the other side, an extensive tests campaign where the numerical failure load would be validated against experimental data could be carried out, to provide evidence of the accuracy of hFE models on a different level.

Chapter 5

Conclusion

In the last chapter, the main achievements of this PhD project are summarised, focusing on the original contribution that this thesis brings to the biomechanics field. After that, the major limitations of the presented studies are recalled, and to conclude, the possible direction in which this work can proceed are listed.

5.1. General

The aim of this PhD thesis was to assess the accuracy of subject-specific homogenised finite element models of multi-vertebrae segments generated from clinical CT scans in predicting the minimum load required to induce a vertebral fracture. The accuracy of the predictions of such models was assessed through comparison with experimental data obtained adopting two distinct full-field techniques: DIC measuring the displacements on the bone surface and DVC acquiring three-dimensional displacement fields across a specimen. The project has been developed in multiple steps, described in Chapters 2, 3, and 4. The work started with the validation of the superficial predictions of a multi-vertebral model. Then the focus was shifted to the single vertebrae models.

In Chapter 2, a multi-vertebral segment (with both healthy and metastatic vertebrae) was imaged with a clinical CT scanner and experimentally tested in presso-flexion conditions. The displacement field on the vertebral surfaces was tracked using the DIC technique. Then, an FE model was generated from the CT scan, loaded in accordance with the experiments, and validated against the previously acquired experimental data. The model showed good accuracy in the replication of spine kinematics: the FE model predicted displacements with an R^2 higher than 0.94 and a RMSE% lower than 8%. While the DIC technique had already been used to validate bone models, showing interesting results (Ghosh et al., 2012; Grassi et al., 2013; Gustafson et al., 2017), this was the first time it was employed to validate the model of a multi-vertebra segment subjected to physiological loading.

In Chapter 3, the same model was used, but the focus was shifted towards its strain prediction accuracy assessment. The working hypothesis of the project was that in order to predict the risk of vertebral fracture, it would be sufficient to use subject-specific information from clinical CT to inform the geometry and material properties of each vertebral body, while it would have been sufficient to use population-specific information to characterise the material properties of the intervertebral disc. Because of this assumption, we used the simplest possible constitutive equation to model the disc, as any more complex law would have been more sensitive to the uncertainty of the material properties. The hypothesis of linear elastic isotropic material properties was made for the discs, and the range of Young's modulus values available in the literature was explored. The study showed that varying disc properties inside the physiological values reported in the literature caused significant variations in the vertebral strains field. These findings suggest that an accurate prediction of bone deformation would also require a personalisation of the mechanical properties of the discs, which, unfortunately, may also require a clinical MRI exam.

In light of the discrepancies observed in the strain prediction, the last part of this work, described in Chapter 4, was conceived. Here the focus was shifted to the analysis of the three-dimensional strain field inside individual vertebrae, aiming to establish whether a homogenised FE model of a single

vertebra could only provide accurate predictions of displacements and strains when provided with boundary conditions coming from the experimental tests and, in particular, determined using DVC technique. Both healthy and metastatic human vertebrae were analysed. The results showed that linear elastic FE models exhibited accuracy comparable to DVC within the elastic range for both displacement and strain. In particular, the displacements were characterised by RMSE% settling in the 3÷22% (controls, max errors < 45 μm) and 5÷18% (metastatic, max errors < 54 μm) ranges. These findings were in agreement with previous works performed on healthy vertebrae (Jackman et al., 2016, on displacements) and scapular bone (Kusins et al., 2019 on displacements; Kusins et al., 2020, on strains), where similar approaches were used. Furthermore, the study also highlighted the FE models' capability to identify the regions where the highest strains were located experimentally. The homogenised FE model displacement fields were also compared to the ones of micro-FE models subjected to the same boundary conditions, obtaining comparable accuracy (R^2 higher than 0.95, RMSE equal to a tenth of a voxel, RMSE% in the range 3÷29% and 95th percentile in the range 2÷61 μm) until the elastic limit is exceeded. Once validated, these *in-silico* tools could support clinical decisions where the subject-specific fracture risk assessment is of interest; thus, the homogenised micro-CT based FE model was also compared to a clinical CT-based model of the same specimen and subjected to the same boundary conditions, achieving excellent agreement ($R^2 = 0.99$, RMSE% < 1.3%, max error = 6 μm). Although the displacement prediction errors appear small, the prediction of the risk of fracture is based on the prediction of strain; if we use numerical methods to estimate the prediction error on the strain given the prediction error on displacements (the derivation of these errors from displacements to strains is reported Appendix B), we see that strain prediction errors of the FE model are comparable to the accuracy on strain measurements expected for the DVC method at that imaging resolution, as estimated with zero-strain studies (Cavazzoni et al., 2023; Dall'Ara et al., 2017).

So, while the DVC methodology appears to be a promising validation pipeline for these in silico predictors with respect to the predicted displacements, in these conditions, it is difficult to draw conclusions on the accuracy of the FE model in predicting strains. For this purpose, we would need to reduce the measurement error (accuracy) of the DVC by at least one order of magnitude. This is possible only by drastically increasing the spatial resolution of the micro-CT images used in the DVC calculation. While this is possible (for example, by using synchrotron-light Computed Tomography), the limitations of the CCD sensors would impose a much smaller field of view. This would require validation only in a small region of the vertebrae or the development of a multi-scan protocol with all the issues of spatial registration of the scans.

Another point of view is to conclude from this validation campaign that the displacement fields the in silico predictor provides are not significantly different from those experimentally measured with digital volume correlation. Thus, this validation study did not falsify the assumption that our in silico

predictor is sufficiently accurate to predict the clinical risk of vertebral fracture. We could then proceed to the next step of the credibility assessment of the predictor by exploring if the load to failure predicted by the FE model, assuming certain loading conditions do correlate with the fracture events observed in a sufficiently large clinical cohort.

In summary, this work highlighted that when the boundary conditions are accurately modelled, subject-specific CT-based FE vertebral models can predict displacements and strains with accuracies comparable to that of the experimental method used for the validation. Still, looking at multi-segment models, the model's predictions are highly sensitive to the biomechanical properties of intervertebral discs. Thus, our hypothesis that an accurate model can be built with population-specific properties for the intervertebral disc is falsified.

5.2. Limitations and future perspectives

In the following sections, the thesis limitations are presented and discussed, along with potential improvements.

A first critical consideration involves the mechanical properties assigned to the intervertebral discs, according to what was described in Chapters 2 and 3. The discs were modelled using the simplest possible approach. This obviously does not accurately reproduce the reality. Moreover, no distinction between annulus and nucleus was implemented because it is not possible to extract this information from the CT scans. More complex constitutive laws to model the mechanical behaviour of the IVD might have been examined in addition to the linear elastic one adopted. Still, the unavailability of patient-specific information retrievable from the CT images would have required the identification of the constitutive model's parameters either 1) through minimisation of the error between the numerical and experimental strains or 2) by assigning literature-based population values. As far as the first case is concerned, in light of the challenging identification of one single parameter able to minimise errors on strains, the inclusion of additional parameters to handle a more complex law (such as viscoelastic or hyper-elastic) would decrease the chances of discovering an optimal condition. In the second case, the adoption of more complex constitutive models using population-based parameters would be limited by the lack of experimental literature for the definition of such multiple coefficients.

Therefore, the adoption of more complicated constitutive laws to model the IVD was not considered within the specific focus of this thesis, which was to assess the possibility of predicting the vertebral fracture risk *in silico* starting from a clinical CT. In this respect, the conclusion that could be drawn from the work presented in this thesis is that IVD modelling is pivotal in determining the mechanical response at the vertebral level and thus should be modelled accounting for its patient-specific and heterogeneous structural features. In this context, the adoption of more complex constitutive modelling, still lacking patient-specific information, would not be sufficient to improve the strains' prediction accuracy.

Experimental evidence supporting this point can also be found in a recent study carried out by Dr Palanca, part of Prof Cristofolini's research group at the University of Bologna, where the effect of the IVD mechanical properties on the collapse of the vertebral bone was experimentally highlighted. The presence of a healthy IVD was indeed shown to lead to the collapse of the vertebra at the region of the endplates (Fig. 5.1A), differently from the buckling in the central part of the vertebral body (Fig. 5.2B) in the case the IVD had been enzymatically degraded.
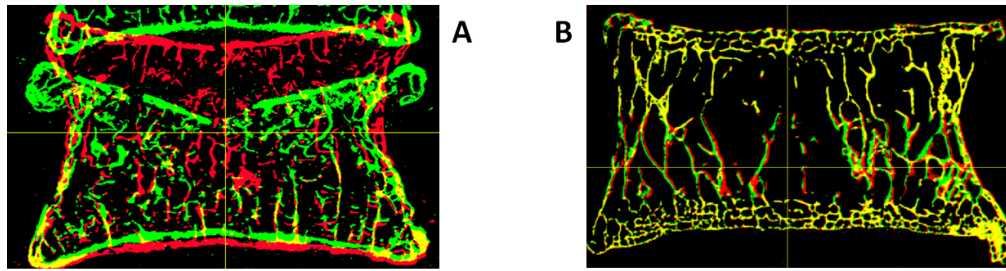
Fig. 5.1: µCT scans of vertebrae after the collapse, when the load is transmitted through a healthy (left, A) or a degenerated disc (right, B). The scans of the unloaded vertebrae are reported in red, while the scans of the vertebrae after failure are reported in green. The yellow regions represent the perfect overlap of the two scans, namely the regions in which no failure appeared.

The transmission of load through the vertebral bodies thus appears to take place in a way that is unique to each individual and is a result of the vertebral organogenesis process that takes around 15 years. Therefore, it is essential to have information about the material properties of a specific IVD in order to generate a model of the spine. Even if the complexity of the IVD model is increased, there would still be the risk of incorrectly predicting the vertebral deformation unless subject-specific material properties are also taken into account for the IVD.

An alternative possible strategy would involve the use of additional/alternative imaging information (e.g., magnetic resonance imaging information) as input, aiming to integrate the IVD mode with patient-specific and heterogeneous information. Having said this, this would require the definition of a mathematical relation between the images' local information and the discs' local material properties, which is not yet available in the literature.

The second area of limitations concerns the boundary conditions assignment. In fact, as far as the FE models of the spine segment are concerned, it was assumed that no relative motion occurred between the cranial potted vertebra and the cement it was potted in, as well as between the cement and the metal pot in which it was inserted and locked. However, this assumption was reasonable due to the considerably greater stiffness of the metal pots compared to the specimen, also given the secure connection ensured by the screws. As far as the DVC-based FE model validation, the main issue was related to the use of experimental information in the vertebral body portion closer to the endplates to apply boundary conditions to the model. In fact, this choice, which is strictly linked to a single vertebra FE model, prevented us from considering the endplates in the analyses, which, however, do represent regions where fracture often originates (Palanca et al., 2023). To overcome this limitation, a potential approach could be to include DVC information on the discs when it is possible to apply this technique to the discs as well. This would indeed allow a more accurate comparison between model

and experiment, as the model boundary conditions could come from the discs and not from the vertebral endplates as in the here presented study.

The third point is connected to the material properties assigned to the vertebral bone. As explained, the same constitutive laws were employed for all the vertebrae analysed in the different studies without taking into account the vertebrae's health status. While this choice may have introduced some inaccuracies, it was aligned with the findings of other authors who observed similarities in the mechanical properties of trabecular bone with and without lesions (Nazarian et al., 2008; M. A. Stadelmann et al., 2020). If this assumption holds when metastatic lesions can be characterised as low-density bone tissue, as in the case of lytic lesions, it might not be accurate enough for blastic lesions. If evident signs of blastic metastatic lesions are detected, other constitutive models may be used to reproduce better the real mechanical behaviour of that kind of tissue.

Last, it should also be noted that in the first two parts of the work (Chapters 2 and 3), the developed method was presented on one specimen only because they were methodological works. However, the procedure could also be applied to multiple specimens to strengthen the obtained results.

In conclusion, the accurate prediction of the risk of vertebral fracture using a subject-specific finite element model of the spine informed only by a clinical CT scan does not seem to be feasible. In the context of fragility fracture, further work may explore if the use of an MRI exam in place of the CT exam would provide better results. MRI may provide more information on the mechanical properties of the intervertebral discs but would lack the excellent correlation between X-ray attenuation and mineral content that CT data provide. We are optimistic that the combination of MRI and CT data would allow the development of an accurate predictor, but the clinical applicability of such protocol seems unlikely in the context of fragility fractures.

This may be different when the model is used to predict the risk of vertebral fracture in patients with metastatic lesions in the spine as a decision-support for treatment stratification (e.g., radiotherapy vs vertebroplasty). These patients are normally examined with CT and MRI; thus, the theoretical possibility of developing a sufficiently accurate decision-support system exists in this context. However, for now, accurate predictions would be limited to patients with clastic lesions, as the modelling of blastic lesions probably requires additional research.

Appendix A
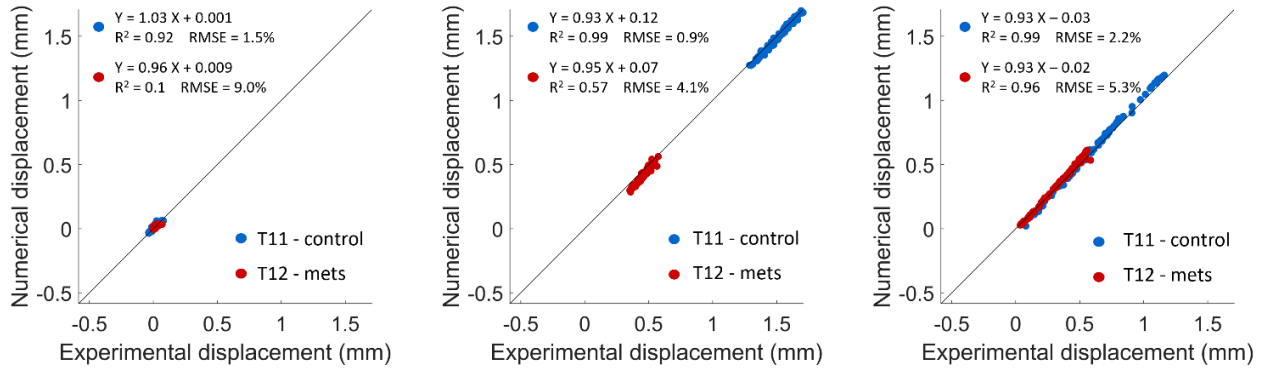
Fig.1s: Comparison between the displacements intensity measured using DIC and the ones predicted by the FE model on the vertebral surfaces. Linear regression, coefficient of determination and root mean squared error are also reported.

	E_{disc} (MPa)	control								lesioned							
		left		central		right		total		left		central		right		total	
		ε_{MIN}	ε_{MAX}	ε_{MIN}	ε_{MAX}	ε_{MIN}	ε_{MAX}	ε_{MIN}	ε_{MAX}	ε_{MIN}	ε_{MAX}	ε_{MIN}	ε_{MAX}	ε_{MIN}	ε_{MAX}	ε_{MIN}	ε_{MAX}
RMSE ($\mu\varepsilon$)	4.15	3439	2166	3464	2067	1945	1472	2955	2030	3789	1396	8023	2307	8333	1944	7515	2096
	10	2931	2005	2762	1903	1408	1366	2407	1890	3202	1232	7084	2064	7532	1767	6797	1915
	25	2017	1666	1600	1552	528	1128	1477	1589	2201	921	5413	1584	5993	1419	5463	1562
	30	1833	1572	1466	1453	562	1058	1342	1504	2039	846	5068	1463	5616	1330	5157	1471
	35	1709	1485	1471	1363	741	992	1301	1426	1966	784	4819	1356	5297	1252	4910	1393
	50	1660	1265	1988	1130	1437	817	1584	1223	2162	666	4570	1137	4642	1073	4480	1216
RMSE%	4.15	105	101	86	100	84	106	100	108	96	104	132	102	141	102	157	116
	10	89	93	65	92	53	96	79	96	77	89	122	91	132	94	149	109
	25	65	75	39	74	28	84	53	84	49	63	108	71	112	78	135	93
	30	62	71	43	70	35	80	56	80	52	58	104	66	108	74	128	90
	35	56	70	50	69	47	72	62	72	57	54	104	64	104	71	96	87
	50	68	60	77	59	85	62	81	65	80	54	104	58	98	65	77	84
R²	4.15	< 0.1	< 0.1	0.55	< 0.1	0.46	0.21	0.15	0.10	0.20	0.14	< 0.1	< 0.1	0.24	< 0.1	0.11	< 0.1
	10	< 0.1	< 0.1	0.54	< 0.1	0.46	0.20	0.15	0.10	0.20	0.14	< 0.1	< 0.1	0.24	< 0.1	0.11	< 0.1
	25	< 0.1	< 0.1	0.54	< 0.1	0.46	0.17	0.15	0.10	0.20	0.13	< 0.1	< 0.1	0.25	< 0.1	0.11	< 0.1
	30	< 0.1	< 0.1	0.53	< 0.1	0.47	0.17	0.14	0.10	0.20	0.13	< 0.1	< 0.1	0.25	< 0.1	0.11	0.10
	35	< 0.1	< 0.1	0.53	< 0.1	0.48	0.16	0.14	0.10	0.20	0.13	< 0.1	< 0.1	0.26	< 0.1	0.11	0.10
	50	< 0.1	< 0.1	0.53	< 0.1	0.48	0.14	0.14	0.10	0.20	0.12	< 0.1	< 0.1	0.26	< 0.1	0.11	0.11

Table 1s: Correlation indexes between predicted and experimental local displacements. RMSE, RMSE%, and R^2 between experimental and FE local strain measurements for all the E_{disc} considered were reported, for both the control and the lesioned vertebra, considering each RoI as well as the total analysed lateral surface.

Appendix B

The following two sections report tests performed on one vertebra only. The first aimed at assessing if the inclusion of a simple bilinear plastic behaviour to the hFE model can improve the models accuracy. The second aimed at defining a way to propagate the errors on displacement to errors on the strains.

Plasticity

An elastoplastic behaviour was also integrated in the hFE model development using a bilinear, isotropic behaviour, and a symmetric yield stress criterion. Similar approach have already been applied in the estimation of the mechanical competence of vertebrae with lytic metastases (Costa et al., 2019). The plasticity coefficients were taken from the literature and were defined as follows.

$\sigma_{y1} = 21.70 * \rho_{app}^{1.52}$ [g/$cm3$]   (Morgan & Keaveny, 2001)   (Eq.2)

$Ep_y = 0.05 \times E$ [MPa]   (Bayraktar et al., 2004; Morgan et al., 2003)   (Eq.3)

The elastoplastic hFE displacement field was compared to the elastic hFE displacement field, as well as to the experimental measurements.

Elastic and elastoplastic hFE models showed good accordance in the craniocaudal direction (RMSE% = 2%), while lower accordance in the anterior-posterior one (RMSE% = 10%), and looking at the validation against the DVC measurement, it was possible to highlight a strong decrease in the data fitting (Fig.2s).

Since the correlations instead of improving worsen slightly, it was concluded that non-inclusion of the plasticity in the model was not the main source of the error in the prediction of the experimental outcomes.
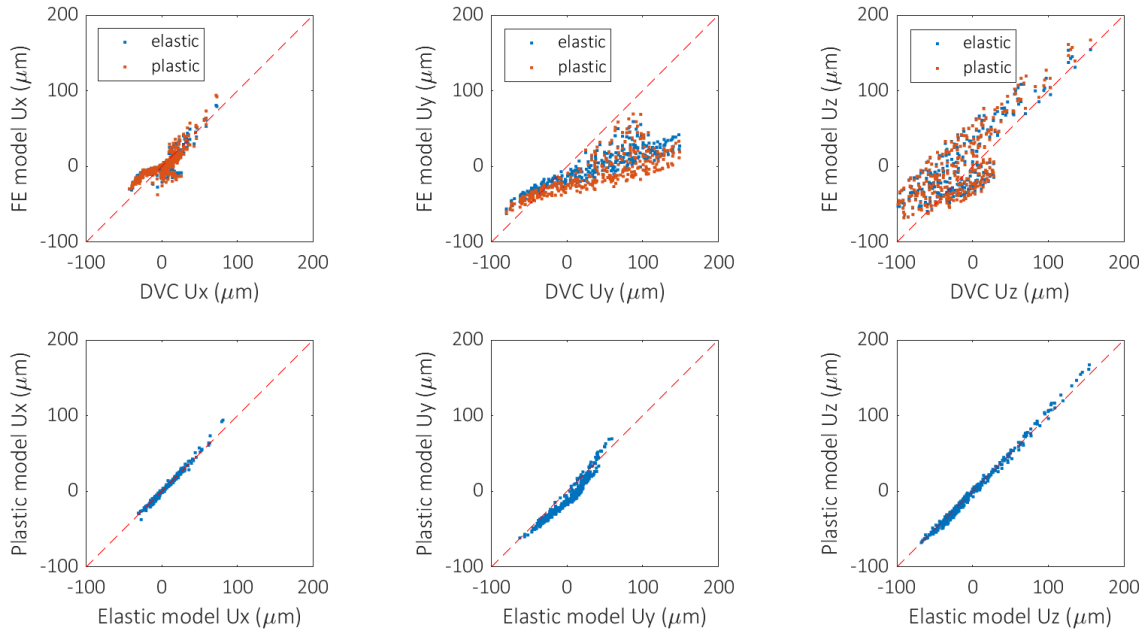
Fig.2s: In the first row, the correlations between displacement fields calculated by DVC (horizontal axis) and predicted by the FE (vertical axis) models, both with elastic (blue) and elastoplastic (orange) material properties assigned. In the second row, the correlations between the two models are also reported.

# Error Propagation

The possibility of propagating the error on displacement to an error on strain was analysed, considering that the displacement is the original variable computed by the experimental procedure. Firstly, an estimation of the error on strain was performed considering the predictive error on displacement given by the difference between FE and DVC displacements and dividing it by the grid nodal spacing (~ 2 mm). The order of the error was compared to the order of the uncertainty on strains. Then, the point-to-point difference between hFE and DVC displacements at the DVC points locations was superimposed to each node of the hexahedral DVC mesh and the FE simulation environment (ANSYS, Inc.) was used to derivate the local errors on the strain field. Subsequently, the zero-strain value at the relative point was used to reduce the error on strains, to remove the portion of error explained by the experimental uncertainty, and the distribution of the residual error was examined.

Considering the correlations obtained for the displacement field, the estimation of the error on the strains resulted in the range 0.001-0.025 ε while the experimental zero-strain were in the order of 0.001 ε, at worst an order of magnitude less. These results were confirmed also analysing the point-to-point distribution of the error on strains (Fig.2s). The comparison between the distribution of the error

on the strains and the distribution of the experimental uncertainty for the same vertebra is also reported in Fig.3s.
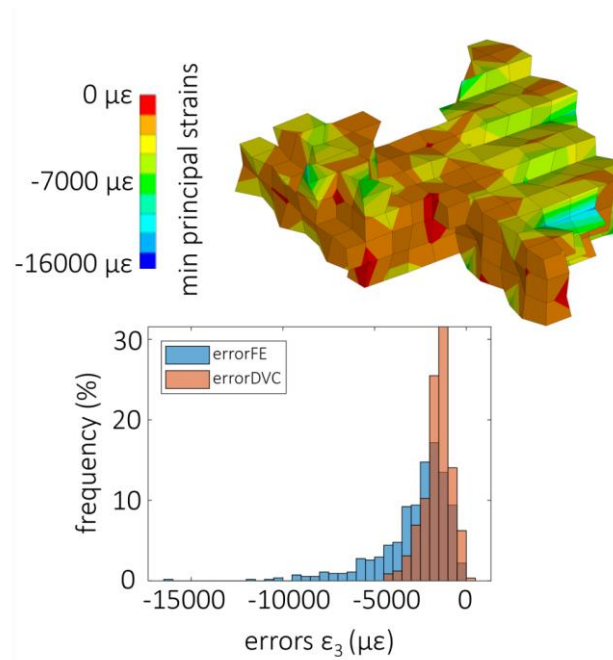

Fig.3s: On the top, the contour plot of the minimum principal strain due to the derivation of the displacement error is presented. On the bottom, the histogram of the predictive error (errorFE in blue) on the minimum principal strain is compared to the one of the experimental uncertainties (errorDVC in pink) for the same vertebra.

Appendix C

Among the analysed vertebrae, three have been excluded from the validation because they fitted one of the Exclusion Criteria, as reported below:

1) One vertebra showed experimental deformations over Bayraktar failure limits in more than 20% of the correlation points (Fig.4s).
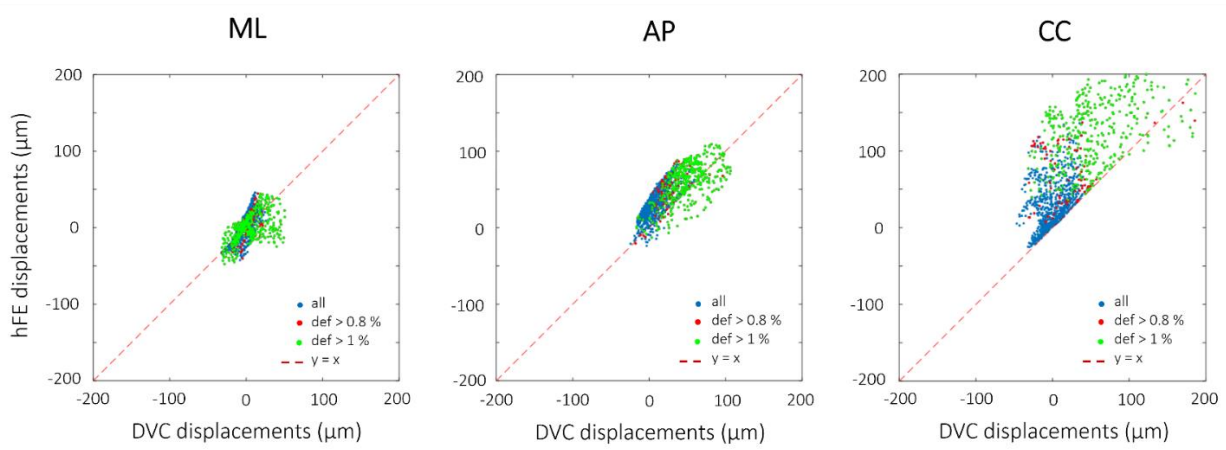
Fig.4s: Scatter plots between DVC (horizontal axis) and hFE (vertical axis) displacements, on mediolateral (ML), anteroposterior (AP) and craniocaudal (CC) directions respectively. The points in which the maximum and/or the minimum principal experimental strains overcome 0.8% (red) and then 1% (green) are highlighted in order to show that in the points with higher deformations the model have higher difficulties in reproducing the experimental data. The points in which all the strain components are lower than 0.8% are reported in blue.

2) One vertebra had a lytic metastatic lesion that had destroyed the trabecular lattice for more than half of its body. This strongly reduced the points of the DVC grid inside the bone (Fig.5s).
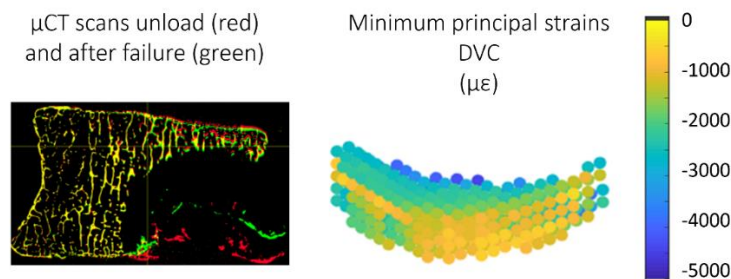
Fig.5s: The lytic lesion in this vertebra was bigger than half of the vertebral body as is possible to see from the μCT scan on the left. On the right the DVC points able to correlate are reported.

3) One vertebra showed a strong dependence of the prediction errors to the DVC uncertainties at the same locations (Fig.6s). Predictive error was computed has the absolute difference between DVC and FE displacements at each correlation point. DVC errors at zero-strain conditions were computed as the average of the six components of the strains derived from the experimental displacements computed applying BoneDVC algorithm to two unloaded scans of the same vertebra (Cavazzoni et al., 2023).
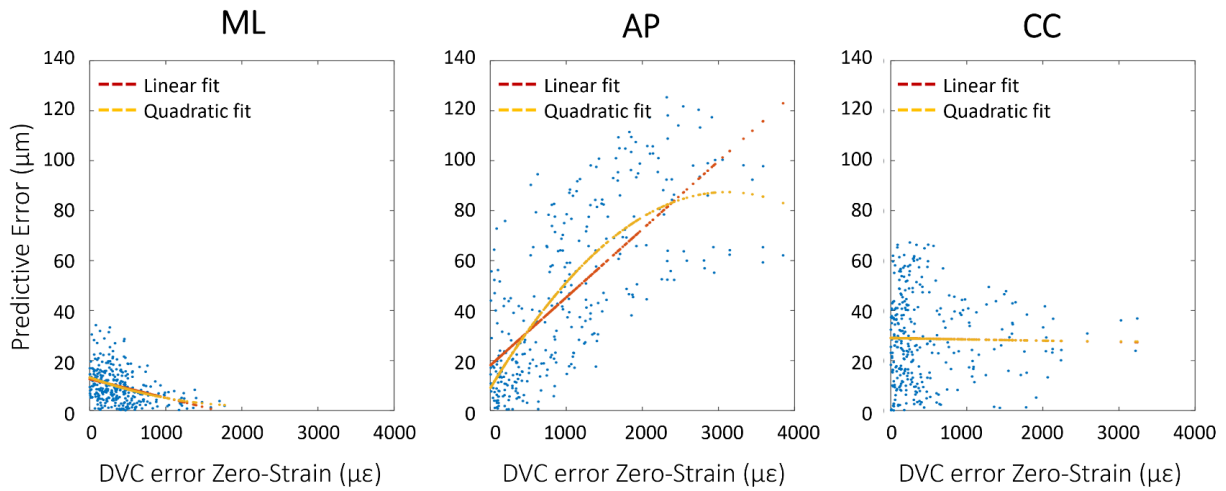
Fig.6s: Scatter plots between DVC uncertainties (horizontal axis) and predictive errors on displacements (vertical axis), on mediolateral (ML), anteroposterior (AP) and craniocaudal (CC) directions respectively. In the AP direction strong dependence was highlighted.

Bibliography

Acciaioli, A., Falco, L., & Baleani, M. (2020). Measurement of apparent mechanical properties of trabecular bone tissue: Accuracy and limitation of digital image correlation technique. *Journal of the Mechanical Behavior of Biomedical Materials*, *103*, 103542. https://doi.org/10.1016/j.jmbbm.2019.103542

Adachi, J. D., Olszynski, W. P., Hanley, D. A., Kendler, D. L., Siminoski, K. G., Brown, J., Cowden, E. A., Ioannidis, G., Josse, R. G., Ste, L.-G., Davison, K. S., Blocka, K. L. N., Pollock, A. P., & Sibley, J. (s.d.). *Management of Corticosteroid-Induced Osteoporosis*.

Adams, M. A., Pollintine, P., Tobias, J. H., Wakley, G. K., & Dolan, P. (2006). Intervertebral Disc Degeneration Can Predispose to Anterior Vertebral Fractures in the Thoracolumbar Spine. *Journal of Bone and Mineral Research*, *21*(9), 1409–1416. https://doi.org/10.1359/jbmr.060609

Agostinho Hernandez, B., Gill, H. S., & Gheduzzi, S. (2020). A Novel Modelling Methodology Which Predicts the Structural Behaviour of Vertebral Bodies under Axial Impact Loading: A Finite Element and DIC Study. *Materials*, *13*(19), 4262. https://doi.org/10.3390/ma13194262

Albrecht, B. M., Stalling, I., Foettinger, L., Recke, C., & Bammann, K. (2022). Adherence to Lifestyle Recommendations for Bone Health in Older Adults with and without Osteoporosis: Cross-Sectional Results of the OUTDOOR ACTIVE Study. *Nutrients*, *14*(12), 2463. https://doi.org/10.3390/nu14122463

Aldieri, A., Bhattacharya, P., Paggiosi, M., Eastell, R., Audenino, A. L., Bignardi, C., Morbiducci, U., & Terzini, M. (2022). Improving the Hip Fracture Risk Prediction with a Statistical Shape-and-Intensity Model of the Proximal Femur. *Annals of Biomedical Engineering*, *50*(2), 211–221. https://doi.org/10.1007/s10439-022-02918-z

Aldieri, A., Terzini, M., Audenino, A. L., Bignardi, C., Paggiosi, M., Eastell, R., Viceconti, M., & Bhattacharya, P. (2022). Personalised 3D Assessment of Trochanteric Soft Tissues Improves HIP Fracture Classification Accuracy. *Annals of Biomedical Engineering*, *50*(3), 303–313. https://doi.org/10.1007/s10439-022-02924-1

Alexandru, D. (2012). Evaluation and Management of Vertebral Compression Fractures. *The Permanente Journal*, 46–51. https://doi.org/10.7812/TPP/12-037

Allaire, B. T., Lu, D., Johannesdottir, F., Kopperdahl, D., Keaveny, T. M., Jarraya, M., Guermazi, A., Bredella, M. A., Samelson, E. J., Kiel, D. P., Anderson, D. E., Demissie, S., & Bouxsein, M. L. (2019). Prediction of incident vertebral fracture using CT-based finite element analysis. *Osteoporosis International*, *30*(2), 323–331. https://doi.org/10.1007/s00198-018-4716-1

Anderson, A. E., Ellis, B. J., & Weiss, J. A. (2007). Verification, validation and sensitivity studies in computational biomechanics. *Computer Methods in Biomechanics and Biomedical Engineering*, *10*(3), 171–184. https://doi.org/10.1080/10255840601160484

Anitha, D. P., Baum, T., Kirschke, J. S., & Subburaj, K. (2020). Effect of the intervertebral disc on vertebral bone strength prediction: A finite-element study. *The Spine Journal*, *20*(4), 665–671. https://doi.org/10.1016/j.spinee.2019.11.015

Antoniou, J., Epure, L. M., Michalek, A. J., Grant, M. P., Iatridis, J. C., & Mwale, F. (2013). Analysis of quantitative magnetic resonance imaging and biomechanical parameters on human discs with

different grades of degeneration: Quantitative MRI of Degenerated Human Discs. *Journal of Magnetic Resonance Imaging*, *38*(6), 1402–1414. https://doi.org/10.1002/jmri.24120

Argoubi, M., & Shirazi-Adl, A. (1996). Poroelastic creep response analysis of a lumbar motion segment in compression. *Journal of Biomechanics*, *29*(10), 1331–1339. https://doi.org/10.1016/0021-9290(96)00035-8

ASME. (2018). *V&V 40—2018: Assessing Credibility of Computational Modeling through Verification and Validation: Application to Medical Devices*.

Babuska, I., & Oden, J. T. (2004). Verification and validation in computational engineering and science: Basic concepts. *Computer Methods in Applied Mechanics and Engineering*, *193*(36–38), 4057–4066. https://doi.org/10.1016/j.cma.2004.03.002

Baleani, M., Fraterrigo, G., Erani, P., Rota, G., Berni, M., Taddei, F., & Schileo, E. (2023). Applying a homogeneous pressure distribution to the upper vertebral endplate: Validation of a new loading system, pilot application to human vertebral bodies, and finite element predictions of DIC measured displacements and strains. *Journal of the Mechanical Behavior of Biomedical Materials*, *140*, 105706. https://doi.org/10.1016/j.jmbbm.2023.105706

Barber, D., & Hose, D. (2005). Automatic segmentation of medical images using image registration: Diagnostic and simulation applications. *Journal of Medical Engineering & Technology*, *29*(2), 53–63. https://doi.org/10.1080/03091900412331289889

Barlev, A. (2010). Payer Costs for Inpatient Treatment of Pathologic Fracture, Surgery to Bone, and Spinal Cord Compression Among Patients with Multiple Myeloma or Bone Metastasis Secondary to Prostate or Breast Cancer. *Journal of Managed Care Pharmacy*, *16*(9), 693–702. https://doi.org/10.18553/jmcp.2010.16.9.693

Basu, P. K., Beall, A. G., Simmons, D. J., & Vannier, M. (1985). 3-D Femoral Stress Analysis Using Ct Scans and P-Version Fem. *Biomaterials, Medical Devices, and Artificial Organs*, *13*(3–4), 163–186. https://doi.org/10.3109/10731198509118849

Bayraktar, H. H., Morgan, E. F., Niebur, G. L., Morris, G. E., Wong, E. K., & Keaveny, T. M. (2004). Comparison of the elastic and yield properties of human femoral trabecular and cortical bone tissue. *Journal of Biomechanics*, *37*(1), 27–35. https://doi.org/10.1016/S0021-9290(03)00257-4

Bhattacharya, P., Altai, Z., Qasim, M., & Viceconti, M. (2019). A multiscale model to predict current absolute risk of femoral fracture in a postmenopausal population. *Biomechanics and Modeling in Mechanobiology*, *18*(2), 301–318. https://doi.org/10.1007/s10237-018-1081-0

Bianchi, D., Falcinelli, C., Molinari, L., Gizzi, A., & Di Martino, A. (2022). Osteolytic vs. Osteoblastic Metastatic Lesion: Computational Modeling of the Mechanical Behavior in the Human Vertebra after Screws Fixation Procedure. *Journal of Clinical Medicine*, *11*(10), 2850. https://doi.org/10.3390/jcm11102850

Bishr, M., & Saad, F. (2012). Preventing bone complications in prostate cancer. *Current Opinion in Supportive and Palliative Care*, *6*(3), 299–303. https://doi.org/10.1097/SPC.0b013e328356da87

Borgström, F., Karlsson, L., Ortsäter, G., Norton, N., Halbout, P., Cooper, C., Lorentzon, M., McCloskey, E. V., Harvey, N. C., Javaid, M. K., & Kanis, J. A. (2020). Fragility fractures in Europe: Burden, management and opportunities. *Archives of Osteoporosis*, *15*(1), 59. https://doi.org/10.1007/s11657-020-0706-y

Buckley, J. M., Loo, K., & Motherway, J. (2007). Comparison of quantitative computed tomography-based measures in predicting vertebral compressive strength. *Bone*, *40*(3), 767–774. https://doi.org/10.1016/j.bone.2006.10.025

Burke, M., Atkins, A., Kiss, A., Akens, M., Yee, A., & Whyne, C. (2017). The impact of metastasis on the mineral phase of vertebral bone tissue. *Journal of the Mechanical Behavior of Biomedical Materials*, *69*, 75–84. https://doi.org/10.1016/j.jmbbm.2016.12.017

Campbell, G., Pena, J., Giravent, S., Thomsen, F., Damm, T., Gluer, C., & Borggrefe, J. (2017). *Assessment of Bone Fragility in Patients With MultipleMyeloma Using QCT-Based Finite Element Modeling*. https://doi.org/DOI: 10.1002/jbmr.2924

Cassidy, J. J., Hiltner, A., & Baer, E. (s.d.). *Hierarchical Structure of the Intervertebral Disc*.

Cavazzoni, G., Cristofolini, L., Dall'Ara, E., & Palanca, M. (2023). Bone metastases do not affect the measurement uncertainties of a global digital volume correlation algorithm. *Frontiers in Bioengineering and Biotechnology*, *11*, 1152358. https://doi.org/10.3389/fbioe.2023.1152358

Chen, Y., Dall'Ara, E., Sales, E., Manda, K., Wallace, R., Pankaj, P., & Viceconti, M. (2017). Micro-CT based finite element models of cancellous bone predict accurately displacement once the boundary condition is well replicated: A validation study. *Journal of the Mechanical Behavior of Biomedical Materials*, *65*, 644–651. https://doi.org/10.1016/j.jmbbm.2016.09.014

Cheng, X. G., Nicholson, P. H. F., Boonen, S., Lowet, G., Brys, P., Aerssens, J., van der Perre, G., & Dequeker, J. (1997). Prediction of Vertebral Strength In Vitro by Spinal Bone Densitometry and Calcaneal Ultrasound. *Journal of Bone and Mineral Research*, *12*(10), 1721–1728. https://doi.org/10.1359/jbmr.1997.12.10.1721

Chevalier, Y., Pahr, D., & Zysset, P. K. (2009). The Role of Cortical Shell and Trabecular Fabric in Finite Element Analysis of the Human Vertebral Body. *Journal of Biomechanical Engineering*, *131*(11), 111003. https://doi.org/10.1115/1.3212097

Chevalier, Y., Quek, E., Borah, B., Gross, G., Stewart, J., Lang, T., & Zysset, P. (2010). Biomechanical effects of teriparatide in women with osteoporosis treated previously with alendronate and risedronate: Results from quantitative computed tomography-based finite element analysis of the vertebral body. *Bone*, *46*(1), 41–48. https://doi.org/10.1016/j.bone.2009.09.032

Choplin, R. H., Lenchik, L., & Wuertzer, S. (2014). A Practical Approach to Interpretation of Dual-Energy X-ray Absorptiometry (DXA) for Assessment of Bone Density. *Current Radiology Reports*, *2*(6), 48. https://doi.org/10.1007/s40134-014-0048-x

Christen, D., Levchuk, A., Schori, S., Schneider, P., Boyd, S. K., & Müller, R. (2012). Deformable image registration and 3D strain mapping for the quantitative assessment of cortical bone microdamage. *Journal of the Mechanical Behavior of Biomedical Materials*, *8*, 184–193. https://doi.org/10.1016/j.jmbbm.2011.12.009

Clouthier, A. L., Hosseini, H. S., Maquer, G., & Zysset, P. K. (2015). Finite element analysis predicts experimental failure patterns in vertebral bodies loaded via intervertebral discs up to large deformation. *Medical Engineering & Physics*, *37*(6), 599–604. https://doi.org/10.1016/j.medengphy.2015.03.007

Coleman, R., Brown, J., & Ingunn, H. (2019). Bone Metastases. In *Abeloff's Clinical Oncology (Sixth Edition)*.

Combes, R., & Shah, A. (2016). *The Use of In Vivo, Ex Vivo, In Vitro, Computational Models and Volunteer Studies in Vision Research and Therapy, and Their Contribution to the Three Rs*.

Cooper, C., & Iii, L. J. M. (s.d.). *Epidemiology of Osteoporosis*.

Costa, M. C., Eltes, P., Lazary, A., Varga, P. P., Viceconti, M., & Dall'Ara, E. (2019). Biomechanical assessment of vertebrae with lytic metastases with subject-specific finite element models. *Journal of the Mechanical Behavior of Biomedical Materials*, *98*, 268–290. https://doi.org/10.1016/j.jmbbm.2019.06.027

Costa, M. C., Tozzi, G., Cristofolini, L., Danesi, V., Viceconti, M., & Dall'Ara, E. (2017). Micro Finite Element models of the vertebral body: Validation of local displacement predictions. *PLOS ONE*, *12*(7), e0180151. https://doi.org/10.1371/journal.pone.0180151

Crandall, C. J., Larson, J. C., Watts, N. B., Gourlay, M. L., Donaldson, M. G., LaCroix, A., Cauley, J. A., Wactawski-Wende, J., Gass, M. L., Robbins, J. A., & Ensrud, K. E. (2014). Comparison of Fracture Risk Prediction by the US Preventive Services Task Force Strategy and Two Alternative Strategies in Women 50–64 Years Old in the Women's Health Initiative. *The Journal of Clinical Endocrinology & Metabolism*, *99*(12), 4514–4522. https://doi.org/10.1210/jc.2014-2332

Cranney, A., Jamal, S. A., Tsang, J. F., Josse, R. G., & Leslie, W. D. (2007). Low bone mineral density and fracture burden in postmenopausal women. *Canadian Medical Association Journal*, *177*(6), 575–580. https://doi.org/10.1503/cmaj.070234

Crawford, R. P., Cann, C. E., & Keaveny, T. M. (2003). Finite element models predict in vitro vertebral body compressive strength better than quantitative computed tomography. *Bone*, *33*(4), 744–750. https://doi.org/10.1016/S8756-3282(03)00210-2

Cristofolini, L. (2015). In vitro evidence of the structural optimization of the human skeletal bones. *Journal of Biomechanics*, *48*(5), 787–796. https://doi.org/10.1016/j.jbiomech.2014.12.010

Cristofolini, L., Brandolini, N., Danesi, V., Juszczyk, M. M., Erani, P., & Viceconti, M. (2013). Strain distribution in the lumbar vertebrae under different loading configurations. *The Spine Journal*, *13*(10), 1281–1292. https://doi.org/10.1016/j.spinee.2013.06.014

Cristofolini, L., Schileo, E., Juszczyk, M., Taddei, F., Martelli, S., & Viceconti, M. (2010). Mechanical testing of bones: The positive synergy of finite–element models and *in vitro* experiments. *Philosophical Transactions of the Royal Society A: Mathematical, Physical and Engineering Sciences*, *368*(1920), 2725–2763. https://doi.org/10.1098/rsta.2010.0046

Cristofolini, L., & Viceconti, M. (1997). Comparison of uniaxial and triaxial rosette gages for strain measurement in the femur. *Experimental Mechanics*, *37*(3), 350–354. https://doi.org/10.1007/BF02317430

Dall'Ara, E., Barber, D., & Viceconti, M. (2014). About the inevitable compromise between spatial resolution and accuracy of strain measurement for bone tissue: A 3D zero-strain study. *Journal of Biomechanics*, *47*(12), 2956–2963. https://doi.org/10.1016/j.jbiomech.2014.07.019

Dall'Ara, E., Pahr, D., Varga, P., Kainberger, F., & Zysset, P. (2012). QCT-based finite element models predict human vertebral strength in vitro significantly better than simulated DEXA. *Osteoporosis International: A Journal Established as Result of Cooperation between the European Foundation for Osteoporosis and the National Osteoporosis Foundation of the USA*, *23*(2), 563–572. https://doi.org/10.1007/s00198-011-1568-3

Dall'Ara, E., Peña-Fernández, M., Palanca, M., Giorgi, M., Cristofolini, L., & Tozzi, G. (2017). Precision of Digital Volume Correlation Approaches for Strain Analysis in Bone Imaged with Micro-Computed Tomography at Different Dimensional Levels. *Frontiers in Materials*, *4*, 31. https://doi.org/10.3389/fmats.2017.00031

Dall'Ara, E., Schmidt, R., Pahr, D., Varga, P., Chevalier, Y., Patsch, J., Kainberger, F., & Zysset, P. (2010). A nonlinear finite element model validation study based on a novel experimental technique for inducing anterior wedge-shape fractures in human vertebral bodies in vitro. *Journal of Biomechanics*, *43*(12), 2374–2380. https://doi.org/10.1016/j.jbiomech.2010.04.023

Dall'Ara, E., & Tozzi, G. (2022). Digital volume correlation for the characterization of musculoskeletal tissues: Current challenges and future developments. *Frontiers in Bioengineering and Biotechnology*, *10*, 1010056. https://doi.org/10.3389/fbioe.2022.1010056

Danesi, V., Erani, P., Brandolini, N., Juszczyk, M. M., & Cristofolini, L. (2016). Effect of the In Vitro Boundary Conditions on the Surface Strain Experienced by the Vertebral Body in the Elastic Regime. *Journal of Biomechanical Engineering*, *138*(10), 104503. https://doi.org/10.1115/1.4034383

Danesi, V., Zani, L., Scheele, A., Berra, F., & Cristofolini, L. (2014). Reproducible reference frame for in vitro testing of the human vertebrae. *Journal of Biomechanics*, *47*(1), 313–318. https://doi.org/10.1016/j.jbiomech.2013.10.005

Dickinson, A. S., Taylor, A. C., Ozturk, H., & Browne, M. (2011). Experimental Validation of a Finite Element Model of the Proximal Femur Using Digital Image Correlation and a Composite Bone Model. *Journal of Biomechanical Engineering*, *133*(1), 014504. https://doi.org/10.1115/1.4003129

Dionyssiotis, Y. (2010). Management of osteoporotic vertebral fractures. *International Journal of General Medicine*, 167. https://doi.org/10.2147/IJGM.S11751

Disney, C. M., Lee, P. D., Hoyland, J. A., Sherratt, M. J., & Bay, B. K. (2018). *A review of techniques for visualising soft tissue microstructure deformation and quantifying strain Ex Vivo*. https://doi.org/10.1111/jmi.12701

Engelke, K., Van Rietbergen, B., & Zysset, P. (2016). FEA to Measure Bone Strength: A Review. *Clinical Reviews in Bone and Mineral Metabolism*, *14*(1), 26–37. https://doi.org/10.1007/s12018-015-9201-1

Ensrud, K. E., & Schousboe, J. T. (2011). Vertebral Fractures. *New England Journal of Medicine*, *364*(17), 1634–1642. https://doi.org/10.1056/NEJMcp1009697

Eswaran, S. K., Fields, A. J., Nagarathnam, P., & Keaveny, T. M. (2008). MULTI-SCALE MODELING OF THE HUMAN VERTEBRAL BODY: COMPARISON OF MICRO-CT BASED HIGH-RESOLUTION AND CONTINUUM-LEVEL MODELS. *Biocomputing 2009*, 293–303. https://doi.org/10.1142/9789812836939_0028

Ferlay, J., Colombet, M., Soerjomataram, I., Parkin, D. M., Piñeros, M., Znaor, A., & Bray, F. (2021). Cancer statistics for the year 2020: An overview. *International Journal of Cancer*, *149*(4), 778–789. https://doi.org/10.1002/ijc.33588

Fisher, C. G., DiPaola, C. P., Ryken, T. C., Bilsky, M. H., Shaffrey, C. I., Berven, S. H., Harrop, J. S., Fehlings, M. G., Boriani, S., Chou, D., Schmidt, M. H., Polly, D. W., Biagini, R., Burch, S., Dekutoski, M. B., Ganju, A., Gerszten, P. C., Gokaslan, Z. L., Groff, M. W., … Fourney, D. R. (2010). A Novel Classification System for Spinal Instability in Neoplastic Disease: An Evidence-Based Approach and Expert Consensus From the Spine Oncology Study Group. *Spine*, *35*(22), E1221. https://doi.org/10.1097/BRS.0b013e3181e16ae2

Fisher, C. G., Schouten, R., Versteeg, A. L., Boriani, S., Varga, P. P., Rhines, L. D., Kawahara, N., Fourney, D., Weir, L., Reynolds, J. J., Sahgal, A., Fehlings, M. G., & Gokaslan, Z. L. (2014). Reliability of the Spinal Instability Neoplastic Score (SINS) among radiation oncologists: An assessment of instability secondary to spinal metastases. *Radiation Oncology*, *9*(1), 69. https://doi.org/10.1186/1748-717X-9-69

Fleps, I., & Morgan, E. F. (2022). A Review of CT-Based Fracture Risk Assessment with Finite Element Modeling and Machine Learning. *Current Osteoporosis Reports*, *20*(5), 309–319. https://doi.org/10.1007/s11914-022-00743-w

Fonseca, H., Moreira-Gonçalves, D., Coriolano, H.-J. A., & Duarte, J. A. (2014). Bone Quality: The Determinants of Bone Strength and Fragility. *Sports Medicine*, *44*(1), 37–53. https://doi.org/10.1007/s40279-013-0100-7

Fourney, D. R., Frangou, E. M., Ryken, T. C., DiPaola, C. P., Shaffrey, C. I., Berven, S. H., Bilsky, M. H., Harrop, J. S., Fehlings, M. G., Boriani, S., Chou, D., Schmidt, M. H., Polly, D. W., Biagini, R., Burch, S., Dekutoski, M. B., Ganju, A., Gerszten, P. C., Gokaslan, Z. L., … Fisher, C. G. (2011). Spinal Instability Neoplastic Score: An Analysis of Reliability and Validity From the Spine Oncology Study Group. *Journal of Clinical Oncology*, *29*(22), 3072–3077. https://doi.org/10.1200/JCO.2010.34.3897

Galbusera, F., Qian, Z., Casaroli, G., Bassani, T., Costa, F., Schlager, B., & Wilke, H.-J. (2018). The Role of the Size and Location of the Tumors and of the Vertebral Anatomy in Determining the Structural Stability of the Metastatically Involved Spine: A Finite Element Study. *Translational Oncology*, *11*(3), 639–646. https://doi.org/10.1016/j.tranon.2018.03.002

Garavelli, C., Curreli, C., Palanca, M., Aldieri, A., Cristofolini, L., & Viceconti, M. (2022). Experimental validation of a subject-specific finite element model of lumbar spine segment using digital image correlation. *PLOS ONE*, *17*(9), e0272529. https://doi.org/10.1371/journal.pone.0272529

Gaweda, A. E., Lederer, E. D., & Brier, M. E. (2022). Artificial intelligence–guided precision treatment of chronic kidney DISEASE – MINERAL bone disorder. *CPT: Pharmacometrics & Systems Pharmacology*, *11*(10), 1305–1315. https://doi.org/10.1002/psp4.12843

Genant, H. K., Wu, C. Y., Van Kuijk, C., & Nevitt, M. C. (1993). Vertebral fracture assessment using a semiquantitative technique. *Journal of Bone and Mineral Research*, *8*(9), 1137–1148. https://doi.org/10.1002/jbmr.5650080915

Ghosh, R., Gupta, S., Dickinson, A., & Browne, M. (2012). Experimental Validation of Finite Element Models of Intact and Implanted Composite Hemipelvises Using Digital Image Correlation. *Journal of Biomechanical Engineering*, *134*(8), 081003. https://doi.org/10.1115/1.4007173

Goldman, L. W. (2007). Principles of CT: Radiation Dose and Image Quality. *Journal of Nuclear Medicine Technology*, *35*(4), 213–225. https://doi.org/10.2967/jnmt.106.037846

Graeff, C., Chevalier, Y., Charlebois, M., Varga, P., Pahr, D., Nickelsen, T. N., Morlock, M. M., Glüer, C. C., & Zysset, P. K. (2009). Improvements in Vertebral Body Strength Under Teriparatide Treatment Assessed In Vivo by Finite Element Analysis: Results From the EUROFORS Study. *Journal of Bone and Mineral Research*, *24*(10), 1672–1680. https://doi.org/10.1359/jbmr.090416

Grassi, L., & Isaksson, H. (2015). Extracting accurate strain measurements in bone mechanics: A critical review of current methods. *Journal of the Mechanical Behavior of Biomedical Materials*, *50*, 43–54. https://doi.org/10.1016/j.jmbbm.2015.06.006

Grassi, L., Väänänen, S. P., Amin Yavari, S., Weinans, H., Jurvelin, J. S., Zadpoor, A. A., & Isaksson, H. (2013). Experimental validation of finite element model for proximal composite femur using optical measurements. *Journal of the Mechanical Behavior of Biomedical Materials*, *21*, 86–94. https://doi.org/10.1016/j.jmbbm.2013.02.006

Grassi, L., Väänänen, S. P., Ristinmaa, M., Jurvelin, J. S., & Isaksson, H. (2016). How accurately can subject-specific finite element models predict strains and strength of human femora? Investigation

using full-field measurements. *Journal of Biomechanics*. https://doi.org/10.1016/j.jbiomech.2016.02.032

Gray, H. (s.d.). *Gray's Anatomy* (38ª ed.). Churchill Livingstone.

Griffith, J. F., & Genant, H. K. (2008). Bone mass and architecture determination: State of the art. *Best Practice & Research Clinical Endocrinology & Metabolism*, *22*(5), 737–764. https://doi.org/10.1016/j.beem.2008.07.003

Groenen, K. H. J., Bitter, T., van Veluwen, T. C. G., van der Linden, Y. M., Verdonschot, N., Tanck, E., & Janssen, D. (2018). Case-specific non-linear finite element models to predict failure behavior in two functional spinal units: FE TO PREDICT VERTEBRAL FAILURE. *Journal of Orthopaedic Research®*, *36*(12), 3208–3218. https://doi.org/10.1002/jor.24117

Guise, T. A., Mohammad, K. S., Clines, G., Stebbins, E. G., Wong, D. H., Higgins, L. S., Vessella, R., Corey, E., Padalecki, S., Suva, L., & Chirgwin, J. M. (2006). Basic Mechanisms Responsible for Osteolytic and Osteoblastic Bone Metastases. *Clinical Cancer Research*, *12*(20), 6213s–6216s. https://doi.org/10.1158/1078-0432.CCR-06-1007

Gustafson, H. M., Cripton, P. A., Ferguson, S. J., & Helgason, B. (2017). Comparison of specimen-specific vertebral body finite element models with experimental digital image correlation measurements. *Journal of the Mechanical Behavior of Biomedical Materials*, *65*(September 2016), 801–807. https://doi.org/10.1016/j.jmbbm.2016.10.002

Harrigan, T. P., & Mann, R. W. (1984). *Characterization of microstructural anisotropy in orthotropic materials using a second rank tensor*.

Hasserius, R., Karlsson, M. K., Jónsson, B., Redlund-Johnell, I., & Johnell, O. (2005). Long-Term Morbidity and Mortality After a Clinically Diagnosed Vertebral Fracture in the Elderly—A 12- and 22-Year Follow-up of 257 Patients. *Calcified Tissue International*, *76*(4), 235–242. https://doi.org/10.1007/s00223-004-2222-2

Helgason, B., Perilli, E., Schileo, E., Taddei, F., Brynjólfsson, S., & Viceconti, M. (2008). Mathematical relationships between bone density and mechanical properties: A literature review. *Clinical Biomechanics*, *23*(2), 135–146. https://doi.org/10.1016/j.clinbiomech.2007.08.024

Helgason, B., S.Gilchrist, Ariza, O., Chak, J. D., Zheng, G., Widmer, R. P., Ferguson, S. J., Guy, P., & Cripton, P. A. (2014). Development of a balanced experimental–computational approach to understanding the mechanics of proximal femur fractures. *Medical Engineering & Physics*, *36*(6), 793–799. https://doi.org/10.1016/j.medengphy.2014.02.019

Hoc, T., Henry, L., Verdier, M., Aubry, D., Sedel, L., & Meunier, A. (2006). Effect of microstructure on the mechanical properties of Haversian cortical bone. *Bone*, *38*(4), 466–474. https://doi.org/10.1016/j.bone.2005.09.017

Hosseini, H. S., Clouthier, A. L., & Zysset, P. K. (2014). Experimental Validation of Finite Element Analysis of Human Vertebral Collapse Under Large Compressive Strains. *Journal of Biomechanical Engineering*, *136*(4), 041006. https://doi.org/10.1115/1.4026409

Huang, J.-F., Shen, J., Li, X., Rengan, R., Silvestris, N., Wang, M., Derosa, L., Zheng, X., Belli, A., Zhang, X.-L., Li, Y. M., & Wu, A. (2020). Incidence of patients with bone metastases at diagnosis of solid tumors in adults: A large population-based study. *Annals of Translational Medicine*, *8*(7), 482–482. https://doi.org/10.21037/atm.2020.03.55

Hussein, A. I., Louzeiro, D. T., Unnikrishnan, G. U., & Morgan, E. F. (2018). Differences in Trabecular Microarchitecture and Simplified Boundary Conditions Limit the Accuracy of Quantitative

Computed Tomography-Based Finite Element Models of Vertebral Failure. *Journal of Biomechanical Engineering*, *140*(2), 021004. https://doi.org/10.1115/1.4038609

Hussein, A. I., Mason, Z. D., & Morgan, E. F. (2013). Presence of intervertebral discs alters observed stiffness and failure mechanisms in the vertebra. *Journal of Biomechanics*, *46*(10), 1683–1688. https://doi.org/10.1016/j.jbiomech.2013.04.004

Imai, K. (2015). Computed tomography-based finite element analysis to assess fracture risk and osteoporosis treatment. *World Journal of Experimental Medicine*, *5*(3), 182. https://doi.org/10.5493/wjem.v5.i3.182

Imai, K., Ohnishi, I., Bessho, M., & Nakamura, K. (2006). Nonlinear Finite Element Model Predicts Vertebral Bone Strength and Fracture Site: *Spine*, *31*(16), 1789–1794. https://doi.org/10.1097/01.brs.0000225993.57349.df

Imai, K., Ohnishi, I., Matsumoto, T., Yamamoto, S., & Nakamura, K. (2009). Assessment of vertebral fracture risk and therapeutic effects of alendronate in postmenopausal women using a quantitative computed tomography-based nonlinear finite element method. *Osteoporosis International*, *20*(5), 801–810. https://doi.org/10.1007/s00198-008-0750-8

Incidence of Vertebral Fracture in Europe: Results From the European Prospective Osteoporosis Study (EPOS). (2002). *Journal of Bone and Mineral Research*, *17*(4), 716–724. https://doi.org/10.1359/jbmr.2002.17.4.716

Jackman, T. M., DelMonaco, A. M., & Morgan, E. F. (2016). Accuracy of finite element analyses of CT scans in predictions of vertebral failure patterns under axial compression and anterior flexion. *Journal of Biomechanics*, *49*(2), 267–275. https://doi.org/10.1016/j.jbiomech.2015.12.004

Johannesdottir, F., Allaire, B., & Bouxsein, M. L. (2018). Fracture Prediction by Computed Tomography and Finite Element Analysis: Current and Future Perspectives. *Current Osteoporosis Reports*, *16*(4), 411–422. https://doi.org/10.1007/s11914-018-0450-z

Johnell, O. (1997). The socioeconomic burden of fractures: Today and in the 21st century. *The American Journal of Medicine*, *103*(2), S20–S26. https://doi.org/10.1016/S0002-9343(97)90023-1

Johnell, O., & Kanis, J. A. (2006). An estimate of the worldwide prevalence and disability associated with osteoporotic fractures. *Osteoporosis International*, *17*(12), 1726–1733. https://doi.org/10.1007/s00198-006-0172-4

Jones, A. C., & Wilcox, R. K. (2008). Finite element analysis of the spine: Towards a framework of verification, validation and sensitivity analysis. *Medical Engineering & Physics*, *30*(10), 1287–1304. https://doi.org/10.1016/j.medengphy.2008.09.006

Jungmann, R., Szabo, M. E., Schitter, G., Yue-Sing Tang, R., Vashishth, D., Hansma, P. K., & Thurner, P. J. (2011). Local strain and damage mapping in single trabeculae during three-point bending tests. *Journal of the Mechanical Behavior of Biomedical Materials*, *4*(4), 523–534. https://doi.org/10.1016/j.jmbbm.2010.12.009

Kado, D., Browner, W., Palermo, L., Nevitt, M., Genant, H. K., & Cummings, S. R. (1999). *Vertebral Fractures and Mortality in Older Women: A Prospective Study*. https://doi.org/doi:10.1001/archinte.159.11.1215

Kakhki, V. R. D., Anvari, K., Sadeghi, R., Mahmoudian, A.-S., & Torabian-Kakhki, M. (2013). Pattern and distribution of bone metastases in common malignant tumors. *Nuclear Medicine Review*, *16*(2), 66–69. https://doi.org/10.5603/NMR.2013.0037

Kaneko, T. S., Bell, J. S., Pejcic, M. R., Tehranzadeh, J., & Keyak, J. H. (2004). Mechanical properties, density and quantitative CT scan data of trabecular bone with and without metastases. *Journal of Biomechanics*, *37*(4), 523–530. https://doi.org/10.1016/j.jbiomech.2003.08.010

Kanis, J., Harvey, N. C., Johansson, H., Oden, A., McCloskey, E. V., & Leslie, W. D. (2017). *Overview of Fracture Prediction Tools*. https://doi.org/10.1016/j.jocd.2017.06.013

Katz, Y., & Yosibash, Z. (2020). New insights on the proximal femur biomechanics using Digital Image Correlation. *Journal of Biomechanics*, *101*, 109599. https://doi.org/10.1016/j.jbiomech.2020.109599

Keaveny, T. M., Clarke, B. L., Cosman, F., Orwoll, E. S., Siris, E. S., Khosla, S., & Bouxsein, M. L. (2020). Biomechanical Computed Tomography analysis (BCT) for clinical assessment of osteoporosis. *Osteoporosis International: A Journal Established as Result of Cooperation between the European Foundation for Osteoporosis and the National Osteoporosis Foundation of the USA*, *31*(6), 1025–1048. https://doi.org/10.1007/s00198-020-05384-2

Keaveny, T. M., Donley, D. W., Hoffmann, P. F., Mitlak, B. H., Glass, E. V., & San Martin, J. A. (2007). Effects of Teriparatide and Alendronate on Vertebral Strength as Assessed by Finite Element Modeling of QCT Scans in Women With Osteoporosis. *Journal of Bone and Mineral Research*, *22*(1), 149–157. https://doi.org/10.1359/jbmr.061011

Keaveny, T. M., Pinilla, T. P., Crawford, R. P., Kopperdahl, D. L., & Lou, A. (1997). Systematic and random errors in compression testing of trabecular bone. *Journal of Orthopaedic Research*, *15*(1), 101–110. https://doi.org/10.1002/jor.1100150115

Keller, T. S., Spengler, D. M., & Hansson, T. H. (1987). Mechanical behavior of the human lumbar spine. I. Creep analysis during static compressive loading. *Journal of Orthopaedic Research*, *5*(4), 467–478. https://doi.org/10.1002/jor.1100050402

Keyak, J. H., Rossi, S. A., Jones, K. A., Les, C. M., & Skinner, H. B. (2001). Prediction of fracture location in the proximal femur using finite element models. *Medical Engineering & Physics*, *23*(9), 657–664. https://doi.org/10.1016/S1350-4533(01)00094-7

Kim, H.-J., Park, S., Park, S.-H., Park, J., Chang, B.-S., Lee, C.-K., & Yeom, J. S. (2018). Prevalence of Frailty in Patients with Osteoporotic Vertebral Compression Fracture and Its Association with Numbers of Fractures. *Yonsei Medical Journal*, *59*(2), 317. https://doi.org/10.3349/ymj.2018.59.2.317

Kim, Y. R., Lee, C.-H., Yang, S. H., Hyun, S.-J., Kim, C. H., Park, S. B., Kim, K.-J., & Chung, C. K. (2021). Accuracy and precision of the spinal instability neoplastic score (SINS) for predicting vertebral compression fractures after radiotherapy in spinal metastases: A meta-analysis. *Scientific Reports*, *11*(1), 5553. https://doi.org/10.1038/s41598-021-84975-3

Klintstrom, E. (s.d.). *Image Analysis for Trabecular Bone Properties on Cone-Beam CT Data*.

Klotzbuecher, C. M., Ross, P. D., Landsman, P. B., Abbott, T. A., & Berger, M. (2000). Patients with Prior Fractures Have an Increased Risk of Future Fractures: A Summary of the Literature and Statistical Synthesis. *Journal of Bone and Mineral Research*, *15*(4), 721–739. https://doi.org/10.1359/jbmr.2000.15.4.721

Kok, J., Odin, K., Rokkones, S., Grassi, L., & Isaksson, H. (2022). The influence of foramina on femoral neck fractures and strains predicted with finite element analysis. *Journal of the Mechanical Behavior of Biomedical Materials*, *134*, 105364. https://doi.org/10.1016/j.jmbbm.2022.105364

Kopperdahl, D. L., Aspelund, T., Hoffmann, P. F., Sigurdsson, S., Siggeirsdottir, K., Harris, T. B., Gudnason, V., & Keaveny, T. M. (2014). Assessment of incident spine and hip fractures in women and

men using finite element analysis of CT scans: INCIDENT FRACTURE ASSESSMENT USING FEA OF CT SCANS. *Journal of Bone and Mineral Research*, *29*(3), 570–580. https://doi.org/10.1002/jbmr.2069

Kopperdahl, D. L., Morgan, E. F., & Keaveny, T. M. (2002). Quantitative computed tomography estimates of the mechanical properties of human vertebral trabecular bone. *Journal of Orthopaedic Research*, *20*(4), 801–805. https://doi.org/10.1016/S0736-0266(01)00185-1

Kusins, J., Knowles, N., Columbus, M., Oliviero, S., Dall'Ara, E., Athwal, G. S., & Ferreira, L. M. (2020). The Application of Digital Volume Correlation (DVC) to Evaluate Strain Predictions Generated by Finite Element Models of the Osteoarthritic Humeral Head. *Annals of Biomedical Engineering*, *48*(12), 2859–2869. https://doi.org/10.1007/s10439-020-02549-2

Kusins, J., Knowles, N., Ryan, M., Dall'Ara, E., & Ferreira, L. (2019). Performance of QCT-Derived scapula finite element models in predicting local displacements using digital volume correlation. *Journal of the Mechanical Behavior of Biomedical Materials*, *97*, 339–345. https://doi.org/10.1016/j.jmbbm.2019.05.021

Lanyon, L. E. (1987). Functional strain in bone tissue as an objective and controlling stimulus for adaptive bone remodelling. *Functional strain in bone tissue as an objective and controlling stimulus for adaptive bone remodelling*, *Journal of Biomechanics*(20), 1083–1093.

Laufer, I., Rubin, D. G., Lis, E., Cox, B. W., Stubblefield, M. D., Yamada, Y., & Bilsky, M. H. (2013). The NOMS framework: Approach to the treatment of spinal metastatic tumors. *The Oncologist*, *18*(6), 744–751. https://doi.org/10.1634/theoncologist.2012-0293

LeBoff, M. S., Greenspan, S. L., Insogna, K. L., Lewiecki, E. M., Saag, K. G., Singer, A. J., & Siris, E. S. (2022). The clinician's guide to prevention and treatment of osteoporosis. *Osteoporosis International*, *33*(10), 2049–2102. https://doi.org/10.1007/s00198-021-05900-y

Martelli, S., Giorgi, M., Dall'Ara, E., & Perilli, E. (2021). Damage tolerance and toughness of elderly human femora. *Acta Biomaterialia*, *123*, 167–177. https://doi.org/10.1016/j.actbio.2021.01.011

Matsumoto, T., Ohnishi, I., Bessho, M., Imai, K., Ohashi, S., & Nakamura, K. (2009). Prediction of Vertebral Strength Under Loading Conditions Occurring in Activities of Daily Living Using a Computed Tomography-Based Nonlinear Finite Element Method: *Spine*, *34*(14), 1464–1469. https://doi.org/10.1097/BRS.0b013e3181a55636

McCloskey, E., Johansson, H., Oden, A., & Kanis, J. A. (2012). Fracture risk assessment. *Clinical Biochemistry*, *45*(12), 887–893. https://doi.org/10.1016/j.clinbiochem.2012.05.001

McCloskey, E. V., Vasireddy, S., Threlkeld, J., Eastaugh, J., Parry, A., Bonnet, N., Beneton, M., Kanis, J. A., & Charlesworth, D. (2008). Vertebral Fracture Assessment (VFA) With a Densitometer Predicts Future Fractures in Elderly Women Unselected for Osteoporosis. *Journal of Bone and Mineral Research*, *23*(10), 1561–1568. https://doi.org/10.1359/jbmr.080515

Melton, J. (s.d.). *Epidemiology of Spinal Osteoporosis*.

Miller, K. D., Nogueira, L., Devasia, T., Mariotto, A. B., Yabroff, K. R., Jemal, A., Kramer, J., & Siegel, R. L. (2022). Cancer treatment and survivorship statistics, 2022. *CA: A Cancer Journal for Clinicians*, *72*(5), 409–436. https://doi.org/10.3322/caac.21731

Mobbs, R. J., Loganathan, A., Yeung, V., & Rao, P. J. (2013). Indications for Anterior Lumbar Interbody Fusion. *Orthopaedic Surgery*, *5*(3), 153–163. https://doi.org/10.1111/os.12048

Molinari, L., & Falcinelli, C. (2022). On the human vertebra computational modeling: A literature review. *Meccanica*, *57*(3), 599–622. https://doi.org/10.1007/s11012-021-01452-x

Morgan, E. F., Bayraktar, H. H., & Keaveny, T. M. (2003). Trabecular bone modulus–density relationships depend on anatomic site. *Journal of Biomechanics*, *36*(7), 897–904. https://doi.org/10.1016/S0021-9290(03)00071-X

Morgan, E. F., & Keaveny, T. M. (2001). Dependence of yield strain of human trabecular bone on anatomic site. *Journal of Biomechanics*, *34*(5), 569–577. https://doi.org/10.1016/S0021-9290(01)00011-2

Morita, M., Ebihara, A., Itoman, M., & Sasada, T. (1994). Progression of osteoporosis in cancellous bone depending on trabecular structure. *Annals of Biomedical Engineering*, *22*(5), 532–539. https://doi.org/10.1007/BF02367089

Naoum, S., Vasiliadis, A. V., Koutserimpas, C., Mylonakis, N., Kotsapas, M., & Katakalos, K. (2021). Finite Element Method for the Evaluation of the Human Spine: A Literature Overview. *Journal of Functional Biomaterials*, *12*(3), 43. https://doi.org/10.3390/jfb12030043

Nazarian, A., von Stechow, D., Zurakowski, D., Müller, R., & Snyder, B. D. (2008). Bone Volume Fraction Explains the Variation in Strength and Stiffness of Cancellous Bone Affected by Metastatic Cancer and Osteoporosis. *Calcified Tissue International*, *83*(6), 368–379. https://doi.org/10.1007/s00223-008-9174-x

Nicolella, D. P., Nicholls, A. E., Lankford, J., & Davy, D. T. (2001). Machine vision photogrammetry: A technique for measurement of microstructural strain in cortical bone. *Journal of Biomechanics*, *34*(1), 135–139. https://doi.org/10.1016/S0021-9290(00)00163-9

Old, J. L., & Calvert, M. (2004). *Vertebral Compression Fractures in the Elderly*. *69*(1).

Op Den Buijs, J., & Dragomir-Daescu, D. (2011). Validated finite element models of the proximal femur using two-dimensional projected geometry and bone density. *Computer Methods and Programs in Biomedicine*, *104*(2), 168–174. https://doi.org/10.1016/j.cmpb.2010.11.008

O'Connell, G. D., Johannessen, W., Vresilovic, E. J., & Elliott, D. M. (2007). Human Internal Disc Strains in Axial Compression Measured Noninvasively Using Magnetic Resonance Imaging: *Spine*, *32*(25), 2860–2868. https://doi.org/10.1097/BRS.0b013e31815b75fb

Palanca, M., Barbanti-Bròdano, G., & Cristofolini, L. (2018). The Size of Simulated Lytic Metastases Affects the Strain Distribution on the Anterior Surface of the Vertebra. *Journal of Biomechanical Engineering*, *140*(11), 1–9. https://doi.org/10.1115/1.4040587

Palanca, M., Barbanti-Bròdano, G., Marras, D., Marciante, M., Serra, M., Gasbarrini, A., Dall'Ara, E., & Cristofolini, L. (2021). Type, size, and position of metastatic lesions explain the deformation of the vertebrae under complex loading conditions. *Bone*, *151*, 116028. https://doi.org/10.1016/j.bone.2021.116028

Palanca, M., Bodey, A. J., Giorgi, M., Viceconti, M., Lacroix, D., Cristofolini, L., & Dall'Ara, E. (2017). Local displacement and strain uncertainties in different bone types by digital volume correlation of synchrotron microtomograms. *Journal of Biomechanics*, *58*, 27–36. https://doi.org/10.1016/j.jbiomech.2017.04.007

Palanca, M., Brugo, T. M., & Cristofolini, L. (2015). Use of digital image correlation to investigate the biomechanics of the vertebra. *Journal of Mechanics in Medicine and Biology*, *15*(2), 1–10. https://doi.org/10.1142/S0219519415400047

Palanca, M., Cavazzoni, G., & Dall'Ara, E. (2023). The role of bone metastases on the mechanical competence of human vertebrae. *Bone*, *173*, 116814. https://doi.org/10.1016/j.bone.2023.116814

Palanca, M., Cristofolini, L., Dall'Ara, E., Curto, M., Innocente, F., Danesi, V., & Tozzi, G. (2016). Digital volume correlation can be used to estimate local strains in natural and augmented vertebrae: An organ-level study. *Journal of Biomechanics*, *49*(16), 3882–3890. https://doi.org/10.1016/j.jbiomech.2016.10.018

Palanca, M., Oliviero, S., & Dall'Ara, E. (2022). MicroFE models of porcine vertebrae with induced bone focal lesions: Validation of predicted displacements with digital volume correlation. *Journal of the Mechanical Behavior of Biomedical Materials*, *125*, 104872. https://doi.org/10.1016/j.jmbbm.2021.104872

Palanca, M., Tozzi, G., & Cristofolini, L. (2016). The use of digital image correlation in the biomechanical area: A review. *International Biomechanics*, *3*(1), 1–21. https://doi.org/10.1080/23335432.2015.1117395

Pasco, J. A., Seeman, E., Henry, M. J., Merriman, E. N., Nicholson, G. C., & Kotowicz, M. A. (2006). The population burden of fractures originates in women with osteopenia, not osteoporosis. *Osteoporosis International*, *17*(9), 1404–1409. https://doi.org/10.1007/s00198-006-0135-9

Peña Fernández, M., Hoxha, D., Chan, O., Mordecai, S., Blunn, G. W., Tozzi, G., & Goldberg, A. (2020). Centre of Rotation of the Human Subtalar Joint Using Weight-Bearing Clinical Computed Tomography. *Scientific Reports*, *10*(1), 1035. https://doi.org/10.1038/s41598-020-57912-z

Peña Fernández, M., Kao, A. P., Bonithon, R., Howells, D., Bodey, A. J., Wanelik, K., Witte, F., Johnston, R., Arora, H., & Tozzi, G. (2021). Time-resolved in situ synchrotron-microCT: 4D deformation of bone and bone analogues using digital volume correlation. *Acta Biomaterialia*, *131*, 424–439. https://doi.org/10.1016/j.actbio.2021.06.014

Peters, W. H., & Ranson, W. F. (1982). *Digital Imaging Techniques In Experimental Stress Analysis*.

Pollintine, P., van Tunen, M. S. L. M., Luo, J., Brown, M. D., Dolan, P., & Adams, M. A. (2010). Time-Dependent Compressive Deformation of the Ageing Spine: Relevance to Spinal Stenosis. *Spine*, *35*(4), 386–394. https://doi.org/10.1097/BRS.0b013e3181b0ef26

Qasim, M., Farinella, G., Zhang, J., Li, X., Yang, L., Eastell, R., & Viceconti, M. (2016). Patient-specific finite element estimated femur strength as a predictor of the risk of hip fracture: The effect of methodological determinants. *Osteoporosis International*, *27*(9), 2815–2822. https://doi.org/10.1007/s00198-016-3597-4

Rayudu, N. M., Subburaj, K., Mohan, R. E., Sollmann, N., Dieckmeyer, M., Kirschke, J. S., & Baum, T. (2022). Patient-Specific Finite Element Modeling of the Whole Lumbar Spine Using Clinical Routine Multi-Detector Computed Tomography (MDCT) Data—A Pilot Study. *Biomedicines*, *10*(7), 1567. https://doi.org/10.3390/biomedicines10071567

Reznikov, N., Chase, H., Brumfeld, V., Shahar, R., & Weiner, S. (2015). The 3D structure of the collagen fibril network in human trabecular bone: Relation to trabecular organization. *Bone*, *71*, 189–195. https://doi.org/10.1016/j.bone.2014.10.017

Rijsbergen, M. van, van Rietbergen, B., Barthelemy, V., Eltes, P., Lazáry, Á., Lacroix, D., Noailly, J., Ho Ba Tho, M.-C., Wilson, W., & Ito, K. (2018). Comparison of patient-specific computational models vs. Clinical follow-up, for adjacent segment disc degeneration and bone remodelling after spinal fusion. *PLOS ONE*, *13*(8), e0200899. https://doi.org/10.1371/journal.pone.0200899

Robson Brown, K., Tarsuslugil, S., Wijayathunga, V. N., & Wilcox, R. K. (2014). Comparative finite-element analysis: A single computational modelling method can estimate the mechanical properties of porcine and human vertebrae. *Journal of The Royal Society Interface*, *11*(95), 20140186. https://doi.org/10.1098/rsif.2014.0186

Rohlmann, A., Zander, T., Graichen, F., Schmidt, H., & Bergmann, G. (2014). How does the way a weight is carried affect spinal loads? *Ergonomics*, *57*(2), 262–270. https://doi.org/10.1080/00140139.2014.887789

Ruspi, M. L., Palanca, M., Faldini, C., & Cristofolini, L. (2017). Full-field in vitro investigation of hard and soft tissue strain in the spine by means of Digital Image Correlation. *Muscles, Ligaments and Tendons Journal*, 538–545. https://doi.org/10.11138/mltj/2017.7.4.538

Ryan, M. K., Oliviero, S., Costa, M. C., Wilkinson, J. M., & Dall'Ara, E. (2020). Heterogeneous Strain Distribution in the Subchondral Bone of Human Osteoarthritic Femoral Heads, Measured with Digital Volume Correlation. *Materials*, *13*(20), 4619. https://doi.org/10.3390/ma13204619

Schileo, E., Dall'Ara, E., Taddei, F., Malandrino, A., Schotkamp, T., Baleani, M., & Viceconti, M. (2008). An accurate estimation of bone density improves the accuracy of subject-specific finite element models. *Journal of Biomechanics*, *41*(11), 2483–2491. https://doi.org/10.1016/j.jbiomech.2008.05.017

Schileo, E., & Taddei, F. (2021). Finite Element Assessment of Bone Fragility from Clinical Images. *Current Osteoporosis Reports*, *19*(6), 688–698. https://doi.org/10.1007/s11914-021-00714-7

Schileo, E., Taddei, F., Malandrino, A., Cristofolini, L., & Viceconti, M. (2007). Subject-specific finite element models can accurately predict strain levels in long bones. *Journal of Biomechanics*, *40*(13), 2982–2989. https://doi.org/10.1016/j.jbiomech.2007.02.010

Schmidt, T., Tyson, J., & Galanulis, K. (2003). FULL-FIELD DYNAMIC DISPLACEMENT AND STRAIN MEASUREMENT USING ADVANCED 3D IMAGE CORRELATION PHOTOGRAMMETRY: PART 1. *Experimental Techniques*, *27*(3), 47–50. https://doi.org/10.1111/j.1747-1567.2003.tb00115.x

Schousboe, J. T. (2016). Epidemiology of Vertebral Fractures. *Journal of Clinical Densitometry*, *19*(1), 8–22. https://doi.org/10.1016/j.jocd.2015.08.004

Silva, M. J., Keaveny, T. M., & Hayes, W. C. (1998). Computed tomography-based finite element analysis predicts failure loads and fracture patterns for vertebral sections. *Journal of Orthopaedic Research: Official Publication of the Orthopaedic Research Society*, *16*(3), 300–308. https://doi.org/10.1002/jor.1100160305

Sorkine, O., & Rabinovich, M. (2009). Least-squares rigid motion using svd. *Technical notes*, *February*, 1–6.

Stadelmann, M. A., Maquer, G., Voumard, B., Grant, A., Hackney, D. B., Vermathen, P., Alkalay, R. N., & Zysset, P. K. (2018). Integrating MRI-based geometry, composition and fiber architecture in a finite element model of the human intervertebral disc. *Journal of the Mechanical Behavior of Biomedical Materials*, *85*, 37–42. https://doi.org/10.1016/j.jmbbm.2018.05.005

Stadelmann, M. A., Schenk, D. E., Maquer, G., Lenherr, C., Buck, F. M., Bosshardt, D. D., Hoppe, S., Theumann, N., Alkalay, R. N., & Zysset, P. K. (2020). Conventional finite element models estimate the strength of metastatic human vertebrae despite alterations of the bone's tissue and structure. *Bone*, *141*, 115598. https://doi.org/10.1016/j.bone.2020.115598

Stadelmann, M., Alkalay, R., Maquer, G., Buck, F., Hoppe, S., & Theumann, N. (2018). Can Micro and Homogenized Finite Element Analysis Estimate the Strength of Human Metastatic Vertebrae. *Word Congress of Biomechanics*.

Stevens, J. P. (1984). *Outliers and Influential Data Points in Regression Analysis*. *95*, 334–344.

Sztefek, P., Vanleene, M., Olsson, R., Collinson, R., Pitsillides, A. A., & Shefelbine, S. (2010). Using digital image correlation to determine bone surface strains during loading and after adaptation of the mouse tibia. *Journal of Biomechanics*, *43*(4), 599–605. https://doi.org/10.1016/j.jbiomech.2009.10.042

Taddei, F., Schileo, E., Helgason, B., Cristofolini, L., & Viceconti, M. (2007). The material mapping strategy influences the accuracy of CT-based finite element models of bones: An evaluation against experimental measurements. *Medical Engineering and Physics*, *29*(9), 973–979. https://doi.org/10.1016/j.medengphy.2006.10.014

Tavana, S., N. Clark, J., Newell, N., Calder, J. D., & Hansen, U. (2020). In Vivo Deformation and Strain Measurements in Human Bone Using Digital Volume Correlation (DVC) and 3T Clinical MRI. *Materials*, *13*(23), 5354. https://doi.org/10.3390/ma13235354

The American College of Radiology. (2018). *ACR–SPR–SSR PRACTICE PARAMETER FOR THE PERFORMANCE OF MUSCULOSKELETAL QUANTITATIVE COMPUTED TOMOGRAPHY (QCT)*.

Tozzi, G., Danesi, V., Palanca, M., & Cristofolini, L. (2016). Elastic Full-Field Strain Analysis and Microdamage Progression in the Vertebral Body from Digital Volume Correlation. *Strain*, *52*(5), 446–455. https://doi.org/10.1111/str.12202

Tschirhart, C. E., Finkelstein, J. A., & Whyne, C. M. (2007). Biomechanics of vertebral level, geometry, and transcortical tumors in the metastatic spine. *Journal of Biomechanics*, *40*(1), 46–54. https://doi.org/10.1016/j.jbiomech.2005.11.014

Tu, K. N., Lie, J. D., Wan, C. K. V., Cameron, M., Austel, A. G., Nguyen, J. K., Van, K., & Hyun, D. (s.d.). *Osteoporosis: A Review of Treatment Options*.

Väänänen, S. P., Jurvelin, J. S., & Isaksson, H. (2012). Estimation of 3D shape, internal density and mechanics of proximal femur by combining bone mineral density images with shape and density templates. *Biomechanics and Modeling in Mechanobiology*, *11*(6), 791–800. https://doi.org/10.1007/s10237-011-0352-9

Van Den Brande, R., Mj Cornips, E., Peeters, M., Ost, P., Billiet, C., & Van De Kelft, E. (2022). Epidemiology of spinal metastases, metastatic epidural spinal cord compression and pathologic vertebral compression fractures in patients with solid tumors: A systematic review. *Journal of Bone Oncology*, *35*, 100446. https://doi.org/10.1016/j.jbo.2022.100446

Viceconti, M., Henney, A., & Morley-Fletcher, E. (2016). In silico clinical trials: How computer simulation will transform the biomedical industry. *International Journal of Clinical Trials*, *3*(2), 37. https://doi.org/10.18203/2349-3259.ijct20161408

Viceconti, M., Olsen, S., Nolte, L.-P., & Burton, K. (2005). Extracting clinically relevant data from finite element simulations. *Clinical Biomechanics*, *20*(5), 451–454. https://doi.org/10.1016/j.clinbiomech.2005.01.010

Viceconti, M., Qasim, M., Bhattacharya, P., & Li, X. (2018). Are CT-Based Finite Element Model Predictions of Femoral Bone Strengthening Clinically Useful? *Current Osteoporosis Reports*, *16*(3), 216–223. https://doi.org/10.1007/s11914-018-0438-8

Wang, W., Wang, D., De Groote, F., Scheys, L., & Jonkers, I. (2020). Implementation of physiological functional spinal units in a rigid-body model of the thoracolumbar spine. *Journal of Biomechanics*, *98*, 109437. https://doi.org/10.1016/j.jbiomech.2019.109437

Wang, X., Sanyal, A., Cawthon, P. M., Palermo, L., Jekir, M., Christensen, J., Ensrud, K. E., Cummings, S. R., Orwoll, E., Black, D. M., for the Osteoporotic Fractures in Men (MrOS) Research Group, & Keaveny, T. M. (2012). Prediction of new clinical vertebral fractures in elderly men using finite element analysis of CT scans. *Journal of Bone and Mineral Research*, *27*(4), 808–816. https://doi.org/10.1002/jbmr.1539

Whyne, C., Hu, S., & Lotz, J. (2003). *Burst Fracture in the Metastatically Involved Spine Development, Validation, and Parametric Analysis of a Three-Dimensional Poroelastic Finite-Element Model*. https://doi.org/DOI: 10.1097/01.BRS.0000051910.97211.BA

Whyne, C. M., Hu, S. S., & Lotz, J. C. (2001). Parametric finite element analysis of vertebral bodies affected by tumors. *Journal of Biomechanics*.

Wijayathunga, V. N., Jones, A. C., Oakland, R. J., Furtado, N. R., Hall, R. M., & Wilcox, R. K. (2008). Development of specimen-specific finite element models of human vertebrae for the analysis of vertebroplasty. *Proceedings of the Institution of Mechanical Engineers, Part H: Journal of Engineering in Medicine*, *222*(2), 221–228. https://doi.org/10.1243/09544119JEIM285

Wilke, H.-J., Herkommer, A., Werner, K., & Liebsch, C. (2017). In vitro analysis of the segmental flexibility of the thoracic spine. *PLOS ONE*, *12*(5), e0177823. https://doi.org/10.1371/journal.pone.0177823

World Health Organization. (2020). *WHO report on cancer: Setting priorities, investing wisely and providing care for all*. World Health Organization. https://iris.who.int/handle/10665/330745

World Health Organization & United Nations Children's Fund (UNICEF). (2022). *Global report on assistive technology*. World Health Organization. https://apps.who.int/iris/handle/10665/354357

Yang, H., Jekir, M. G., Davis, M. W., & Keaveny, T. M. (2016). Effective modulus of the human intervertebral disc and its effect on vertebral bone stress. *Journal of Biomechanics*, *49*(7), 1134–1140. https://doi.org/10.1016/j.jbiomech.2016.02.045

Yang, P. F., Brüggemann, G.-P., & Rittweger, J. (s.d.). *What do we currently know from in vivo bone strain measurements in humans?*

Yeung, L. Y., Rayudu, N. M., Löffler, M., Sekuboyina, A., Burian, E., Sollmann, N., Dieckmeyer, M., Greve, T., Kirschke, J. S., Subburaj, K., & Baum, T. (2021). Prediction of Incidental Osteoporotic Fractures at Vertebral-Specific Level Using 3D Non-Linear Finite Element Parameters Derived from Routine Abdominal MDCT. *Diagnostics*, *11*(2), 208. https://doi.org/10.3390/diagnostics11020208

Zienkiewicz, O. C. (1971). *The finite element method in engineering science*. McGraw-Hill.

Zysset, P., Pahr, D., Engelke, K., Genant, H. K., McClung, M. R., Kendler, D. L., Recknor, C., Kinzl, M., Schwiedrzik, J., Museyko, O., Wang, A., & Libanati, C. (2015). Comparison of proximal femur and vertebral body strength improvements in the FREEDOM trial using an alternative finite element methodology. *Bone*, *81*, 122–130. https://doi.org/10.1016/j.bone.2015.06.025

Acknowledgments

This journey is almost over, and I want to thank everyone who has been by my side during the pilgrimage.

First of all, thanks to my supervisor, Prof. Marco Viceconti, for giving me this opportunity and for sharing with me the roots of this fascinating travel called biomechanics. I learned much more from our meetings during these three years than from all my studies. Thanks to Prof. Enrico Dall'Ara for hosting me at the University of Sheffield; you made me feel welcomed and inspired. Thanks to Dr. Lorenzo Grassi for the corrections and the suggestions. Thanks to the colleagues who helped me during the studies that have composed this thesis, especially Dr. Aldieri, Dr. Curreli, Prof. Cristofolini, and Dr. Palanca, each shared part of their experience with me, helping me improve over the years. A huge hug to all Rizzoli's labmates, especially Maila, Sofi and Ale, who contributed to transforming that place into a second home for me.

Thanks to my friends for having continued to support me through the years; thanks to those who jumped on the first train (or even the first flight) to give me a hug in the darkest moments; thanks for telling me those words I needed; thank you all for being there.

A massive thanks to my family, especially my favourite supporters, my grandparents Carla and Elio, for teaching me never to give up and for being always by my side.

But most of all, thanks to the person to whom this thesis is dedicated for having made me the person I am today. Only when we see ourselves reflected in someone's admiring gaze can we fly to infinity and beyond. Only by caring for someone do we realize that we are really needed in this world. You used to complain about the time I used to spend studying, and I know if you found out that my models sometimes still don't work, you'd laugh and shake your head. You were, you are, and you will always be the light of my eyes, Michele.

Chiara

Scientific Publications of the candidate

Paper in International Journal

<u>Garavelli C.</u> et al., "Experimental validation of a subject-specific finite element model of lumbar spine segment using digital image correlation", 2022, PLoS ONE 17(9): e0272529.

<u>Garavelli C.</u> et al., "Multi-vertebral CT-based FE models implementing linear isotropic population-based material properties for the intervertebral discs cannot accurately predict strains", (*submitted*)

Proceedings of International Conferences

<u>Garavelli C.</u> et al., "Validation of homogenized finite element models of human metastatic vertebrae using digital volume correlation", European Society of Biomechanics, July 2023, Maastricht (oral presentation)

<u>Garavelli C.</u> et al., "Use of displacements field to validate subject-specific finite element models of spine segments with metastasis", European Society of Biomechanics, June 2022, Porto (oral presentation)

<u>Garavelli C.</u> et al.," Development and validation of a subject-specific finite element model of pathological lumbar spine", 2021, Brain and Spine, https://doi.org/10.1016/j.bas.2021.100076 (poster)